DEPARTMENT OF PARTICLE PHYSICS AND
GALICIAN INSTITUTE OF HIGH-ENERGY PHYSICS
UNIVERSIDADE DE SANTIAGO DE COMPOSTELA

RADIATION OF PHOTONS AND GLUONS IN A HOT AND DENSE QCD MEDIUM

BY
HAO MA

Academic Dissertation
for the Degree of
Doctor of Philosophy

Santiago de Compostela, Spain
May 28, 2013

Carlos Alberto Salgado López, Profesor Contratado Doutor da Universidade de Santiago de Compostela

CERTIFICA: que a memoria titulada *Radiation of photons and gluons in a hot and dense QCD medium* foi realizada, baixo a súa dirección, por Hao Ma, no Departamento de Física de Partículas desta universidade e constitúe o traballo de tese que presenta para optar ao Grao de Doutor en Física.

Asinado:

Carlos Alberto Salgado López
Santiago de Compostela, May 28, 2013.

USC
UNIVERSIDADE
DE SANTIAGO
DE COMPOSTELA

Acknowledgement

I would like to thank my advisor Prof. Dr. Carlos A. Salgado for all the discussions and his encouragement throughout my Ph.D. study at Universidade de Santiago de Compostela.
During my stay in Santiago de Compostela, I commenced my academic work for my Ph.D. thesis, which is inspired by the discussions with Prof. Dr. Néstor Armesto, Dr. Yacine Mehtar-Tani, Prof. Dr. Carlos A. Salgado, and Dr. Konrad Tywoniuk.
I will always remember the scientific atmosphere in the Faculty of Physics at Universidade de Santiago de Compostela. I enjoyed the interesting discussions with Dr. Yun Guo, Dr. Hai Lin, Dr. Yacine Mehtar-Tani, Dr. Hannu Paukkunen, and Dr. Konrad Tywoniuk.
I want to thank again all of those people for their patience, without which this thesis might not have been completed.

Santiago de Compostela, May 28, 2013
Hao Ma

Contents

USC UNIVERSIDADE DE SANTIAGO DE COMPOSTELA

USC UNIVERSIDADE DE SANTIAGO DE COMPOSTELA

Chapter 1

Summary

1.1 English version

My doctorate study spreads over different theoretical and phenomenological aspects of Quantum Chromo-Dynamics (QCD) at high energies and high parton densities as well as their connections to the phenomenology of relativistic nucleus-nucleus (AA) and proton-nucleus (pA) collisions and Deep Inelastic Scattering experiments with nucleons and nuclear targets. Generally speaking, these studies are relevant for the phenomenology of the experiments carried on at Relativistic Heavy-ion Collider (RHIC) in Brookhaven National Laboratory and the Large Hadron Collider (LHC) in CERN.

The introduction is presented in Chapter 2, where some aspects to heavy-ion physics are introduced with the time evolution of the relativistic heavy-ion collisions. Radiation of photons in a hot and dense QCD medium is discussed in Chapter 3. Photon interacts with the particles in a hot and dense QCD medium through electromagnetic interaction, which is negligible as compared with the strong interaction. Following the BDMPS-Z-W approach, we calculate the medium-induced two-photon ladder emission spectrum [1], and find that in the Molière limit the Landau-Pomeranchuk-Migdal effect still holds and the spectrum can not be factorized as a product of two medium-induced single-photon radiation spectra because of the structure of the Molière factor. Radiation of gluons in a hot and dense QCD medium is discussed in Chapter 4. Due to the non-Abelian nature, gluon interacts with the particles in a hot and dense QCD medium through strong interaction. The medium-induced gluon radiation off a single emitter is discussed. Then we study the in-medium color coherence effect by introducing a double-emitter set-up, i.e. a quark-antiquark antenna. As an extension, the medium-induced one-gluon radiation spectrum off a massive quark-antiquark antenna in the color singlet state traversing a color decon-

fined medium is calculated [2]. The interference between the quark and the antiquark dominates the spectrum when the antenna opening angle is small and the emitted gluon is soft, whereas the antenna behaves like a superposition of two independent emitters when the opening angle is large and the radiated gluon is hard. We investigate the average radiative energy loss of the antenna. More collimated antenna loses less energy. The broadening of the gluon radiation off the antenna is also studied. In the soft gluon emission limit, the broadening of the emitted gluon is due to the interference between the quark and the antiquark, rather than the gluon rescattering in the medium. This opens more phase space for the soft gluon emission. The in-medium t-channel antenna radiation is also presented in Chapter 5 [3]. The interference between initial and final state radiation is investigated. The medium-induced gluon radiation spectrum is discussed in three limits: the coherent, the incoherent and the soft limits. The soft on-shell gluon radiation off the initial state incoming quark is further broadened by the medium, and more phase space is opened for the soft gluon radiation off the final state outgoing quark. Then we extend the results obtained at first order in the opacity expansion by providing general results for multiple soft scatterings and their specific formulation within the harmonic oscillator approximation [4]. We discuss some phenomenological consequences of this setup in high-energy AA collisions. The conclusions are given in Chapter 6. The metric tensor is defined as $g^{\mu\nu} = \mathrm{diag}\,(1, -1, -1, -1)$. The natural units $c = \hbar = 1$ are chosen in this thesis, and we set the Boltzmann constant as $k_B = 1$.

1.2 Versión en español

Mis estudios de doctorado se extiende sobre diferentes aspectos teóricos y fenomenológicos de la Cromodinámica Cuántica (QCD) a altas energías y densidades partónicas así como sus conexiones con la fenomenología de las colisiones relativistas núcleo-núcleo (AA) y protón-núcleo (pA) y los experimentos de dispersión inelástica profunda con nucleones y núcleos. En general, estos estudios son relevantes para la fenomenología de las experiencias realizadas en el Relativistic Heavy Ion Collider (RHIC) en el Brookhaven National Laboratory y el Large Hadron Collider (LHC) en el CERN.
La introducción se presenta en el capítulo 2, donde algunos aspectos de la física de iones pesados se introducen siguiendo la evolución temporal de las colisiones de iones pesados relativistas. La radiación de fotones en un medio QCD caliente y denso se discute en el capítulo 3. Los fotones interactúa con las partículas en un medio QCD a través de la interacción electromagnética, que es insignificante en comparación con la interacción

fuerte. Siguiendo el enfoque BDMPS-Z-W, se calcula el espectro de emisión *ladder* de dos fotones inducida por el medio [1], y se encuentra, en el límite de Moliére que el efecto Landau-Pomeranchuk-Migdal se mantiene y que el espectro de dos fotones no puede ser factorizado como un producto de dos espectros de un fotón inducidos por el medio. La radiación de gluones en un medio de QCD caliente y denso se discute en el capítulo 4. Debido a la naturaleza no-abeliana, los gluones interactúa con las partículas en el medio de QCD a través de la interacción fuerte. Se discute la radiación de gluones inducida por el medio de un único emisor. A continuación, se estudia el efecto de la coherencia de color en medio mediante la introducción de un doble emisor en un caso sencillo, una *antena* quark-antiquark. Como una extensión, el espectro de la radiación de un gluon inducida por el medio de una antena de quark-antiquark masivos en estado singlete es calculada [2]. La interferencia entre el quark y el antiquark domina el espectro cuando el ángulo de apertura de la antena es pequeña y el gluon emitido es *soft*, mientras que la antena se comporta como una superposición de dos emisores independientes cuando el ángulo de apertura es grande y el gluon radiado es *hard*. Investigamos la pérdida promedio de energía por radiación de la antena. La antena más colimada pierde menos energía. El aumento de la radiación de gluones de la antena también se estudia. En el límite de emisión de gluones soft, el aumento de la radiación de gluones emitida es debido a la interferencia entre el quark y el antiquark, y no a la redifusión de gluones en el medio. Esto abre más espacio de fase para la emisión de gluones. La radiación por una antena en canal-t también se presenta en el capítulo 5 [3]. La interferencia entre la radiación inicial y final del estado es investigado. El espectro de la radiación de gluones inducida por el medio se analiza en tres límites: coherente, incoherente y el límite soft. Los gluones reales emitidos por el quark incidente sufren un proceso de *broadening* por interacción con el medio, al mismo tiempo que se aumenta el espacio de fase para radiación del quark saliente. Por último, extendemos los resultados obtenidos en el primer orden en la expansión de la opacidad presentando resultados para el caso de scattering múltiple, así como su formulación específica dentro de la aproximación del oscilador armónico [4]. Se discuten algunas consecuencias fenomenológicas de esta configuración en colisiones AA de alta energía. Las conclusiones se presentan en el capítulo 6.

El tensor métrico se define como $g^{\mu\nu} = \mathrm{diag}\,(1, -1, -1, -1)$. Las unidades naturales $c = \hbar = 1$ se eligen en esta tesis, y se toma la constante de Boltzmann como $k_B = 1$.

USC
UNIVERSIDADE
DE SANTIAGO
DE COMPOSTELA

Chapter 2

Some aspects to heavy-ion physics

2.1 Within the Standard Model

The Standard Model is a unified gauge theory with U(1) $\times$ SU(2) $\times$ SU(3) gauge symmetry. U(1) gauge theory is called Quantum Electro-Dynamics (QED). It is an Abelian gauge theory describing the electromagnetic interactions between fermions and photon. Photons do not interact with each other because of the Abelian nature of QED. SU(2) gauge theory describes the weak interactions between fermions and $W^{\pm}$, Z^0 bosons. The weak interaction supports transformations among quarks and among leptons, respectively. SU(3) gauge theory is called Quantum Chromo-Dynamics (QCD).

2.1.1 Quarks and gluons

QCD is a non-Abelian gauge theory of the strong interactions among partons, i.e. quarks and gluons, in the Standard Model. Quarks are spin-$1/2$ fermions, which means that they are matter and they obey the Fermi-Dirac statistics and follow the Pauli exclusion principle. Gluons are spin-1 gauge bosons, which means that they are strong interaction carriers and they obey the Bose-Einstein statistics. In QCD, quarks interact with each other by exchanging gluons. Moreover, the interactions among quarks and gluons and among gluons themselves can also happen because of the non-Abelian nature of QCD. Quarks are described by the Dirac fields with color degrees of freedom. Note that the color of quarks and gluons has nothing to do with visual perception of color, but rather color charge has properties analogous to electric charge. Quark has six flavors: up, down, charm, strange, top, and bottom. Gluons are described in terms of the gauge fields with eight color degrees of freedom. The gauge fields belong to the SU(3) color group.

Here it is the elegant and beautiful QCD Lagrangian density:

$$\mathcal{L}_{\rm QCD} = -\frac{1}{4}\, F_a^{\mu\nu}\, F^a_{\mu\nu} + \bar{\psi}^i_f \left(i \not{D} - m_f\right)_{ij} \psi^j_f + \mathcal{L}_{\rm gauge-fixing} + \mathcal{L}_{\rm ghost}. \quad (2.1)$$

μ and ν in Eq.(2.1) are Lorentz indices. A repeated index implies a summation with respect to that index in this thesis. The non-Abelian field strength tensor for the gluon gauge field in Eq.(2.1) reads

$$F_a^{\mu\nu} = \partial^\mu A_a^\nu - \partial^\nu A_a^\mu + g\, f^{abc}\, A_b^\mu\, A_c^\nu. \quad (2.2)$$

g in Eq.(2.2) is the strong coupling constant and f^{abc} is the structure constant of SU(3). The covariant derivative in Eq.(2.1) reads

$$(D^\mu)_{ij} = \partial^\mu \delta_{ij} - i\, g\, A_a^\mu\, t^a_{ij}. \quad (2.3)$$

$t^a_{ij} = \lambda^a_{ij}/2$ and λ^a_{ij} are the eight generators of SU(3). Note that the color matrices in the fundamental representation are different from the ones in the adjoint representation. There are still free parameters entering the QCD Lagrangian density: quark rest masses m_f and the QCD energy scale $\Lambda_{\rm QCD}$.

2.1.2 Choice of gauge

Gluon propagator is impossible to be defined without a choice of gauge. The light-cone gauge, for example, is described by

$$n \cdot A^a = 0, \quad n^2 = 0 \quad (2.4)$$

corresponding to a gauge-fixing term

$$\mathcal{L}_{\rm gauge-fixing} = -\frac{1}{2\,\xi} \left(n \cdot A^a\right)^2, \quad \xi \to 0. \quad (2.5)$$

n in Eq.(2.4) is a fixed 4-vector, which defines a preferred axis in space. For the gauge parameter approaches zero in Eq.(2.5), a nonzero value of $n \cdot A^a$ leads to an infinite action, and therefore in the homogeneous axial gauge one has $n \cdot A^a = 0$. The light-cone gauge is the most convenient choice of gauge in high-energy processes and is therefore chosen for this thesis. The gluon propagator in the light-cone gauge reads

$$D^{\mu\nu} = \frac{-i}{k^2 + i\,\epsilon}\left(g^{\mu\nu} - \frac{k^\mu\, n^\nu + k^\nu\, n^\mu}{k \cdot n}\right). \tag{2.6}$$

For the physical polarization states of on-shell gluon, one has $k \cdot \epsilon = 0$ and $n \cdot \epsilon = 0$. The sum over two physical polarization states normalized by $|\epsilon_\lambda|^2 = -1$ reads

$$\epsilon_\lambda^\mu\, \epsilon_\lambda^{\nu *} \to -g^{\mu\nu} + \frac{k^\mu\, n^\nu + k^\nu\, n^\mu}{k \cdot n}. \tag{2.7}$$

The sum of photon polarization is analogous but simpler than the one of gluon. The gluon propagator in the light-cone gauge can thus be replaced by the polarization sum over two physical states:

$$D^{\mu\nu} = \frac{i}{k^2 + i\,\epsilon}\,\epsilon_\lambda^\mu\, \epsilon_\lambda^{\nu *}. \tag{2.8}$$

The ghost degrees of freedom in Eq.(2.1) depends on the choice of the gauge-fixing degrees of freedom. The wonderful thing is that the ghost degrees of freedom is eliminated in the light-cone gauge since the gauge parameter is taken to be zero. Another good news is that the number of contributing Feynman diagrams can be reduced if the calculation is performed in the light-cone gauge. These simplifications are the reason why we choose the light-cone gauge here.

2.1.3 Asymptotic freedom

The strong coupling constant satisfies the renormalization group equation

$$\mu^2\, \frac{\mathrm{d}\alpha_s}{\mathrm{d}\mu^2} = \beta = -\left(b_0\, \alpha_s^2 + b_1\, \alpha_s^3 + b_2\, \alpha_s^4 + \cdots\right). \tag{2.9}$$

$b_0 = (11\, N_c - 2\, N_f)\,/\,(4\,\pi\, N_c)$ in Eq.(2.9) is referred to as the 1-loop beta function coefficient, and so on. $N_c = 3$ is of course the number of quark colors. N_f is the number of active light quark flavors. The solution of the beta function for QCD at the second order of α_s in Eq.(2.9) reads

$$\alpha_s\left(Q^2\right) = \frac{\left[g\left(Q^2\right)\right]^2}{4\,\pi} = \frac{1}{b_0 \ln(Q^2/\Lambda^2_{\mathrm{QCD}})}. \tag{2.10}$$

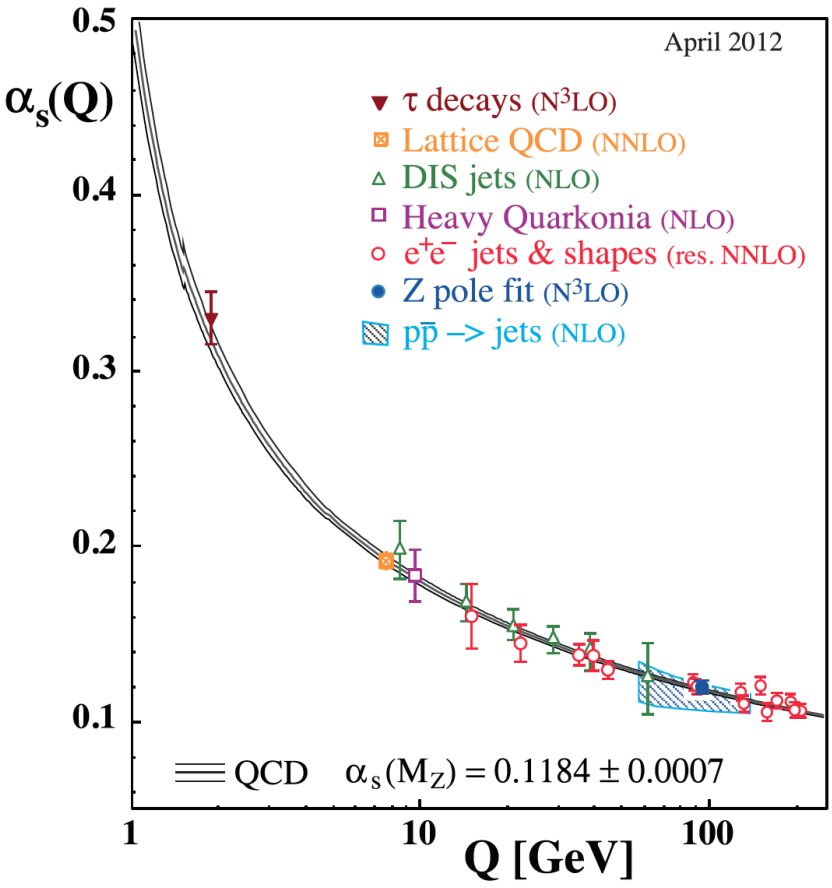

Figure 2.1: The values of α_s at various energy scales [5]

α_s must be positive, so the 1-loop beta function coefficient has to be positive, i.e. gluonic vacuum fluctuations produce an anti-screening between two quarks, which overwhelms the screening produced by fermionic vacuum fluctuations. The strong coupling constant is actually not a constant. The strong coupling constant approaches zero at a logarithmic rate as the energy scale approaches the positive infinity (see figure 2.1). Such a feature of the strong coupling constant of QCD is named asymptotic freedom [6, 7]. On the other hand, $\alpha_s(Q^2)$ is very large in the infrared region $Q^2 \sim \Lambda^2_{\rm QCD}$. The value of α_s can be measured in, e.g. $e^+\,e^-$ annihilation into hadrons. The energy associated with the bare quark is enough to produce a neutralizing quark of the opposite color charge. The running property of the strong coupling constant naturally separates the study of the system of quarks and gluons into perturbative QCD and nonperturbative QCD. Perturbative

QCD is the tool for the study in this thesis. One important application and also justification of asymptotic freedom is the prediction of the existence of jets in high-energy scattering processes.

2.1.4 Color confinement

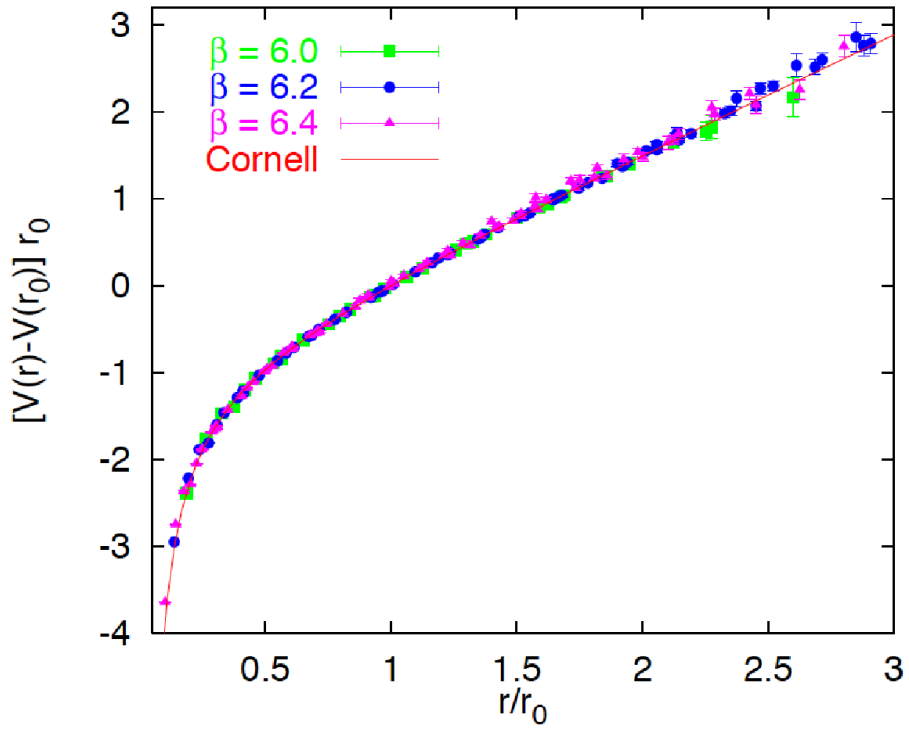

Figure 2.2: Quark potential as a function of length scale with three different β values (6.0, 6.2 and 6.4) in units of $r_0 \approx 0.5$ fm [8]

The radius of color confinement is around the inverse of the QCD energy scale, which is the characteristic size of the hadron. The quark potential increases linearly with an increasing separation between quarks (see figure 2.2). In cold nuclear matter, color confinement is controlled by the non-perturbative scale. All physical observables are in the color singlet state, i.e. their colors are confined. In order to study the dynamics of free quarks and gluons, relativistic heavy-ion collisions are performed to create a quark-gluon plasma phase, which is different from the hadronic phase with the lack of the observation of isolated quarks and gluons (see 2.4.1).

2.2 Light-cone variables

Before getting to know more about such a brand new phase, let us first be familiar with the light-cone variables that I use in my work. In the light-cone coordinate system, one writes the 4-coordinate as $x = (x^+, x^-, \mathbf{x})$, with $x^\pm = \left(x^0 \pm x^3\right)/\sqrt{2}$ and the transverse coordinates $\mathbf{x} = \left(x^1, x^2\right)$, and the 4-momentum is given by $p = (p^+, p^-, \mathbf{p})$, with $p^\pm = \left(p^0 \pm p^3\right)/\sqrt{2}$ and the transverse coordinates $\mathbf{p} = \left(p^1, p^2\right)$. Therefore the Lorentz invariant scalar products are

$$x^2 = 2\,x^+\,x^- - \mathbf{x}^2, \quad p^2 = 2\,p^+\,p^- - \mathbf{p}^2, \tag{2.11}$$

and

$$p \cdot x = p^+\,x^- + p^-\,x^+ - \mathbf{p} \cdot \mathbf{x}. \tag{2.12}$$

The 4-momentum of an on-shell particle of rest mass m and transverse momentum $\mathbf{p}$ can also be expressed as

$$p = \left(\sqrt{\frac{\mathbf{p}^2 + m^2}{2}}\,e^y, \sqrt{\frac{\mathbf{p}^2 + m^2}{2}}\,e^{-y}, \mathbf{p}\right). \tag{2.13}$$

The rapidity in Eq.(2.13) is defined as

$$y = \frac{1}{2}\,\ln\frac{p^+}{p^-}. \tag{2.14}$$

When the 3-momentum is large, one can substitute the energy of the particle by its 3-momentum in Eq.(2.14) to define the pseudorapidity. Note that if a (positive or negative) boost along the p^3-direction is very large, only one of the first two components in the parentheses of Eq.(2.13) is large and another is exponentially suppressed. Consider two colliding particles p_1 and p_2. We suppose that p_1 is highly boosted along the p^3-direction relative to p_2, say p_1^+ is large and p_1^- is suppressed without loss of generality, and accordingly p_2^- is large and p_2^+ is suppressed. Then the scalar product of the sum of these two particles simplifies

$$(p_1 + p_2)^2 \approx 2\,p_1^+\,p_2^-. \tag{2.15}$$

It is clear that it is easier to analyze the size of the scalar product of highly boosted particles by using the light-cone coordinates than by using the ordinary coordinates.
One useful variable that is going to appear frequently in the rest of my thesis is the forward light-cone variable of the emitted daughter particle k relative to the parent particle p, which is defined as

$$x = \frac{k^+}{p^+}. \tag{2.16}$$

Since the daughter particle is always softer than the parent particle, one always has $0 \leq x \leq 1$. The forward light-cone variable is equal to the longitudinal momentum fraction in the high-energy limit.

2.3 Initial state evolution

Now let us go back to the process of relativistic heavy-ion collisions and see how such an exotic phase of quark-gluon plasma is created and how it further evolves. If we want to study such a color deconfined medium, we have to first create it by accelerating two heavy nuclei and then smash them. A nucleon at rest contains quantum fluctuations at all space-time scales smaller than its own size. Only quantum fluctuations that have longer life time than the external probe can be resolved by such probe. The short lived quantum fluctuations, on the other hand, are of the role to just renormalize the couplings and the masses. Contrary to the nucleon at rest, time dilation of all internal time-scales happens for a high-energy nucleon accelerated by a machine, e.g. RHIC or the LHC. The constituents of the nucleon behave as if they were free since the interactions among the constituents take place over time-scales that are much longer than the characteristic time-scale of the external probe. Therefore more quantum fluctuations can be resolved by the probe for the nucleon at high energy than at rest. Pre-existing quantum fluctuations are completely static as compared with the time-scale of the external probe, and therefore act as static color sources of new partons. It motivates the utility of the classical gauge field approximation (see 4.2.1).

2.3.1 Pure bremsstrahlung

What happens in the early stage of the acceleration? The nucleon can be seen as a collection of partons described by non-perturbative parton distributions, which depend on the longitudinal momentum fraction of the parton and a transverse resolution scale. In a simplified picture, only valence quarks

are present inside the hadron in the very beginning of the acceleration, but more and more partons are emitted during the acceleration. The increase of the number of partons inside the hadron is linear in energy as long as the density of the partons is small during the acceleration. The way to probe the inner structure of a nucleon is by using Deep Inelastic Scattering experiments to kind of taking a snapshot of the inner structure of the accelerated nucleon.

2.3.2 Gluon saturation

An estimate of the gluon density, i.e. the number of gluons per unit area, is

$$\rho \sim \frac{x\,G\left(x,Q^2\right)}{\pi\,R^2}, \tag{2.17}$$

where R is the radius of the nucleon. When the density of the partons is large enough, the evolution of the partons inside the hadron becomes non-linear because they start to overlap, i.e. the process of gluon fusion starts to compete against the one of gluon splitting. This effect is known as gluon saturation. The cross section of the merge of two gluons reads

$$\sigma_{gg\to g} \sim \frac{\pi\,\alpha_s\left(Q^2\right)}{Q^2}. \tag{2.18}$$

Gluon saturation happens when $\rho\,\sigma_{gg\to g} \gtrsim 1$, which is equivalent to $Q^2 \lesssim Q_s^2$. The saturation scale Q_s is defined here as

$$Q_s^2 \sim \frac{\pi\,\alpha_s\,x\,G\left(x,Q_s^2\right)}{\pi\,R^2}, \tag{2.19}$$

At gluon saturation, the phase space density reads

$$\frac{\mathrm{d}N_g}{\mathrm{d}^2\mathbf{x}\,\mathrm{d}^2\mathbf{p}} \sim \frac{\rho}{Q^2} \sim \frac{1}{\alpha_s}. \tag{2.20}$$

2.4 Color deconfinement

2.4.1 Deconfinement transition

Relativistic heavy-ion collisions are able to create a color deconfined medium, i.e. the quark-gluon plasma, with initial energy densities above the critical values indicated by lattice QCD. The size of such a hot and dense QCD medium depends on the collision area of two heavy ions, which is defined as centrality. At $\tau \sim 0$, hard particles, e.g. jets, heavy quarks, quarkonia and direct photons are produced at this stage. And I would like to remind the reader that perturbative QCD is a valid theoretical tool here. At $\tau \sim 0.2$ fm, most of the multiplicity with relatively small transverse momentum around $1-2$ GeV is made up. Semi-hard particles, i.e. gluons and light quarks are produced in this time interval. At $\tau \sim 1-2$ fm, a fast thermalization is indicated by experiments. At 2 fm/c $\leq \tau \lesssim 10$ fm, new phase of matter, i.e. the quark-gluon plasma is believed to be created with temperature higher than the critical temperature. A basic difference between the quark-gluon plasma and the gas of protons, neutrons and pions is that the quark-gluon plasma has a much larger number of degrees of freedom than the hadron gas (see Eq.(2.21) below).
In discussing the temperature dependence of the pressure of the system, the QCD phase can be divided into three regions: the low-temperature region with the temperature of the system of interest lower than the critical temperature, the critical region with the temperature of the system of interest around the critical temperature, and the high-temperature region with the temperature of the system of interest higher than the critical temperature. At high-temperature and zero chemical potential, the energy density asymptotically approaches the Stefan-Boltzmann limit for an ideal gas of gluons and N_f massless quarks:

$$\frac{\varepsilon_{\rm SB}}{T^4} = \frac{3\,p_{\rm SB}}{T^4} = \left(16 + \frac{21}{2}\,N_f\right)\frac{\pi^2}{30}, \tag{2.21}$$

where the number 16 comes from the product of helicity and color of gluon, and the fraction $21/2$ comes from the product of spin, quark/antiquark, color and Fermi-Dirac statistics. The pressure divided by T^4 in Eq.(2.21) increases drastically above the critical temperature, and then starts to saturate by around twice the critical temperature, which is still below the Stefan-Boltzmann limit (see figure 2.3). Lattice QCD indicates a 1st order phase transition for the pure gauge at around 270 MeV, and a cross-over for the light quarks at around $150-170$ MeV, depending on the number of the flavors of light quarks.

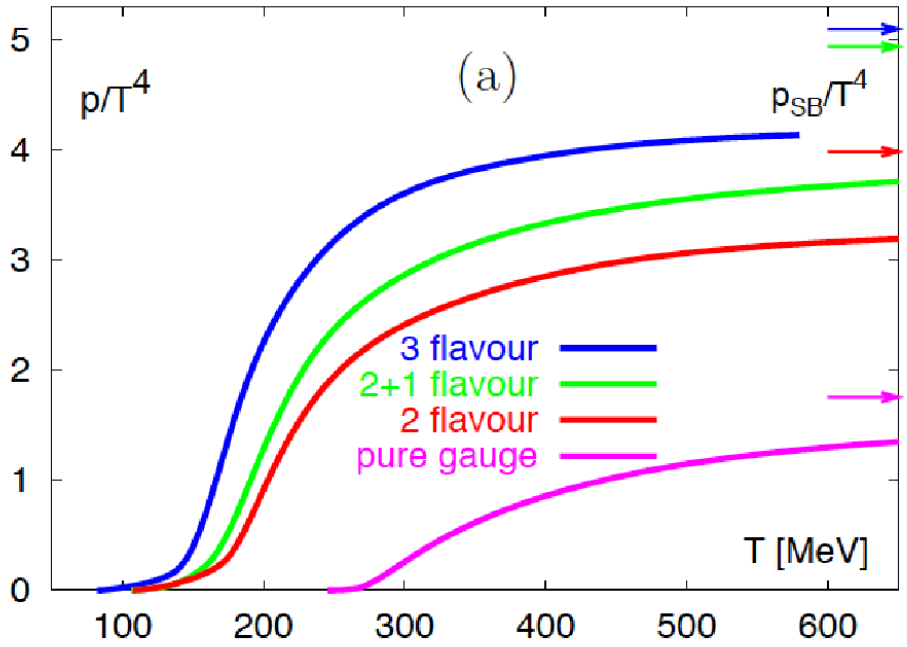

Figure 2.3: The QCD color deconfinement transition [9]

At low temperature, the typical correlation length among color charges in a nucleon is of the order of the nucleon size. Nucleons merge with each other as far as the temperature of the nucleons reaches a critical value, and then the quarks and gluons gain extra degrees of freedom to move inside the entire nuclear volume rather than only the nucleonic one. All kinds of hadrons and nuclei behave in the same way at high temperature. Note that the same explanation works with respect to the change of the density of normal cold nucleons, but does not work with respect to the change of the density of nuclear matter with very large net baryon density at low temperature.

2.4.2 Heavy flavor and quarkonia

The completely different behaviors of the Debye screening mass divided by temperature around the critical temperature predicted by both the perturbative QCD and the lattice QCD calculations (see figure 2.4) show clearly the large non-perturbative effects in the vicinity of the critical temperature. Perturbative QCD is therefore proved to be not valid at low energy scales. The effective potential between a heavy quark-antiquark pair is described

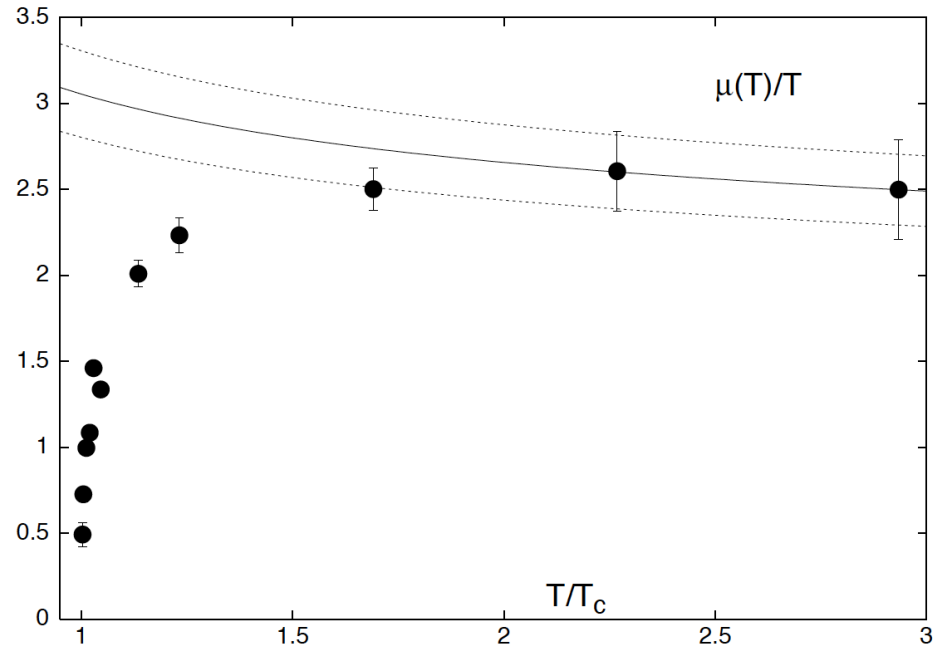

Figure 2.4: Temperature dependence of the Debye screening mass divided by temperature [10] (T_c is the critical temperature and note that $\mu(T) = m_D$ as introduced in the text. The solid curve represents the result from perturbative QCD calculations and the dots denote the lattice QCD result.)

by the screened Coulomb potential. From figure 2.4 one can see that the Debye screening mass increases with increasing temperature, which means a decreasing screening length, and therefore a shortening of the range of the interaction between the quark and the antiquark. A suppression of the quarkonium production in the quark-gluon plasma has been argued based on this behavior.

2.5 Jet evolution

A jet is a spray of highly energetic particles produced in a collision and appearing in the detector in a close by region, which is so hard that it can be easily and clearly identified from the background of softer particles. The generation of jets is due to the asymptotic freedom. On one hand, a hard parton can be produced directly from the initial hard process. On the other hand, it is much easier to decohere a parton from the parent hard parton collinearly, i.e. with a negligible separation, than to emit a parton with a

distinguishable separation from the parent hard parton. The structure of the final state is determined by parton branching and hadronization, i.e. a hard parton, produced in some initial hard process, traveling in vacuum with some initial virtuality will radiate gluons to become on-shell.

2.5.1 Medium modification on the QCD branching

The color deconfined medium can not be studied directly from experiments to date. Therefore one has to study some indirect probes in order to study the properties of the hot and dense QCD medium, and the hard probes, i.e. the jets, are the perfect choice for this aim. The reason that one can study the hard probes in order to indirectly study the properties of the created color deconfined medium is that the production of hard partons occurs at $0 < \tau \ll 1$ fm, i.e. before the formation of the quark-gluon plasma. Photon and gluon radiation is modified when the hard parton, again produced in some initial hard process, traverses a hot and dense QCD medium. Still, we have to show some experimental evidences to justify our argument. The nuclear modification factor (see figure 2.5), which is the number of the charged particle yields observed in AA collisions divided by the expected one in the binary scaled pp collisions, reads

$$R_{AA}\left(\mathbf{p}\right) = \frac{\mathrm{d}N_{\mathrm{ch}}^{AA} / \left(\mathrm{d}\eta\, \mathrm{d}^2\mathbf{p}\right)}{\langle N_{\mathrm{coll}} \rangle\, \mathrm{d}N_{\mathrm{ch}}^{pp} / \left(\mathrm{d}\eta\, \mathrm{d}^2\mathbf{p}\right)}. \tag{2.22}$$

The nuclear modification factor in the high-$\mathbf{p}$ range is much smaller than 1, so it is obvious that the quenching of inclusive hadron spectra is a final state effect due to parton energy loss in the medium.
High-$\mathbf{p}$ hadrons with the magnitude of the transverse momentum larger than ~ 5 GeV are interesting and important in studying the hot and dense QCD medium formed in relativistic heavy-ion collisions due to several reasons. First: The medium effect modifies the hadron spectrum, so the hadrons can be used to study the color deconfined medium produced in relativistic heavy-ion collisions. Second: The high-$\mathbf{p}$ hadrons occupy a small part of the total hadron multiplicity (see figure 2.6), so the suppression of high-$\mathbf{p}$ hadrons is easy to see in experiments. Third: High-$\mathbf{p}$ probes are produced in relativistic heavy-ion collisions in extremely short time scales, and perturbative QCD is therefore a valid theoretical tool to study QCD matter. The high-$\mathbf{p}$ partons emit particles when they traverse a hot and dense QCD medium. This phenomenon is called medium-induced radiation. Due to the medium-induced radiation, the jets stemming from parton fragmentation

lose energy and therefore exhibit a significant broadening and softening. The phenomenon of jet energy loss is called jet quenching.
Now it is the time to end this chapter with the motivation of my doctorate work. How to improve our knowledge about the QCD branching in a color deconfined medium? This question will be addressed in Chapters 3, 4 and 5.

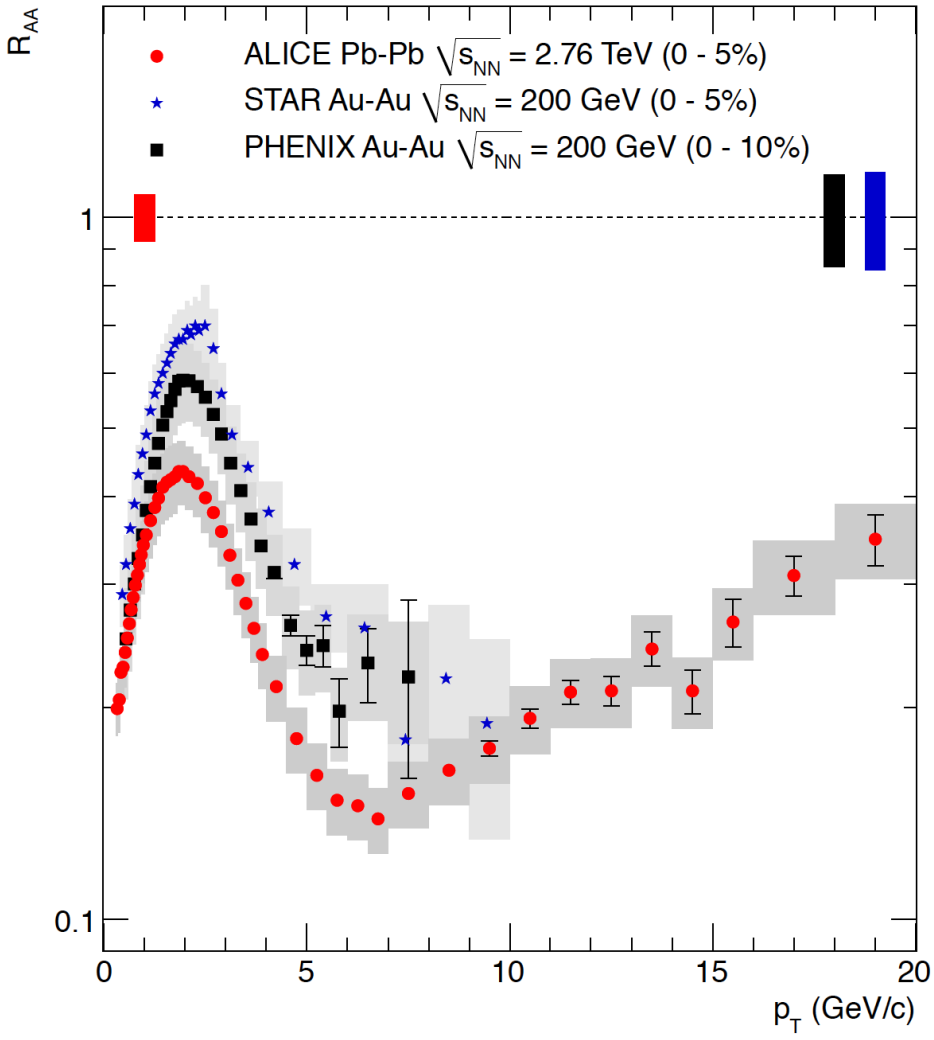

Figure 2.5: R_{AA} in central $(0-5\%)$ Pb-Pb collisions at $\sqrt{s_{\mathrm{NN}}} = 2.76$ TeV at ALICE, in central $(0-5\%)$ Au-Au collisions at $\sqrt{s_{\mathrm{NN}}} = 200$ GeV at STAR, and in central $(0-10\%)$ Au-Au collisions at $\sqrt{s_{\mathrm{NN}}} = 200$ GeV at PHENIX [11]

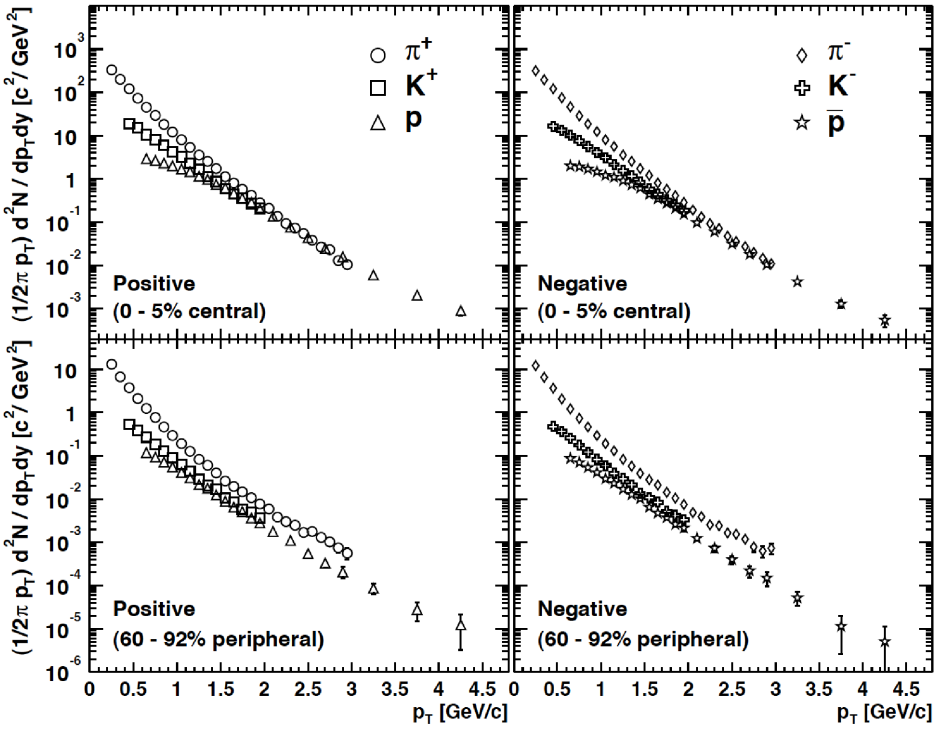

Figure 2.6: Transverse momentum distributions of different hadrons (pions, kaons, protons and antiprotons) in Au+Au collisions at $\sqrt{s_{\mathrm{NN}}} = 200$ GeV [12]

USC
UNIVERSIDADE
DE SANTIAGO
DE COMPOSTELA

Chapter 3

Medium-induced photon radiation

3.1 Medium-induced one-photon radiation

Because of the Abelian nature, photon interacts with a hot and dense QCD medium through electromagnetic interaction. The electromagnetic coupling is negligible as compared with the strong coupling. Therefore photon is an important probe for studying QCD matter formed after the relativistic heavy-ion collisions, and is classified into electroweak collision products, which can be used to characterize the bulk properties during the early collision stages.

3.1.1 The Gyulassy-Wang model

The Gyulassy-Wang model [13] is employed in this thesis to describe the scattering centers in a hot and dense QCD medium. The key feature of this model is that the scattering centers are assumed to be static. Therefore the collisional energy loss of a hard parton traversing the medium is zero and the total energy loss will be only due to the radiation. This model is applicable for hot nuclear matter with the temperature higher than the critical temperature. In hot nuclear matter a quark or a gluon polarizes the partons in its vicinity in order to screen its color charge. This is the so-called Debye screening. According to the Gyulassy-Wang model and the assumption that the static scattering centers are located at fixed longitudinal positions, the created color screened Coulomb potential in configuration space reduces to

$$\mathcal{V}_i^a = \frac{g\, t_i^a}{4\,\pi}\, \frac{e^{-m_D|\mathbf{x}-\mathbf{x}_i|}}{|\mathbf{x}-\mathbf{x}_i|}. \tag{3.1}$$

The Debye mass is defined in Eq.(3.1), which is the typical transverse momentum transfer from a single static scattering center to the hard parton. Debye mass is the minimum energy scale that the hard parton must have in order to be able to exchange a gluon with the scattering center. The effective range of the screened Coulomb potential is the inverse of the Debye mass. It is considered that the effective range of the screened Coulomb potential is much smaller than the mean free path of the hard parton, and therefore the successive scattering centers are independent and the hard parton propagation is path-ordered. In momentum space, the color screened Coulomb potential of the static scattering center at fixed longitudinal position reduces to

$$\mathcal{V}_i^a = \frac{g\, t_i^a}{|\mathbf{q}|^2 + m_D^2}\, e^{-i\,\mathbf{q}\cdot\mathbf{x}_i}. \tag{3.2}$$

$\mathbf{q}$ in Eq.(3.2) is the transverse momentum transfer from the medium to the hard parton, since in the high-energy limit the $+$ and $-$-components are negligible.

3.1.2 One-photon emission induced by a single scattering

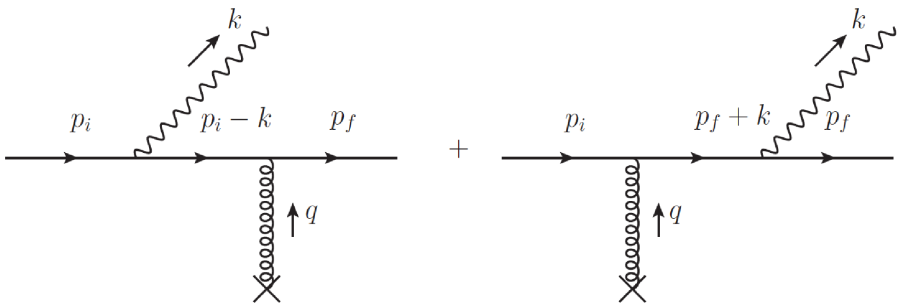

Figure 3.1: One-photon emission induced by a single scattering

The one-photon emission induced by a single scattering is depicted in figure 3.1. In order to deal with the pure perturbative process, hadronization is

considered to occur outside of the medium in this thesis. From now on, we fix the coupling constant. The initial and the final quarks and the emitted photon are all on-shell. Alternatively, one can consider the initial quark as a nascent quark produced during a hard collision inside the medium produced in relativistic heavy-ion collisions. The spin effect on the quark is neglected in the eikonal limit, which is that the quark energy is too high to be changed by the medium and the emitted particle is both soft and collinear. Therefore one can get the well-known eikonal vertex by using the Gordon identity. In the light-cone coordinate system, the light-cone gauge specifies $n = (0, 1, \mathbf{0})$, $n \cdot A^a = 0$, and $\epsilon = (0, \mathbf{k} \cdot \boldsymbol{\epsilon}/k^+, \boldsymbol{\epsilon})$. The amplitude of soft photon emission in figure 3.1 reads

$$i\,\mathcal{M}_{(1)} \approx 2\,Q\,e\left(\frac{p_i \cdot \epsilon^*}{p_i \cdot k} - \frac{p_f \cdot \epsilon^*}{p_f \cdot k}\right) i\,g\,p^+\,A_a^-\,t^a. \tag{3.3}$$

e in Eq.(3.3) is the electromagnetic coupling constant and the amount of the electric charge depends on the specific flavor of the quark, and A is a gauge field modeling the medium interaction. The longitudinal momentum fraction of the emitted photon relative to the parent quark is defined as the ratio of the $+$-component of the emitted photon to the one of the parent quark. In the high-energy limit and to the leading order of the longitudinal momentum fraction of the emitted photon, one has

$$\frac{p_i \cdot \epsilon^*}{p_i \cdot k} \approx \frac{p_f \cdot \epsilon^*}{p_f \cdot k} \approx 2\,\frac{\mathbf{k} \cdot \boldsymbol{\epsilon}}{\mathbf{k}^2}. \tag{3.4}$$

In order to get a nonvanishing contribution from Eq.(3.3), one has to keep all terms in the expansion of the scalar product of the 4-momenta and distinguish the transverse components of the final quark momentum from the initial ones by the transverse momentum transfer from the single scattering. In order to simplify the calculation without loss of generality, one can choose that the transverse momentum of the initial quark is zero. The high-energy limit of the Bethe-Heitler spectrum [14] can be readily obtained by squaring the amplitude discussed above, which reads

$$\frac{\mathrm{d}N^{\mathrm{BH}}}{\mathrm{d}^2\mathbf{q}\,\mathrm{d}^2\mathbf{k}\,\mathrm{d}\,(\ln x)} \propto \frac{\alpha_{em}\,C_F}{\pi^2}\,\frac{x^2\,\mathbf{q}^2}{\mathbf{k}^2\,(\mathbf{k} - x\,\mathbf{q})^2}, \tag{3.5}$$

where $\mathbf{q}$ is the transverse momentum transfer from the medium. Only quark interacts with the hot and dense QCD medium, but photon does not because of its Abelian nature. The scattering is most effective for soft particles, therefore the Bethe-Heitler spectrum peaks at $x = 1$.

3.1.3 Photon emission induced by multiple soft scatterings

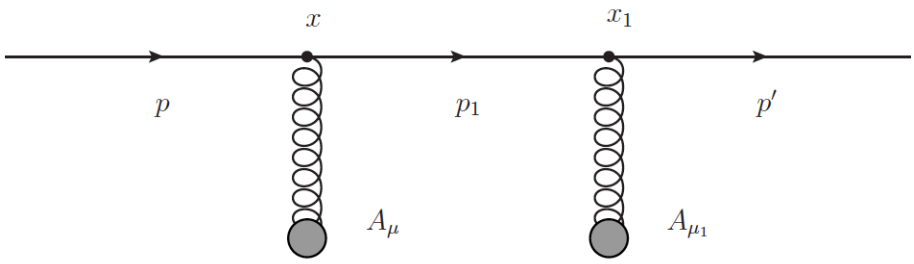

Figure 3.2: The trajectory of two scatterings centers

Next, we study the photon emission induced by multiple soft scatterings. Let us start from the case of two scattering centers. The contribution to the S-matrix of two scattering centers (see figure 3.2) is given by

$$\begin{aligned}\mathcal{M}_2 = \int \frac{\mathrm{d}^4 p_1}{(2\,\pi)^4}\,\mathrm{d}^4 x\,\mathrm{d}^4 x_1 e^{i(p_1-p)\cdot x} e^{i(p'-p_1)\cdot x_1} \\ \times\,\bar{u}^s\left(p'\right)\,i\,g\,\gamma^{\mu_1}\,A^{a_1}_{\mu_1}\left(x_1\right)\,t^{a_1}\,\frac{i\,\left(\not{p}_1+m\right)}{p_1^2-m^2+i\,\epsilon} \\ \times\,i\,g\,\gamma^{\mu}\,A^{a}_{\mu}\left(x\right)\,t^{a}\,u^s\left(p\right),\end{aligned} \tag{3.6}$$

where A is the same as in Eq.(3.3). In the eikonal approximation, the hard quark traverses the color deconfined medium with only its color rotated. One can neglect the dependence of the target fields on the $-$-component of the position of the scattering center, because the hard quark propagates in the $+z$ direction and thus only feels the target fields at the origin of the $-$-component of the position of the scattering center. With this, the integration on the x^- component of the position of the scattering center is trivial and gives the constraint on the $+$-component of the quark momentum. The integration on $-$-component of the quark momentum gives

$$\begin{aligned}&\int \mathrm{d}p_1^-\,\frac{1}{p_1^- - \frac{m^2}{2\,p^+}+i\,\epsilon}\,\exp\left[i\,p_1^-\left(x^+-x_1^+\right)\right] \\ &= -\,2\,\pi\,i\,\Theta\left(x_1^+-x^+\right)\,\exp\left[i\,\frac{m^2}{2\,p^+}\left(x^+-x_1^+\right)\right].\end{aligned} \tag{3.7}$$

The integration on the transverse momentum is trivial and gives the constraint on the transverse position. Hence the amplitude, i.e. Eq.(3.6), can be simplified in the eikonal approximation as

$$\mathcal{M}_2 \simeq 2\,\pi\,\delta\left(p'^{+}-p^{+}\right)\,2\,p^{+}\,e^{i\,\frac{m^2}{2\,p^{+}}\left(x^{+}-x_1^{+}\right)}\int \mathrm{d}^2\mathbf{x}\,e^{-i\,\mathbf{x}\cdot\left(\mathbf{p}'-\mathbf{p}\right)} \times \frac{1}{2}\,\mathcal{P}\left[i\,g\int \mathrm{d}\xi\,A_a^{-}\left(\xi,\mathbf{x}\right)\,t^a\right]^2 . \tag{3.8}$$

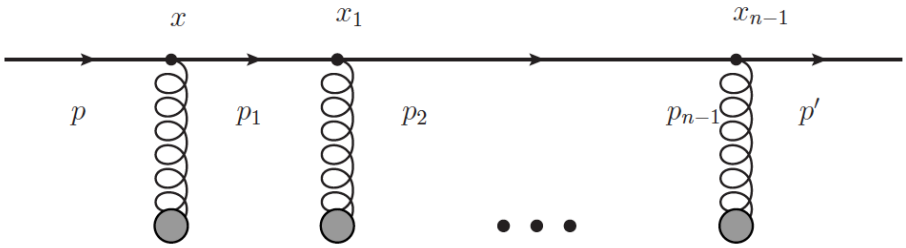

Figure 3.3: The trajectory of multiple soft scatterings

The generalization to the contribution of n-fold scattering centers (see figure 3.3) in the eikonal approximation reads

$$\mathcal{M}_n \simeq 2\,\pi\,\delta\left(p'^{+}-p^{+}\right)\,2\,p^{+}\,e^{i\,\frac{m^2}{2\,p^{+}}\left(x^{+}-x_f^{+}\right)}\int \mathrm{d}^2\mathbf{x}\,e^{-i\,\mathbf{x}\cdot\left(\mathbf{p}'-\mathbf{p}\right)} \times \frac{1}{n!}\,\mathcal{P}\left[i\,g\int \mathrm{d}\xi\,A_a^{-}\left(\xi,\mathbf{x}\right)\,t^a\right]^n . \tag{3.9}$$

After performing the resummation of n-fold scattering centers in Eq.(3.9), one gets

$$\mathcal{M} \simeq 2\,\pi\,\delta\left(p'^{+}-p^{+}\right)\,2\,p^{+}\,e^{i\,\frac{m^2}{2\,p^{+}}\left(x^{+}-x_f^{+}\right)}\int \mathrm{d}^2\mathbf{x}\,e^{-i\,\mathbf{x}\cdot\left(\mathbf{p}'-\mathbf{p}\right)}\,U\left(\mathbf{x}\right). \tag{3.10}$$

The Dirac delta function in Eq.(3.10) indicates that the quark energy is too high to be changed by the medium. The Wilson line in Eq.(3.10) is defined to describe the eikonal phase acquired by the hard quark when it goes through the medium, which reads

$$U\left(\left[\mathbf{r}\left(\xi\right)\right];x^{+},x_0^{+}\right)=\mathcal{P}\,\exp\left[i\,g\int_{x_0^{+}}^{x^{+}}\mathrm{d}\xi\,A_a^{-}\left(\xi,\left[\mathbf{r}\left(\xi\right)\right]\right)\,t^a\right]. \tag{3.11}$$

$\mathcal{P}$ in Eq.(3.11) denotes the path ordering of the color fields.
In some applications, as e.g. the photon emission the eikonal approximation needs to be relaxed. If one keeps the terms in the norm to the leading order of the inverse of the $+$-component of the quark momentum, and keeps the terms in the phase to the next-to-leading order of the inverse of the $+$-component of the quark momentum, the integration on $-$-component of the quark momentum (see Eq.(3.7)) is slightly modified as

$$\begin{aligned}&\int \mathrm{d}p_1^- \, \frac{1}{p_1^- - \frac{\mathbf{p}_1^2+m^2}{2\,p^+} + i\,\epsilon} \, \exp\left[i\,p_1^-\,\left(x^+ - x_1^+\right)\right] \\ =& -2\,\pi\,i\,\Theta\left(x_1^+ - x^+\right)\,\exp\left[i\,\frac{\mathbf{p}_1^2+m^2}{2\,p^+}\left(x^+ - x_1^+\right)\right].\end{aligned} \tag{3.12}$$

In the massless case, the integration on the transverse momentum gives the Feynman propagator

$$G_0\left(\mathbf{r}(x_1^+), x_1^+; \mathbf{r}(x^+), x^+ | p^+\right) = \int \mathcal{D}\mathbf{r}\left(\xi\right) \exp\left[\frac{i\,p^+}{2}\int_{x^+}^{x_1^+} \mathrm{d}\xi\,\dot{\mathbf{r}}^2\left(\xi\right)\right], \tag{3.13}$$

which describes the Brownian motion of the free particle in the transverse plane. Then one can get the Green function with the higher order correction to the phase of the eikonal Wilson line included:

$$\begin{aligned}&G\left(\mathbf{r}(x^+), x^+; \mathbf{r}(x_0^+), x_0^+ | p^+\right) \\ =& \int \mathcal{D}\mathbf{r}\left(\xi\right) \exp\left[\frac{i\,p^+}{2}\int_{x_0^+}^{x^+} \mathrm{d}\xi\,\dot{\mathbf{r}}^2\left(\xi\right)\right] U\left(\left[\mathbf{r}\left(\xi\right)\right]; x^+, x_0^+\right).\end{aligned} \tag{3.14}$$

3.1.4 Medium average

Due to the locality, the two point function can be written as [15]

$$\begin{aligned}&\frac{1}{N_c}\left\langle \mathbf{tr}\, U\left(x^+, y^+; \mathbf{r}\left(\xi\right)\right)\, U^\dagger\left(x^+, y^+; \mathbf{z}\right)\right\rangle \\ =& \exp\left[-\frac{1}{2}\int_{y^+}^{x^+} \mathrm{d}\xi\, n\left(\xi\right)\,\sigma\left(\mathbf{r}-\mathbf{z}\right)\right],\end{aligned} \tag{3.15}$$

where $n\left(\xi\right)$ is the one-dimensional medium density. The dipole cross section in Eq.(3.15) is defined as

$$\sigma\left(\mathbf{r}-\mathbf{z}\right)=2\int\frac{\mathrm{d}^{2}\mathbf{q}}{\left(2\,\pi\right)^{2}}\left|a_{a}^{-}\left(\mathbf{q}\right)\right|^{2}\left[1-e^{i(\mathbf{r}-\mathbf{z})\cdot\mathbf{q}}\right], \tag{3.16}$$

where $C_F=\left(N_c^2-1\right)/\left(2\,N_c\right)$ is the Casimir operator in the fundamental representation, and $a\left(q\right)$ is the Fourier transform of the gauge field $A\left(x\right)$. The elastic high-energy cross section for a single scattering in Eq.(3.16) is usually taken as that of a color screened Coulomb potential

$$\left|a_{a}^{-}\left(\mathbf{q}\right)\right|^{2}=\left(2\,\pi\right)^{2}g^{2}\,C_{F}\,\frac{m_{D}^{2}}{\pi\left(\mathbf{q}^{2}+m_{D}^{2}\right)^{2}}, \tag{3.17}$$

where m_D, the Debye mass, corresponds to the typical momentum exchanged in a scattering. Fixing $|\mathbf{z}|=0$ for simplicity, the leading quadratic dependence of the dipole cross section (see Eq.(3.16)) for $m_D\,|\mathbf{r}|\ll 1$ is

$$\sigma\left(\mathbf{r}\right)\approx C\,\mathbf{r}^{2}, \tag{3.18}$$

with

$$C=4\,\pi\,\alpha_{s}\,C_{F}\,m_{D}^{2}\left(\frac{1}{2}-\gamma+\log\frac{2}{m_{D}\,|\mathbf{r}|}\right). \tag{3.19}$$

In Eq.(3.19) the logarithm can be treated as a constant for small value of transverse size, and hence C is a constant, which denotes the probability of a scattering center in the medium interacting with the hard quark. In this approximation the two point function for the leading quadratic dependence reads

$$\begin{aligned}&\frac{1}{N_{c}}\left\langle\mathbf{tr}\,U^{\dagger}\left(x^{+},y^{+};\mathbf{z}\right)\,U\left(x^{+},y^{+};\mathbf{z}'\right)\right\rangle\\&=\exp\left[-\frac{1}{4}\int_{y^{+}}^{x^{+}}\mathrm{d}\xi\,\hat{q}\left(\xi\right)\,\left(\mathbf{z}-\mathbf{z}'\right)^{2}\right].\end{aligned} \tag{3.20}$$

The transport coefficient in Eq.(3.20) is defined as

$$n\left(\xi\right)\,\sigma\left(\mathbf{r}\right)\simeq\frac{1}{2}\,\hat{q}\left(\xi\right)\,\mathbf{r}^{2}, \tag{3.21}$$

where $\mathbf{r} = \mathbf{z} - \mathbf{z}'$ is defined as the transverse distance. The transport coefficient encodes all the information about the medium properties, and characterizes the average transverse momentum transfer from the medium to the hard quark per mean free path:

$$\hat{q}\left(\xi\right) \simeq \frac{\left\langle \mathbf{q}^2 \right\rangle}{\lambda} = n\left(\xi\right) \int \frac{\mathrm{d}^2\mathbf{q}}{\left(2\,\pi\right)^2}\, \mathbf{q}^2\, \left|a_a^-\left(\mathbf{q}\right)\right|^2, \tag{3.22}$$

where λ is the mean free path. A initial condition for the transport coefficient can be related to the saturation scale, i.e.

$$\hat{q}\left(\xi = 0\right) \sim \hat{q}_{cold} \sim Q_s^2/L^+. \tag{3.23}$$

Therefore the two point function can be written as

$$\frac{1}{N_c} \left\langle \mathbf{tr}\, U^\dagger\left(L^+, 0; \mathbf{z}\right) U\left(L^+, 0; \mathbf{z}'\right) \right\rangle = \exp\left[-\frac{1}{4}\, Q_s^2\, \left(\mathbf{z} - \mathbf{z}'\right)^2 \right], \tag{3.24}$$

where the square of the saturation scale reads

$$Q_s^2 = \int_0^{L^+} \mathrm{d}\xi\, n\left(\xi\right) \int \frac{\mathrm{d}^2\mathbf{q}}{\left(2\,\pi\right)^2}\, \mathbf{q}^2\, \left|a_a^-\left(\mathbf{q}\right)\right|^2. \tag{3.25}$$

Once the medium average of a dipole is known, the medium average of two Green functions in the fundamental representation can be easily calculated to be [16]

$$\begin{aligned}
&\int \mathrm{d}^2\mathbf{r}\left(x^+\right)\, \mathrm{d}^2\bar{\mathbf{r}}\left(x^+\right)\, \exp\left\{ -i\,\mathbf{k}\cdot\left[\mathbf{r}\left(x^+\right) - \bar{\mathbf{r}}\left(x^+\right)\right]\right\} \\
&\quad \times \frac{1}{N_c} \left\langle \mathbf{tr}\, G^\dagger\left(\bar{\mathbf{r}}(x^+), x^+; \bar{\mathbf{r}}(x_0^+), x_0^+ | p^+\right)\, G\left(\mathbf{r}(x^+), x^+; \mathbf{r}(x_0^+), x_0^+ | p^+\right) \right\rangle \\
&= \exp\left\{ -i\,\mathbf{k}\cdot\left[\mathbf{r}\left(x_0^+\right) - \bar{\mathbf{r}}\left(x_0^+\right)\right]\right\} \\
&\quad \times \exp\left\{ -\frac{1}{2} \int_{x_0^+}^{x^+} \mathrm{d}\xi\, n\left(\xi\right)\, \sigma\left[\mathbf{r}\left(x_0^+\right) - \bar{\mathbf{r}}\left(x_0^+\right)\right] \right\}.
\end{aligned} \tag{3.26}$$

Also needed in the applications of this thesis, the medium average of one Wilson line and one Green function in the fundamental representation reads [15]

$$\begin{aligned}
&\frac{1}{N_c}\left\langle \mathbf{tr}\, G^{\dagger}\left(\bar{\mathbf{r}}(x^+),x^+;\bar{\mathbf{r}}(x_0^+),x_0^+|p^+\right)\, U\left(x^+,x_0^+;\mathbf{r}\left(\xi\right)\right)\right\rangle \\
&=\int \mathcal{D}\bar{\mathbf{r}}\,\exp\left\{\frac{i\,p^+}{2}\int_{x_0^+}^{x^+}\mathrm{d}\xi\,\dot{\bar{\mathbf{r}}}^2\left(\xi\right)-\frac{1}{2}\int_{x_0^+}^{x^+}\mathrm{d}\xi\,n\left(\xi\right)\,\sigma\left[\bar{\mathbf{r}}\left(\xi\right)-\mathbf{r}\left(\xi\right)\right]\right\} \\
&\equiv\mathcal{K}\left(\bar{\mathbf{r}}(x^+),x^+;\bar{\mathbf{r}}(x_0^+),x_0^+|p^+\right).
\end{aligned} \tag{3.27}$$

3.1.5 The Landau-Pomeranchuk-Migdal effect

At this moment I would like to emphasize an important longitudinal interference effect. Let us first analyze two limits. In the Bethe-Heitler limit, the separation between scattering centers is large enough such that the radiation spectrum is the sum of N Bethe-Heitler spectra, given by

$$\sum_i \frac{\mathrm{d}N^{\mathrm{BH}}}{\mathrm{d}^2\mathbf{q}_i\,\mathrm{d}^2\mathbf{k}\,\mathrm{d}\left(\ln x\right)}\propto\frac{\alpha_{em}\,C_F}{\pi^2}\sum_i\frac{x^2\,\mathbf{q}_i^2}{\mathbf{k}^2\left(\mathbf{k}-x\,\mathbf{q}_i\right)^2}, \tag{3.28}$$

where $\alpha_{em}=e^2/\left(4\,\pi\right)$, the longitudinal momentum fraction x is given by the ratio of the $+$-component of the emitted photon to the one of the parent quark, $\mathbf{k}$ is the transverse momentum of the emitted photon, and $\mathbf{q}_i$ is the transverse momentum transfer from the ith scattering center. In the factorization limit, the fixed N scattering centers are not resolvable by the emitted photon. Therefore the spectrum is given by

$$\frac{\mathrm{d}N^{\mathrm{fac}}}{\mathrm{d}^2\left(\sum_i\mathbf{q}_i\right)\,\mathrm{d}^2\mathbf{k}\,\mathrm{d}\left(\ln x\right)}\propto\frac{\alpha_{em}\,C_F}{\pi^2}\,\frac{x^2\left(\sum_i\mathbf{q}_i\right)^2}{\mathbf{k}^2\left(\mathbf{k}-x\sum_i\mathbf{q}_i\right)^2}. \tag{3.29}$$

The formation length (time) scale is in between the above two limits, which characterizes the Landau-Pomeranchuk-Migdal (LPM) interference effect. The virtual photon can not resolve the scattering centers within its formation length. Scattering amplitudes for the photon radiation off the scattering centers within the photon formation length interfere destructively. The softer photons suffer more the LPM suppression. In QCD, gluon can scatter directly off the scattering centers because of its non-Abelian nature. The relative phases of different contributions to the scattering amplitude determine quantitatively the LPM interference effect. The softer gluons suffer less the LPM suppression.

3.2 Medium-induced two-photon ladder emission

Now we investigate the medium modifications on more exclusive observables, i.e. medium-induced two-photon radiation. In QED, as is well-known, the lack of ordering of the radiation can be traced back to the fact that the photon does not carry color charge. But how is the LPM suppression effect for medium-induced multi-photon radiation? Does this effect still hold for more exclusive observables? As one of the attempts to improve our knowledge about the QCD branching in a color deconfined medium, in the following we study the medium-induced two-photon radiation.

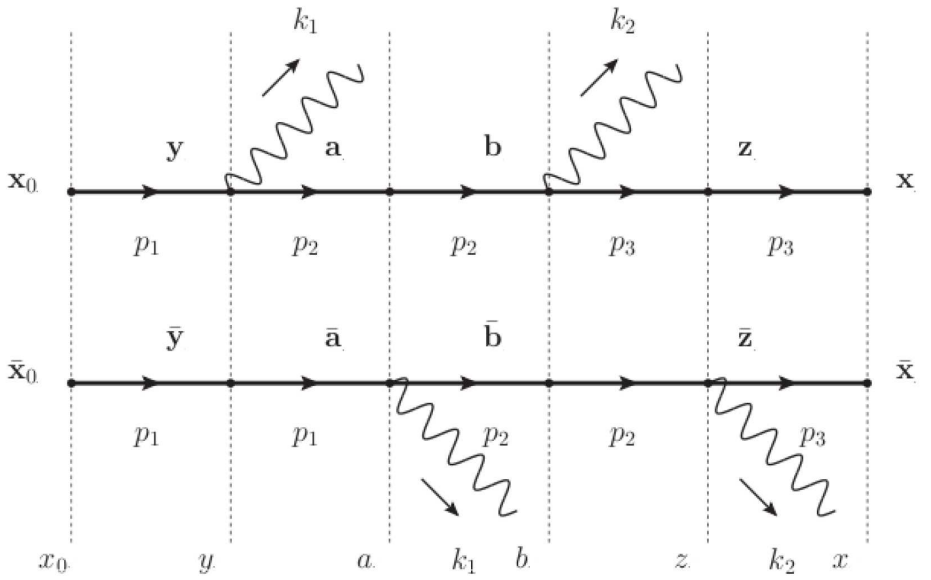

Figure 3.4: Medium-induced two-photon ladder emission (Here $p_1^+ = p^+$, $p_2^+ = (1-x)\,p^+$, $p_3^+ = (1-y)\,(1-x)\,p^+$, $k_1^+ = x\,p^+$ and $k_2^+ = y\,(1-x)\,p^+$. The boldface letters represent the positions of the projectile in the two dimensional transverse plane. The overline is used here to denote the quantities in the complex conjugate.)

The identical extension of the medium-induced one-photon radiation to the medium-induced two-photon radiation in both the amplitude and the complex conjugate amplitude is denoted as a ladder emission (see figure 3.4). The medium-induced two-photon ladder emission spectrum is calculated in [1]. More specifically, first a photon is radiated with transverse momentum $\mathbf{k}_1$ and carrying a momentum fraction x of the parent quark, and subsequently another photon with transverse momentum $\mathbf{k}_2$ and carrying a mo-

mentum fraction y of the quark. Of course, one can have other cases such as exchanging the positions of $\mathbf{k}_1$ and $\mathbf{k}_2$ in the complex conjugate only, or exchanging the positions of $\mathbf{k}_1$ and $\mathbf{k}_2$ in the amplitude only, etc. It might be a solution that one studies the spectrum in a mixture of coordinate and momentum spaces. Back to the two-photon ladder emission, in this case the spectrum is relatively neat:

$$\begin{aligned}
&\frac{\mathrm{d}N^{\mathrm{lad}}}{\mathrm{d}^2\mathbf{p}_f\,\mathrm{d}^2\mathbf{k}_1\,\mathrm{d}^2\mathbf{k}_2\,\mathrm{d}\left(\ln x\right)\,\mathrm{d}\left(\ln y\right)}=\frac{\alpha_{em}^2}{\left(2\,\pi\right)^6}\,\mathrm{Re}\,\frac{2}{x\,y\,\left(1-x\right)^2\,p^{+4}}\\
&\times\int_{x_0^+}^{b^+}\mathrm{d}y^+\int_{y^+}^{b^+}\mathrm{d}a^+\int_{y^+}^{x^+}\mathrm{d}b^+\int_{b^+}^{x^+}\mathrm{d}z^+\int\mathrm{d}^2\boldsymbol{\rho}_1\,\mathrm{d}^2\boldsymbol{\rho}_2\,\mathrm{d}^2\boldsymbol{\rho}_4\\
&\times\exp\left[-\int_{x_0^+}^{y^+}\mathrm{d}\xi_1\,\Sigma\left(\xi_1,x\,\boldsymbol{\rho}_1\right)\right]\exp\left[-\int_{a^+}^{b^+}\mathrm{d}\xi_3\,\Sigma\left(\xi_3,x\,\boldsymbol{\rho}_2\right)\right]\\
&\times\exp\left[-\int_{z^+}^{x^+}\mathrm{d}\xi_5\,\Sigma\left(\xi_5,y\,\boldsymbol{\rho}_4\right)\right]\exp\left[-i\,x\left(\frac{\mathbf{k}_1}{x}+\frac{\mathbf{k}_2}{y}\right)\cdot\boldsymbol{\rho}_1\right]\\
&\times\exp\left[-i\,y\left(\mathbf{p}_f-\frac{1-x}{x}\,\mathbf{k}_1-\frac{1-y}{y}\,\mathbf{k}_2\right)\cdot\boldsymbol{\rho}_4\right]\\
&\times\exp\left[i\left(\bar{q}_1-\frac{\mathbf{k}_1\cdot\mathbf{k}_2}{y\left(1-x\right)p^+}\right)\left(y^+-a^+\right)\right]\\
&\times\exp\left[i\left(\bar{q}_2-\frac{\mathbf{k}_1\cdot\mathbf{k}_2}{x\,p^+}\right)\left(b^+-z^+\right)\right]\\
&\times\left(\partial_1-\frac{i\,x}{y}\,\mathbf{k}_2\right)\cdot\left(\partial_2+\frac{i\,x}{y}\,\mathbf{k}_2\right)\mathcal{K}\left(\boldsymbol{\rho}_2,a^+;\boldsymbol{\rho}_1,y^+|\mu_1\right)\\
&\times\left(\partial_2-i\left(1-x\right)\mathbf{k}_1\right)\cdot\left(\partial_4+\frac{i\left(1-x\right)y}{x}\,\mathbf{k}_1\right)\mathcal{K}\left(\boldsymbol{\rho}_4,z^+;\frac{x}{y}\,\boldsymbol{\rho}_2,b^+\middle|\mu_3\right).
\end{aligned}\tag{3.30}$$

$\boldsymbol{\rho}_1=\mathbf{y}-\bar{\mathbf{y}}$, $\boldsymbol{\rho}_2=\mathbf{a}-\bar{\mathbf{a}}=\mathbf{b}-\bar{\mathbf{b}}$, and $\boldsymbol{\rho}_4=\mathbf{z}-\bar{\mathbf{z}}$ are the dipole sizes at different longitudinal positions. The shorthand notations $\partial_1=\partial/\partial\boldsymbol{\rho}_1$, $\partial_2=\partial/\partial\boldsymbol{\rho}_2$, and $\partial_4=\partial/\partial\boldsymbol{\rho}_4$ are introduced. $\Sigma\left(\xi_1,x\,\boldsymbol{\rho}_1\right)=n\left(\xi_1\right)\,\sigma\left(x\,\boldsymbol{\rho}_1\right)/2$ is defined as the product of the density of scattering centers in the medium $n\left(\xi_1\right)$ and the elastic Mott cross section $\sigma\left(x\,\boldsymbol{\rho}_1\right)$, and analogously for $\Sigma\left(\xi_3,x\,\boldsymbol{\rho}_2\right)=n\left(\xi_3\right)\,\sigma\left(x\,\boldsymbol{\rho}_2\right)/2$ and $\Sigma\left(\xi_5,y\,\boldsymbol{\rho}_4\right)=n\left(\xi_5\right)\,\sigma\left(y\,\boldsymbol{\rho}_4\right)/2$. The shorthand notations $\bar{q}_1=x\,m^2/\left(2\left(1-x\right)p^+\right)$ and $\bar{q}_2=y\,m^2/\left(2\left(1-y\right)\left(1-x\right)p^+\right)$ are the reciprocals of the photon formation lengths. m is the rest mass of the quark. Also the shorthand notations $\mu_1=\left(1-x\right)x\,p^+$ and $\mu_3=\left(1-y\right)y\left(1-x\right)p^+$ are introduced. The path integral in Eq.(3.30) is given by

$$\begin{aligned}
&\mathcal{K}\left(\boldsymbol{\rho}_2, a^+; \boldsymbol{\rho}_1, y^+|\mu_1\right) \\
&= \int \mathcal{D}\mathbf{r}\, \exp\left[\frac{i\,\mu_1}{2}\int_{y^+}^{a^+} \mathrm{d}\xi_2\, \dot{\mathbf{r}}^2\left(\xi_2\right) - \frac{1}{2}\int_{y^+}^{a^+} \mathrm{d}\xi_2\, n\left(\xi_2\right)\, \sigma\left(x\,\mathbf{r}\right)\right],
\end{aligned} \tag{3.31}$$

where $\mathbf{r}\left(y^+\right) = \boldsymbol{\rho}_1$ and $\mathbf{r}\left(a^+\right) = \boldsymbol{\rho}_2$ are boundary conditions. The path integral (see Eq.(3.31)) can be written as a harmonic oscillator for the leading quadratic dependence:

$$\begin{aligned}
&\mathcal{K}_{\mathrm{osc}}\left(\boldsymbol{\rho}_2, a^+; \boldsymbol{\rho}_1, y^+|\mu_1\right) = \frac{\mu_1\,\Omega_1}{2\,\pi\,i\,\sin\left(\Omega_1\,\left(a^+ - y^+\right)\right)} \\
&\times \exp\left\{\frac{i\,\mu_1\,\Omega_1\,\left[\left(\boldsymbol{\rho}_2^2 + \boldsymbol{\rho}_1^2\right)\,\cos\left(\Omega_1\,\left(a^+ - y^+\right)\right) - 2\,\boldsymbol{\rho}_2\cdot\boldsymbol{\rho}_1\right]}{2\,\sin\left(\Omega_1\,\left(a^+ - y^+\right)\right)}\right\},
\end{aligned} \tag{3.32}$$

where the harmonic oscillator frequency is defined as

$$\Omega_1 = \frac{1-i}{\sqrt{2}}\sqrt{\frac{n_0\,C\,x^2}{\mu_1}}, \tag{3.33}$$

and n_0 is a constant for denoting the medium density.
The coherence nature of the photon spectrum becomes most pronounced in the Molière limit written in the light-cone coordinate system:

$$\begin{aligned}
&|\mathbf{q}| \ll |\mathbf{k}| \ll k^+ \ll p^+, \\
&\frac{\mathbf{k}^2}{2\,k^+}\,L^+ \gg 1, \\
&\frac{x\,m^2}{2\,(1-x)\,p^+}\,L^+ \gg 1, \\
&\left|\Omega\,L^+\right| \ll 1.
\end{aligned} \tag{3.34}$$

$|\mathbf{q}| \ll |\mathbf{k}|$ in the first condition in Eq.(3.34) indicates that the transverse momentum transfer from the medium to the quark should be much smaller than the transverse momentum freed from the quark. $|\mathbf{k}| \ll k^+ \ll p^+$ in the first condition in Eq.(3.34) is the eikonal approximation. The second and the third conditions in Eq.(3.34) require that the medium size must be larger than at least one formation length of the photon. The last condition in Eq.(3.34) requires a sufficiently low density medium. With the help of the Molière limit introduced in Eq.(3.34), one can perform all the integrations in Eq.(3.30) analytically, and then the spectrum becomes

$$\frac{\mathrm{d}N^{\mathrm{Mol}}}{\mathrm{d}^2\mathbf{p}_f\,\mathrm{d}^2\mathbf{k}_1\,\mathrm{d}^2\mathbf{k}_2\,\mathrm{d}\,(\ln x)\;\mathrm{d}\,(\ln y)} \propto \exp\left[-\frac{(\mathbf{k}_1+\mathbf{k}_2+\mathbf{p}_f)^2}{2\,n_0\,C\,L^+}\right], \qquad (3.35)$$

where $|\mathbf{k}_1+\mathbf{k}_2+\mathbf{p}_f| = \sum_i \mathbf{q}_i$ is the total transverse momentum transfer from the medium. The appearance of the Molière factor in Eq.(3.35) signals that the LPM effect still holds for the medium induced two-photon ladder emission. In particular, Eq.(3.35) is not simply a superposition of two one-photon radiation spectra as one naively would have expected from independent radiation, e.g. in vacuum. Thus the medium induces some coherence on the multi-photon radiation spectrum.

USC UNIVERSIDADE DE SANTIAGO DE COMPOSTELA

USC
UNIVERSIDADE
DE SANTIAGO
DE COMPOSTELA

Chapter 4

Medium-induced gluon radiation

4.1 Single-emitter set-up

Although the electroweak collision products are important probes for studying QCD matter, their production is scarce and one has to filter them out of those produced in hadron decay and in the final state interactions. Gluon is also an interesting and important probe for the investigation of the color deconfined medium in both the initial and the final state interactions.

4.1.1 One-gluon emission induced by a single scattering

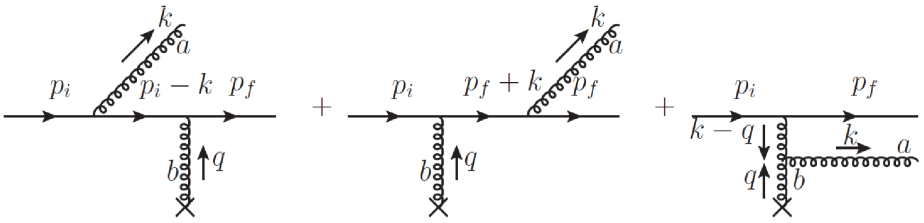

Figure 4.1: One-gluon emission induced by a single scattering

Following the same approach as in the last chapter, here we first discuss the one-gluon emission induced by a single scattering as shown in figure 4.1. The longitudinal momentum transfer from the medium is negligible in the high-energy limit. The initial and the final quarks and the emitted gluon are all on-shell. The gluon propagator here has the support only from the transverse components in the high-energy limit. Also in the high-energy

limit, the spin effect on the quark is neglected. To the leading order of the longitudinal momentum fraction, the amplitude for soft gluon emission in figure 4.1 reads

$$i\,\mathcal{M}_{(1)} \approx -4\,i\,g^2\left[\frac{\mathbf{k}}{\mathbf{k}^2}-\frac{\mathbf{k}-\mathbf{q}}{(\mathbf{k}-\mathbf{q})^2}\right]\cdot\boldsymbol{\epsilon}^*[t^a,t^b]\,p^+\,A_b^-. \tag{4.1}$$

Note that for the gluon emission, one only needs to keep the leading order of the longitudinal momentum fraction term because of the non-Abelian nature. One can get the high-energy limit of the Gunion-Bertsch spectrum from the amplitude discussed above, which is

$$\frac{\mathrm{d}N^{\mathrm{GB}}}{\mathrm{d}^2\mathbf{q}\,\mathrm{d}^2\mathbf{k}\,\mathrm{d}\,(\ln x)}\propto\frac{\alpha_s\,C_A}{\pi^2}\frac{\mathbf{q}^2}{\mathbf{k}^2\,(\mathbf{k}-\mathbf{q})^2}. \tag{4.2}$$

Both quark and gluon interact with the hot and dense QCD medium, therefore the Gunion-Bertsch spectrum is flat in the gluon energy.

4.1.2 Parton radiative energy loss

The parton average radiative energy loss reads

$$\langle\Delta E\rangle=\int_0^E\mathrm{d}\omega\int_0^\omega\mathrm{d}^2\mathbf{k}\,\omega\,\frac{\mathrm{d}^3N}{\mathrm{d}\omega\,\mathrm{d}^2\mathbf{k}}. \tag{4.3}$$

One can easily get the numerical results of the radiative energy loss by plugging Eq.(4.53) in the above one, and performing the numerical calculations by using either Fortran or C++. Analytically, on the other hand, the Baier-Dokshitzer-Mueller-Peigné-Schiff (BDMPS) parton energy loss for an infinite size medium reads [19]

$$-\frac{\mathrm{d}E}{\mathrm{d}z}\simeq\alpha_s\sqrt{\frac{m_D^2\,E}{\lambda}}. \tag{4.4}$$

For a medium with a finite size L, Eq.(4.4) gives

$$L\propto\sqrt{\frac{\lambda\,E}{m_D^2}}, \tag{4.5}$$

where the non-intuitive prediction of the L^2 dependence of the radiative energy loss is a consequence of the destructive interference effects, i.e. the LPM effect. The transverse momentum broadening can be obtained from Eq.(4.5):

$$\left\langle \mathbf{k}^2 \right\rangle \simeq \hat{q}\, L \propto \frac{\langle \Delta E \rangle}{L}. \tag{4.6}$$

4.2 Double-emitter set-up

One important ingredient is missing in the single-emitter set-up, i.e. the interference effects between different emitters. Therefore, one has to introduce at least two emitters in order to study the interference effect between them. Feynman diagrams are powerful tools in performing the perturbative QCD calculations. Alternatively, one can use the classical gauge field approximation to deal with soft particle production in relativistic heavy-ion collisions.

4.2.1 Validity of the classical gauge field approximation

The Feynman diagram language is not the only option for studying the QCD in the high parton density limit. The classical gauge field approximation is valid in this limit because of the large gluon occupation number, i.e. $N_k \sim 1/\alpha_s \gg 1$, and then the Heisenberg commutators between particle creation and annihilation operators are negligible:

$$\left[a_k, a_k^\dagger\right] = 1 \ll a_k^\dagger\, a_k = N_k, \tag{4.7}$$

which signals the validity of the use of the classical gauge field approximation for studying the QCD in the high parton density limit.

4.2.2 s-channel antenna radiation in vacuum

To fix the notation and as a warm-up, we study the well known case of the antenna radiation in vacuum. In the classical gauge field approximation, the single-gluon inclusive radiation spectrum with the gluon 4-momentum $k = (\omega, \vec{k})$ is given by

$$(2\,\pi)^3\; 2\,\omega\, \frac{\mathrm{d}N}{\mathrm{d}^3\vec{k}} = \left|\mathcal{M}_\lambda\right|^2, \tag{4.8}$$

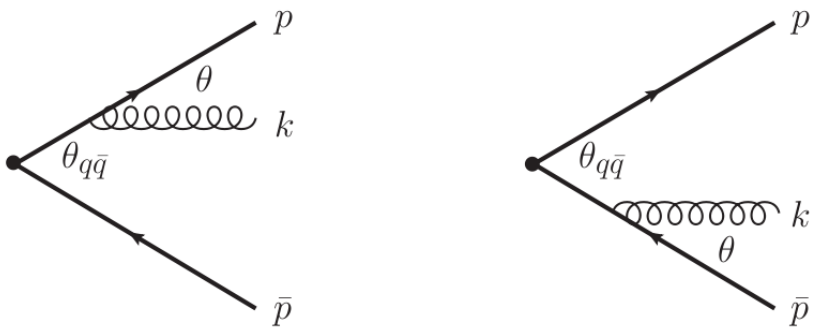

Figure 4.2: Soft gluon radiation off a quark-antiquark antenna in vacuum [17]

where the gluon 3-momentum is $\vec{k} = (\mathbf{k}, k_z)$ and the transverse polarizations of the emitted gluon are the only physical polarization states. The scattering amplitude is related to the classical gauge field by the reduction formula:

$$\mathcal{M}^a_\lambda(\vec{k}) = \lim_{k^2 \to 0} -k^2 \, A^a(k) \cdot \epsilon^*_\lambda. \tag{4.9}$$

The gauge field is the solution of the classical Yang-Mills equations,

$$[D_\mu, F^{\mu\nu}] = J^\nu, \tag{4.10}$$

where the covariant derivative is defined in Eq.(2.3), and the non-Abelian field strength tensor is defined in Eq.(2.2).
A virtual time-like photon or gluon splits into a quark-antiquark antenna with 4-momenta $p = (E, \vec{p})$ and $\bar{p} = (\bar{E}, \vec{\bar{p}})$ for the quark and antiquark, respectively (see figure 4.2). The current is covariantly conserved. The light-cone gauge specifies $n \cdot A^a = 0$ with a specific axial vector $n = (0, 1, \mathbf{0})$. The gauge condition $n \cdot \epsilon = 0$ and the transversality $k \cdot \epsilon = 0$ fix the light-cone decomposition of the polarization vector $\epsilon = (0, \mathbf{k} \cdot \boldsymbol{\epsilon}/k^+, \boldsymbol{\epsilon})$. In vacuum, the classical current that describes the quark-antiquark antenna created at initial time $t_0 = 0$ reads

$$J_{(0)} = J_{q,(0)} + J_{\bar{q},(0)} + J_3, \tag{4.11}$$

where the subscript (0) denotes vacuum quantities, and the third component J_3 is required for 4-current conservation. The currents for the quark and the antiquark, are given by

$$\begin{aligned} J^{\mu,a}_{q,(0)} &= g\,\frac{p^\mu}{E}\,\delta^{(3)}\left(\vec{x}-\frac{\vec{p}}{E}\,t\right)\,\Theta\,(t)\;Q^a_q, \\ J^{\mu,a}_{\bar{q},(0)} &= g\,\frac{\bar{p}^\mu}{\bar{E}}\,\delta^{(3)}\left(\vec{x}-\frac{\vec{\bar{p}}}{\bar{E}}\,t\right)\,\Theta\,(t)\;Q^a_{\bar{q}}, \end{aligned} \tag{4.12}$$

where Q^a_q and $Q^a_{\bar{q}}$ are the color charge of the quark and the antiquark, respectively, and one has analogously Q^a_3 for the third component of the current. In momentum space the total current reads

$$J^\mu_{(0),a} = i\,g\left(\frac{p^\mu}{p\cdot k}\,Q^a_q + \frac{\bar{p}^\mu}{\bar{p}\cdot k}\,Q^a_{\bar{q}} - \frac{p^\mu_3}{p_3\cdot k}\,Q^a_3\right). \tag{4.13}$$

One can prove the color charge conservation $Q^a_q + Q^a_{\bar{q}} = Q^a_3$ by using the current conservation. Then for a color singlet antenna one has $Q^a_3 = 0$, and for a color octet antenna the third component of the current does not contribute in the frame where $p_3 \approx \left(0, p_3^-, \mathbf{0}\right)$ because of the choice of the gauge. Therefore, one has $\left(Q^a_q + Q^a_{\bar{q}}\right)^2 = 0$ and $\left(Q^a_q + Q^a_{\bar{q}}\right)^2 = C_A$ for a color singlet antenna and a color octet one, respectively. Since ${Q^a_q}^2 = {Q^a_{\bar{q}}}^2 = C_F$, one gets

$$Q^a_q \cdot Q^a_{\bar{q}} = \begin{cases} -C_F & \text{color singlet} \\ \frac{C_A}{2} - C_F & \text{color octet} \end{cases} \tag{4.14}$$

One can simplify the classical Yang-Mills equations (4.10) by linearizing it in the strong coupling constant:

$$\partial^2 A^\mu_{(0)} - \partial^\mu\,\partial\cdot A_{(0)} = J^\mu_{(0)}, \tag{4.15}$$

where $A_{(0)}$ is the gauge field of the quark-antiquark antenna in vacuum. With the help of the light-cone gauge, one may break down Eq.(4.15):

$$\begin{aligned} -\,\partial^+\,\partial\cdot A_{(0)} &= J^+_{(0)}, \\ \partial^2 A^i_{(0)} - \partial^i\,\partial\cdot A_{(0)} &= J^i_{(0)}. \end{aligned} \tag{4.16}$$

It is safe to ignore the equality for the negative light-cone component of the gauge field, since only the transverse components of the gauge field are dynamical in the light-cone gauge. Plugging the first equality in the second one, one obtains

$$\partial^2 A^i_{(0)} = -\frac{\partial^i}{\partial^+} J^+_{(0)} + J^i_{(0)}, \tag{4.17}$$

which in momentum space reads

$$-k^2 A^{i,a}_{(0)}(k) = -2\,i\,g\left(\frac{\kappa^i}{\boldsymbol{\kappa}^2} Q^a_q + \frac{\bar{\kappa}^i}{\bar{\boldsymbol{\kappa}}^2} Q^a_{\bar{q}}\right), \tag{4.18}$$

where

$$\begin{aligned} \kappa^i &= k^i - x\,p^i, \\ \bar{\kappa}^i &= k^i - \bar{x}\,\bar{p}^i \end{aligned} \tag{4.19}$$

denote the gluon transverse momenta relative to the ones of the quark and the antiquark, respectively, and the square of each of them reads

$$\begin{aligned} \boldsymbol{\kappa}^2 &= 2\,x\,(p\cdot k), \\ \bar{\boldsymbol{\kappa}}^2 &= 2\,\bar{x}\,(\bar{p}\cdot k). \end{aligned} \tag{4.20}$$

One can now combine the gauge field with the gluon emission amplitude in the soft limit by using the reduction formula (4.9), i.e.

$$\mathcal{M}^a_{(0),\lambda}(\mathbf{k}) = \lim_{k^2\to 0} -k^2\, A^{i,a}_{(0)}(k)\;\epsilon^{i*}_\lambda(\mathbf{k}). \tag{4.21}$$

Then one can get the square of the gluon emission amplitude, which reads

$$|\mathcal{M}^a_{(0),\lambda}|^2 = 4\,g^2\left(\frac{1}{\boldsymbol{\kappa}^2} Q^{a\,2}_q + \frac{1}{\bar{\boldsymbol{\kappa}}^2} Q^{a\,2}_{\bar{q}} + 2\,\frac{\boldsymbol{\kappa}\cdot\bar{\boldsymbol{\kappa}}}{\boldsymbol{\kappa}^2\,\bar{\boldsymbol{\kappa}}^2} Q^a_q\cdot Q^a_{\bar{q}}\right), \tag{4.22}$$

where the sum of the transverse polarizations of the emitted gluon is performed, since it is the only physical contribution to the spectrum. Taking into account the phase space factor, the vacuum spectrum of a soft gluon radiation off a color octet antenna reads

$$\omega \frac{\mathrm{d}N^{\mathrm{vac}}}{\mathrm{d}^3\vec{k}} = \frac{\alpha_s}{(2\,\pi)^2\,\omega^2}\,\left(C_F\,\mathcal{R} + C_A\,\mathcal{J}\right), \tag{4.23}$$

where the shorthand symbol $\mathcal{R} = \mathcal{R}_q + \mathcal{R}_{\bar{q}} - 2\,\mathcal{J}$ is used, and

$$\begin{aligned} \mathcal{R}_q &\equiv \frac{4\,\omega^2}{\boldsymbol{\kappa}^2}, \\ \mathcal{R}_{\bar{q}} &\equiv \frac{4\,\omega^2}{\bar{\boldsymbol{\kappa}}^2} \end{aligned} \tag{4.24}$$

are the independent radiation spectra off the quark and the antiquark, respectively, and

$$\mathcal{J} \equiv 4\,\omega^2\,\frac{\boldsymbol{\kappa}\cdot\bar{\boldsymbol{\kappa}}}{\boldsymbol{\kappa}^2\,\bar{\boldsymbol{\kappa}}^2} \tag{4.25}$$

denotes the interference between the quark and the antiquark. For the case of a color singlet antenna, the spectrum corresponds to taking $C_A = 0$ in Eq.(4.23). A convenient decomposition of the spectrum consists on separating the collinear divergences belonging to either the quark or the antiquark by defining the coherent spectra $\mathcal{P}_q \equiv \mathcal{R}_q - \mathcal{J}$ and $\mathcal{P}_{\bar{q}} \equiv \mathcal{R}_{\bar{q}} - \mathcal{J}$, respectively. For instance, $\mathcal{P}_q$ is divergent along the direction of the quark and vanishes when the gluon is emitted collinearly with respect to the antiquark. After setting the quark momentum on the z-axis and averaging the azimuthal angle of the emitted gluon, one has

$$\int_0^{2\,\pi} \frac{\mathrm{d}\varphi}{2\,\pi}\,\mathcal{P}_q = \frac{2}{1-\cos\theta}\,\Theta\left(\cos\theta - \cos\theta_{q\bar{q}}\right), \tag{4.26}$$

where θ is the gluon emission angle and $\theta_{q\bar{q}}$ is the antenna opening angle. The Heaviside step function in Eq.(4.26) indicates that gluon emissions off the quark are confined within the antenna opening angle and is collinearly divergent along the direction of the quark. The corresponding gluon radiation spectrum reads

$$\langle \mathrm{d}N_q^{\mathrm{vac}} \rangle_\varphi = \frac{\alpha_s\,C_F}{\pi}\,\frac{\mathrm{d}\omega}{\omega}\,\frac{\sin\theta\,\mathrm{d}\theta}{1-\cos\theta}\,\Theta\left(\cos\theta - \cos\theta_{q\bar{q}}\right). \tag{4.27}$$

For the color octet antenna, the second term in the parentheses of Eq.(4.23) should be kept, which is responsible for large angle radiation, i.e.

$$\int_0^{2\pi} \frac{\mathrm{d}\varphi}{2\pi}\,\mathcal{J} = \frac{2}{1-\cos\theta}\,\Theta\left(\cos\theta_{q\bar{q}} - \cos\theta\right). \tag{4.28}$$

The large angle radiation appears along with the total color charge of the antenna, so it can be reinterpreted as the radiation off the parent gluon imagined to be on shell [18].

4.2.3 s-channel antenna radiation in a dilute medium

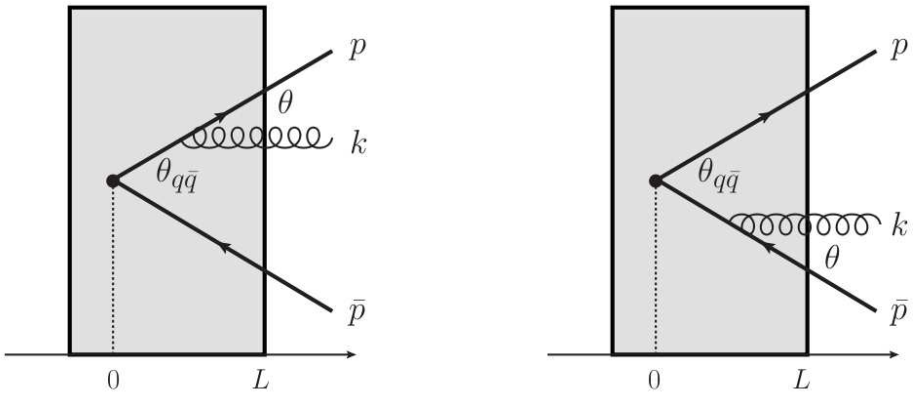

Figure 4.3: Soft gluon radiation off a quark-antiquark antenna in a dilute medium [17]

After reviewing the s-channel antenna radiation in vacuum, now one can consider the same set-up in the environment of a color deconfined medium. The calculation is performed in the infinite momentum frame, i.e. the quark-antiquark antenna is assumed to move nearly at the speed of light in the $+z$ direction while the color deconfined medium moves in the $-z$ direction nearly at the speed of light, but the process is boosted back to the target rest frame at the end of the calculation. Note that this approximation is valid only if the antenna opening angle is very small and the process is in the high-energy limit. The gauge field of a quark-antiquark antenna, originated from a virtual time-like photon, is treated as a perturbation around the strong medium field (the shaded rectangle in figure 4.3), where the strong medium field is described by

$$A^-_{\mathrm{med}}\left(x^+,\mathbf{x}\right) = \int \frac{\mathrm{d}^4 q}{(2\pi)^4}\,2\pi\,\delta\left(q^+\right)\,A^-_{\mathrm{med}}\left(q^-,\mathbf{q}\right)\,e^{-i\,q\cdot x}, \tag{4.29}$$

which is the solution of the 2-dimensional Poisson equation in the asymptotic limit:

$$-\boldsymbol{\partial}^2 A^-_{\rm med}\left(x^+,\mathbf{x}\right)=\rho_{\rm med}\left(x^+,\mathbf{x}\right),\quad A^i_{\rm med}=A^+_{\rm med}=0. \tag{4.30}$$

$\rho_{\rm med}\left(x^+,\mathbf{x}\right)$ in Eq.(4.30) is the medium color charge density. Therefore the total field is written as

$$A\equiv A_{\rm med}+A_{(0)}+A_{(1)}, \tag{4.31}$$

where $A_{(1)}$ is the first order contribution from the medium to the quark. Linearizing the classical Yang-Mills equations in α_s, one gets

$$\begin{aligned}&-\partial^+\,\partial\cdot A_{(1)}=J^+_{(1)},\\&\partial^2\,A^i_{(1)}-2\,i\,g\left[A^-_{\rm med},\partial^+\,A^i_{(0)}\right]=\partial^i\,\partial\cdot A_{(1)}+J^i_{(1)}.\end{aligned} \tag{4.32}$$

As in vacuum, one can omit the equality for the negative light-cone component of the field. Applying the first equality in the second one, one obtains

$$\partial^2\,A^i_{(1)}-2\,i\,g\left[A^-_{\rm med},\partial^+\,A^i_{(0)}\right]=-\frac{\partial^i}{\partial^+}\,J^+_{(1)}+J^i_{(1)}. \tag{4.33}$$

The current obeys the continuity equation:

$$\partial\cdot J_{(1)}=i\,g\left[A^-_{\rm med},J^+_{(0)}\right]. \tag{4.34}$$

The solution of Eq.(4.34) is given by

$$J^\mu_{(1)}=i\,g\,\frac{p^\mu}{p\cdot\partial}\left[A^-_{\rm med},J^+_{q,(0)}\right]+i\,g\,\frac{\bar{p}^\mu}{\bar{p}\cdot\partial}\left[A^-_{\rm med},J^+_{\bar{q},(0)}\right]. \tag{4.35}$$

For the quark, the current in momentum space reads

$$\begin{aligned}J^{\mu,a}_{q,(1)}\left(k\right)=&\left(i\,g\right)^2\,\frac{p^\mu}{-i\,p\cdot k}\int\frac{{\rm d}^4q}{\left(2\,\pi\right)^4}\,\frac{p^+}{p\cdot\left(k-q\right)+i\,\epsilon}\,i\\&\times\left[T\cdot A^-_{\rm med}\left(q\right)\right]^{ab}Q^b_q,\end{aligned} \tag{4.36}$$

where $\left[T\cdot A^{-}_{\mathrm{med}}\left(q\right)\right]^{ab}Q^{b}_{q}=-i\,f^{abc}\,A^{-,c}_{\mathrm{med}}\left(q\right)\,Q^{b}_{q}$. The Dirac delta function in Eq.(4.29) makes it trivial to do the integration of the $+$-component of the momentum transfer from the medium. Integrating out the $-$-component of the momentum transfer from the medium by picking up the pole yields

$$\begin{aligned}J^{\mu,a}_{q,(1)}\left(k\right)=&-i\,g^{2}\,\frac{p^{\mu}}{p\cdot k}\int\frac{\mathrm{d}^{2}\mathbf{q}}{\left(2\,\pi\right)^{2}}\int_{0}^{+\infty}\mathrm{d}x^{+}\,e^{i\,\frac{p^{+}\,k^{-}+p^{-}\,k^{+}-\mathbf{p}\cdot\left(\mathbf{k}-\mathbf{q}\right)}{p^{+}}\,x^{+}}\\&\times\left[T\cdot A^{-}_{\mathrm{med}}\left(x^{+},\mathbf{q}\right)\right]^{ab}Q^{b}_{q}.\end{aligned}\tag{4.37}$$

Inserting the expression Eq.(4.37) into Eq.(4.33), one obtains

$$\begin{aligned}-k^{2}\,A^{i}_{q,(1)}\left(k\right)=&\,2\,g\int\frac{\mathrm{d}^{4}q}{\left(2\,\pi\right)^{4}}\left[A^{-}_{\mathrm{med}}\left(q\right),\left(k-q\right)^{+}\,A^{i}_{q,(0)}\left(k-q\right)\right]\\&-\frac{k^{i}}{k^{+}}\,J^{+}_{q,(1)}\left(k\right)+J^{i}_{q,(1)}\left(k\right),\end{aligned}\tag{4.38}$$

where

$$-\left(k-q\right)^{2}\,A^{i,a}_{q,(0)}\left(k-q\right)=-2\,i\,g\,\frac{\nu^{i}}{\left(\boldsymbol{\kappa}-\mathbf{q}\right)^{2}}\,Q^{a}_{q}.\tag{4.39}$$

It is again trivial to do the integration of the $+$-component of the momentum transfer from the medium in Eq.(4.38) due to the Dirac delta function. Integrating out the $-$-component of the momentum transfer from the medium by picking up the poles yields

$$\begin{aligned}-k^{2}\,A^{i,a}_{q,(1)}\left(k\right)=&\,2\,i\,g^{2}\int\frac{\mathrm{d}^{2}\mathbf{q}}{\left(2\,\pi\right)^{2}}\int_{0}^{\infty}\mathrm{d}x^{+}\left[T\cdot A^{-}_{\mathrm{med}}\left(x^{+},\mathbf{q}\right)\right]^{ab}\\&\times Q^{b}_{q}\,e^{i\left[k^{-}-\frac{\left(\mathbf{k}-\mathbf{q}\right)^{2}}{2\,k^{+}}\right]x^{+}}\\&\times\left\{\frac{\left(\kappa-q\right)^{i}}{\left(\boldsymbol{\kappa}-\mathbf{q}\right)^{2}}\left[1-\exp\left(i\,\frac{\left(\boldsymbol{\kappa}-\mathbf{q}\right)^{2}}{2\,k^{+}}\,x^{+}\right)\right]\right.\\&\left.+\,\frac{\kappa^{i}}{\boldsymbol{\kappa}^{2}}\,\exp\left(i\,\frac{\left(\boldsymbol{\kappa}-\mathbf{q}\right)^{2}}{2\,k^{+}}\,x^{+}\right)\right\}.\end{aligned}\tag{4.40}$$

One can now connect the gauge field with the gluon emission amplitude in the soft limit by using the reduction formula, and the amplitude of medium-induced gluon radiation off the quark reads

$$\mathcal{M}^{a}_{\lambda,q,(1)} = 2\,i\,g^2 \int \frac{\mathrm{d}^2\mathbf{q}}{(2\,\pi)^2} \int_0^\infty \mathrm{d}x^+ \left[T \cdot A^-_{\mathrm{med}}\left(x^+,\mathbf{q}\right)\right]^{ab} Q^b_q \\ \times \left\{ \frac{\boldsymbol{\kappa}-\mathbf{q}}{\left(\boldsymbol{\kappa}-\mathbf{q}\right)^2} - \mathbf{L}\,\exp\left[i\,\frac{\left(\boldsymbol{\kappa}-\mathbf{q}\right)^2}{2\,k^+}\,x^+ \right] \right\} \cdot \boldsymbol{\epsilon}^*_\lambda, \tag{4.41}$$

where

$$\mathbf{L} = \frac{\boldsymbol{\kappa}-\mathbf{q}}{\left(\boldsymbol{\kappa}-\mathbf{q}\right)^2} - \frac{\boldsymbol{\kappa}}{\boldsymbol{\kappa}^2} \tag{4.42}$$

are the transverse components of the Lipatov vertex in the light-cone gauge [19, 20, 21], and it represents the genuine medium-induced gluon radiation off an on-shell quark. The other term in Eq.(4.41) corresponds to the bremsstrahlung off the accelerated quark with a subsequent rescattering of the emitted on-shell gluon. The amplitude of medium-induced gluon radiation off the antiquark can be obtained directly from Eq.(4.41) by substituting the quark momentum and the quark color charge.
The correlation of the color charges in the medium is assumed to be local along the x^+-direction. The medium charge density can therefore be treated as a Gaussian white noise defined by the two-point correlation function

$$\left\langle \rho^a_{\mathrm{med}}\left(x^+,\mathbf{q}\right)\,\rho^{b*}_{\mathrm{med}}\left(x'^+,\mathbf{q}'\right)\right\rangle \\ = \delta^{ab}\,m_D^2\,n\left(x^+\right)\,\delta\left(x^+-x'^+\right)\left(2\,\pi\right)^2\delta^{(2)}\left(\mathbf{q}-\mathbf{q}'\right), \tag{4.43}$$

which gives the medium average of the interaction potential:

$$\left\langle A^{-,a}_{\mathrm{med}}\left(x^+,\mathbf{q}\right)\,A^{-,b*}_{\mathrm{med}}\left(x'^+,\mathbf{q}'\right)\right\rangle \\ = \delta^{ab}\,m_D^2\,n\left(x^+\right)\,\delta\left(x^+-x'^+\right)\left(2\,\pi\right)^2\delta^{(2)}\left(\mathbf{q}-\mathbf{q}'\right)\,\mathcal{V}^2\left(\mathbf{q}\right). \tag{4.44}$$

The interaction potential in Eq.(4.44) is defined to be of the Yukawa-type, i.e.

$$\mathcal{V}\left(\mathbf{q}\right) = \frac{1}{\left|\mathbf{q}\right|^2+m_D^2}. \tag{4.45}$$

m_D in Eq.(4.45) is the Debye screening mass, which serves as an infrared cut-off in the medium. In the following we will assume that the medium is uniform in the longitudinal direction such that the one-dimensional medium density is constant, i.e. $n\left(x^+\right) = n_0\,\Theta\left(L^+ - x^+\right)$. $L = L^+/\sqrt{2}$ is the size of the medium in the longitudinal direction. The medium transport parameter is defined here as

$$\hat{q} = \alpha_s\, C_A\, n_0\, m_D^2, \tag{4.46}$$

which is different from the one in [22] and the one in Eq.(3.21). This is because the standard definition of the medium transport coefficient is done in the multiple soft scattering approximation, while the one here is defined in the single hard scattering approximation. When the smoke clears, one finds the medium-induced radiation spectrum off a quark-antiquark antenna in a singlet configuration

$$\begin{aligned}\omega\,\frac{\mathrm{d}N^{\mathrm{med}}}{\mathrm{d}^3\vec{k}} = {} & \frac{8\,\alpha_s\,C_F\,\hat{q}}{\pi}\int\frac{\mathrm{d}^2\mathbf{q}}{2\,\pi}\,\mathcal{V}^2\left(\mathbf{q}\right)\int_0^{L^+}\mathrm{d}x^+ \\ & \times\left\{\left[1-\cos\left(\frac{\left(\boldsymbol{\kappa}-\mathbf{q}\right)^2}{2\,k^+}\,x^+\right)\right]\mathbf{C}\left(\mathbf{k}-\mathbf{q}\right)\cdot\mathbf{L}\right. \\ & -\left[1-\cos\left(\frac{\left(\bar{\boldsymbol{\kappa}}-\mathbf{q}\right)^2}{2\,k^+}\,x^+\right)\right]\mathbf{C}\left(\mathbf{k}-\mathbf{q}\right)\cdot\bar{\mathbf{L}} \\ & \left.+\left[1-\cos\left(\frac{\boldsymbol{\kappa}+\bar{\boldsymbol{\kappa}}-2\mathbf{q}}{2}\cdot\delta\mathbf{n}\,x^+\right)\right]\mathbf{L}\cdot\bar{\mathbf{L}}\right\},\end{aligned} \tag{4.47}$$

where in order to account for unitarity the virtual corrections, also known as the contact terms [19, 23, 24], have already been added. The explicit form of the contact terms here reads

$$\omega\,\frac{\mathrm{d}N^{\mathrm{med}}}{\mathrm{d}^3\vec{k}}\bigg|_{\mathrm{virtual}} = -\frac{2\,\alpha_s\,C_F}{\pi}\,\frac{p\cdot\bar{p}}{\left(p\cdot k\right)\left(\bar{p}\cdot k\right)}\,\hat{q}\,L^+\int\frac{\mathrm{d}^2\mathbf{q}}{\left(2\,\pi\right)^2}\,\mathcal{V}^2\left(\mathbf{q}\right). \tag{4.48}$$

In other words, adding the contact terms simply corresponds to redefining the square of the interaction potential:

$$\mathcal{V}^2\left(\mathbf{q}\right) \to \mathcal{V}^2\left(\mathbf{q}\right) - \left(2\,\pi\right)^2\,\delta^{(2)}\left(\mathbf{q}\right)\int\frac{\mathrm{d}^2\mathbf{q}'}{\left(2\,\pi\right)^2}\,\mathcal{V}^2\left(\mathbf{q}'\right). \tag{4.49}$$

The spectrum in Eq.(4.47) depends not only on the transverse components of the Lipatov vertex, c.f. Eq.(4.42), but also on the transverse emission current from the hard emission vertex associated with gluon rescattering in the medium, i.e.

$$\mathbf{C}\,(\mathbf{k}-\mathbf{q}) \equiv \frac{\boldsymbol{\kappa}-\mathbf{q}}{(\boldsymbol{\kappa}-\mathbf{q})^2} - \frac{\bar{\boldsymbol{\kappa}}-\mathbf{q}}{(\bar{\boldsymbol{\kappa}}-\mathbf{q})^2}. \tag{4.50}$$

4.2.4 The dead-cone effect

For the up and down quarks, one can safely neglect their masses in the hight-energy limit. But this is not completely correct for the heavy quarks, such as the charm and bottom quarks. In vacuum, the distribution of soft gluon radiation off a massless quark is given by

$$\mathrm{d}N^{\mathrm{vac}}_{m=0} = \frac{\alpha_s\, C_F}{\pi}\,\frac{\mathrm{d}\omega}{\omega}\,\frac{\mathrm{d}\mathbf{k}^2}{\mathbf{k}^2}, \tag{4.51}$$

while that off a massive quark reads

$$\mathrm{d}N^{\mathrm{vac}}_{m\neq 0} = \frac{\alpha_s\, C_F}{\pi}\,\frac{\mathrm{d}\omega}{\omega}\,\frac{\mathbf{k}^2\,\mathrm{d}\mathbf{k}^2}{\left(\mathbf{k}^2+\omega^2\,\theta_0^2\right)^2}, \quad \theta_0 \equiv \frac{m}{E}, \tag{4.52}$$

where θ_0 is the dead-cone angle. The soft gluon emission is suppressed inside the cone set by the dead-cone angle around the parent massive quark as compared with the massless quark (see Eq.(4.51)).
For a dense medium, due to the non-Abelian nature, Wilson line can be used to describe the quark trajectory in the eikonal limit, and the emitted gluon trajectory is described by Green function. The medium-induced single-gluon radiation spectrum off a massive quark reads [28]

$$\begin{aligned}(2\,\pi)^3\,2\,\omega\,\frac{\mathrm{d}N^{\mathrm{med}}_{m\neq 0}}{\mathrm{d}\omega\,\mathrm{d}^2\mathbf{k}} = {} & 8\,(4\,\pi)^2\,\alpha_s^2\,C_A\,C_F\,n_0\int_0^{L^+}\mathrm{d}x^+\int\frac{\mathrm{d}^2\mathbf{q}}{(2\,\pi)^2} \\ & \times\frac{m_D^2}{\left(\mathbf{q}^2+m_D^2\right)^2}\,\frac{(\mathbf{k}-\mathbf{q})^2\;\mathbf{k}\cdot\mathbf{q}-x^2\,m^2\;(\mathbf{k}-\mathbf{q})\cdot\mathbf{q}}{\Big[(\mathbf{k}-\mathbf{q})^2+x^2\,m^2\Big]^2\,(\mathbf{k}^2+x^2\,m^2)} \\ & \times\left\{1-\cos\left[\frac{(\mathbf{k}-\mathbf{q})^2+x^2\,m^2}{2\,k^+}\,x^+\right]\right\}.\end{aligned} \tag{4.53}$$

This spectrum is for both the massless quark ($m = 0$) and the massive one, and one can study the parton energy loss from it by integrating out the entire phase space of the gluon.

4.2.5 Massive s-channel antenna

As an extension to the study of the massless s-channel antenna radiation, the spectrum off an antenna made out of a massive quark-antiquark pair traversing a color deconfined medium assumed to be made out of static scattering centers spaced on average at a typical mean free path λ is studied in [2]. As before, the medium interaction is modeled by a gauge field $A^{\mu}_{\mathrm{med}}(q)$, and q denotes the momentum exchange with the medium. The single elastic differential scattering cross section $\propto |A(q)|^2$ is then usually chosen to be a color screened Coulomb potential with the Debye mass m_D. For the sake of transparency, we study the case when the antenna arises from the decay of a highly virtual time-like photon. Note that the calculation of the decay of a virtual gluon proceeds in the soft limit analogously to the one performed in this thesis, differing only in the color algebra. The 3-momenta are given by $\vec{p} \equiv (\mathbf{p}, p_z)$ and $\vec{\bar{p}} \equiv (\bar{\mathbf{p}}, \bar{p}_z)$ as usual, and $p^2 = \bar{p}^2 = m^2$ defines the rest mass of the on-shell quark (antiquark). The quark-antiquark antenna is characterized by the antenna opening angle. We compute the amplitude at first order in the opacity expansion, i.e. considering the contribution with one scattering center in the amplitude, but due to the unitarity one has to take into account virtual corrections to the interaction, i.e. the so-called contact terms, with two scattering centers in the amplitude in the contact limit (see e.g. [24, 25]). All in all, 64 diagrams coming from the amplitudes with one scattering plus 32 contact terms contribute to the s-channel antenna spectrum.

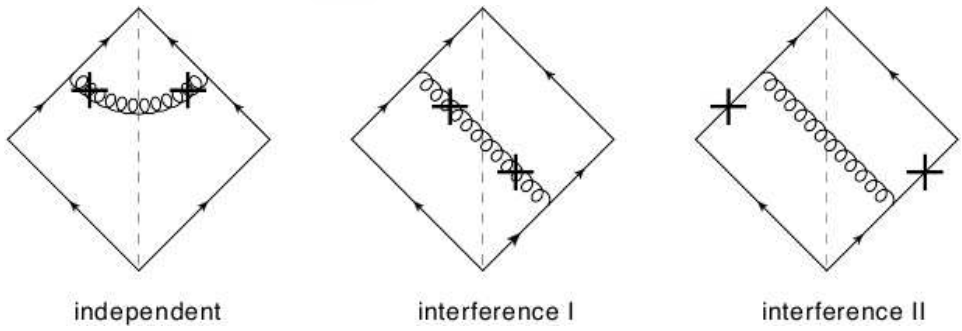

Figure 4.4: Typical contributions to the quark-antiquark antenna spectrum [2]

Since the Born cross section is not altered by the presence of a color deconfined medium, it can be factored out of the expression. Then the medium-induced single-inclusive gluon radiation spectrum off the quark-antiquark antenna, cf. Eq.(4.47), can be decomposed in terms of three characteristic contributions, which are denoted by

$$(2\,\pi)^3\,2\,\omega\,\frac{\mathrm{d}N}{\mathrm{d}\omega\,\mathrm{d}^2\mathbf{k}} = \mathcal{I}_{q\bar{q}}^{\mathrm{indep}} + \mathcal{I}_{q\bar{q}}^{\mathrm{interf\,I}} + \mathcal{I}_{q\bar{q}}^{\mathrm{interf\,II}}. \tag{4.54}$$

The three contributions in Eq.(4.54) are illustrated in figure 4.4. They represent the independent emission off the quark and the antiquark contained in $\mathcal{I}_{q\bar{q}}^{\mathrm{indep}}$, and the interferences given by $\mathcal{I}_{q\bar{q}}^{\mathrm{interf\,I}}$ and $\mathcal{I}_{q\bar{q}}^{\mathrm{interf\,II}}$, i.e. contributions where the gluon is emitted by one of the antenna constituents to the left of the cut and absorbed by the other to the right.
Let us turn to the sum of the independent emission spectra off the quark and the antiquark, denoted as $\mathcal{I}_{q\bar{q}}^{\mathrm{indep}}$ above. Note that this part of the spectrum was denoted as GLV in [26]. This contribution reads

$$\begin{aligned}\mathcal{I}_{q\bar{q}}^{\mathrm{indep}} = 2\,(4\,\pi)^2\,\alpha_s^2\,C_A\,C_F\,n_0 \int_0^{L^+}\mathrm{d}x^+ \int \frac{\mathrm{d}^2\mathbf{q}}{(2\,\pi)^2}\,\frac{m_D^2}{\left(\mathbf{q}^2+m_D^2\right)^2} \\ \times\left\{\left[\frac{\boldsymbol{\nu}^2}{\left(x\,p\cdot v\right)^2} - \frac{\boldsymbol{\nu}\cdot\boldsymbol{\kappa}}{x^2\,(p\cdot v)\,(p\cdot k)}\right]\left[1-\cos\left(\Omega_q\,x^+\right)\right]\right. \\ \left. + \left[\frac{\bar{\boldsymbol{\nu}}^2}{\left(\bar{x}\,\bar{p}\cdot v\right)^2} - \frac{\bar{\boldsymbol{\nu}}\cdot\bar{\boldsymbol{\kappa}}}{\bar{x}^2\,(\bar{p}\cdot v)\,(\bar{p}\cdot k)}\right]\left[1-\cos\left(\Omega_{\bar{q}}\,x^+\right)\right]\right\},\end{aligned} \tag{4.55}$$

where all momenta and positions are written in the light-cone coordinate system. Indeed, $\mathcal{I}_{q\bar{q}}^{\mathrm{indep}}$ is a superposition of the individual spectra off the quark and the antiquark, which are to be found in the second and the third lines of Eq.(4.55), respectively, and therefore does not contain any information about the opening angle of the pair. Above, we have assumed a medium of constant density n_0 which extends over a distance $L^+ = \sqrt{2}\,L$ in the longitudinal direction, such that $n_0\,L^+ = L/\lambda$ gives the average number of scattering centers.
In Eq.(4.55), $\alpha_s\,C_F$ denotes the emission strength in terms of the strong coupling constant, and analogously $\alpha_s\,C_A$ for the interaction with the medium. The 4-momentum of the emitted on-shell gluon is defined in the light-cone coordinate system as $v \equiv \left[k^+, (\mathbf{k}-\mathbf{q})^2/(2\,k^+), \mathbf{k}-\mathbf{q}\right]$. $\boldsymbol{\kappa} = \mathbf{k} - x\,\mathbf{p}$ and $\boldsymbol{\nu} = (\mathbf{k}-\mathbf{q}) - x\,\mathbf{p}$ are the transverse displacement vectors, where $x = k^+/p^+$ is the longitudinal momentum fraction. $\Omega_q = p\cdot v/p^+$ denotes the inverse of

the formation time. Analogous expressions hold for the antiquark contribution simply by substituting $p \to \bar{p}$. Kinematically, the terms proportional to $\boldsymbol{\nu}^2/\left(x\,p\cdot v\right)^2$ account for the contribution purely from gluon rescattering, while those proportional to $\boldsymbol{\nu}\cdot\boldsymbol{\kappa}/\left(x^2\,(p\cdot v)\,(p\cdot k)\right)$ account for the contribution from the destructive interference between gluon and quark (antiquark) rescatterings. The contributions from purely quark rescattering cancel due to the contact terms (see [24, 25]).
The independent spectrum off the quark simplifies in the $|\mathbf{p}| = 0$ frame, where it reads

$$\begin{aligned}\mathcal{I}_q^{\text{indep}} = &\, 8\,(4\,\pi)^2\,\alpha_s^2\,C_A\,C_F\,n_0 \int_0^{L^+} \mathrm{d}x^+ \int \frac{\mathrm{d}^2\mathbf{q}}{(2\,\pi)^2} \\ &\times \frac{m_D^2}{\left(\mathbf{q}^2+m_D^2\right)^2}\,\frac{(\mathbf{k}-\mathbf{q})^2\;\mathbf{k}\cdot\mathbf{q} - x^2\,m^2\;(\mathbf{k}-\mathbf{q})\cdot\mathbf{q}}{\left[(\mathbf{k}-\mathbf{q})^2+x^2\,m^2\right]^2\left(\mathbf{k}^2+x^2\,m^2\right)} \\ &\times \left\{1-\cos\left[\frac{(\mathbf{k}-\mathbf{q})^2+x^2\,m^2}{2\,k^+}\,x^+\right]\right\}.\end{aligned} \tag{4.56}$$

This expression coincides with the one obtained in [27, 28] and the one discussed in Eq.(4.53). We recover the independent spectrum off a massless quark, which was first calculated in [25, 32], by setting $m = 0$ in Eq.(4.56). Qualitatively, the interaction with the medium leads to a characteristic broadening of the mean transverse momentum, i.e. $\langle\mathbf{k}^2\rangle \sim m_D^2$, which further implies a characteristic energy scale. In the first order opacity expansion, this characteristic gluon energy is denoted by $\bar{\omega}_c = m_D^2\,L/2$ (see [22, 28]). The presence of these intrinsic scales in the medium-induced spectrum renders it both the infrared and the collinear convergences in contrast to the vacuum spectrum.
As expected, the non-zero quark mass appears in the effective formation time, i.e. in the argument of the cosine function, and as a dead-cone factor analogously to the vacuum case in Eq.(4.56). For soft gluons, these two modifications work in opposite directions and compensate each other. On the other hand, the dead-cone suppression at small angles is particularly important for hard gluons, which mainly occupy this part of the phase space. Since the energy loss distribution is biased toward the hard sector, it follows that the typical energy loss is smaller in the massive case than in the massless one [28]. The non-zero quark mass does not change the infrared and the collinear convergence of the independent spectrum.
The individual spectra off the two antenna constituents lack the information about the presence of the other emitter. Assuming a strong medium

screening, leaving the quark and the antiquark completely unaware of one another, it can serve as a building block for a cascade of multiple independent medium-induced gluon emissions [33, 34]. Yet, such a heuristic generalization fails to include subtle interference effects which are crucial for soft gluons, most prominently in vacuum [18], and which were calculated recently [2, 26, 29, 35, 36] for the color deconfined medium.

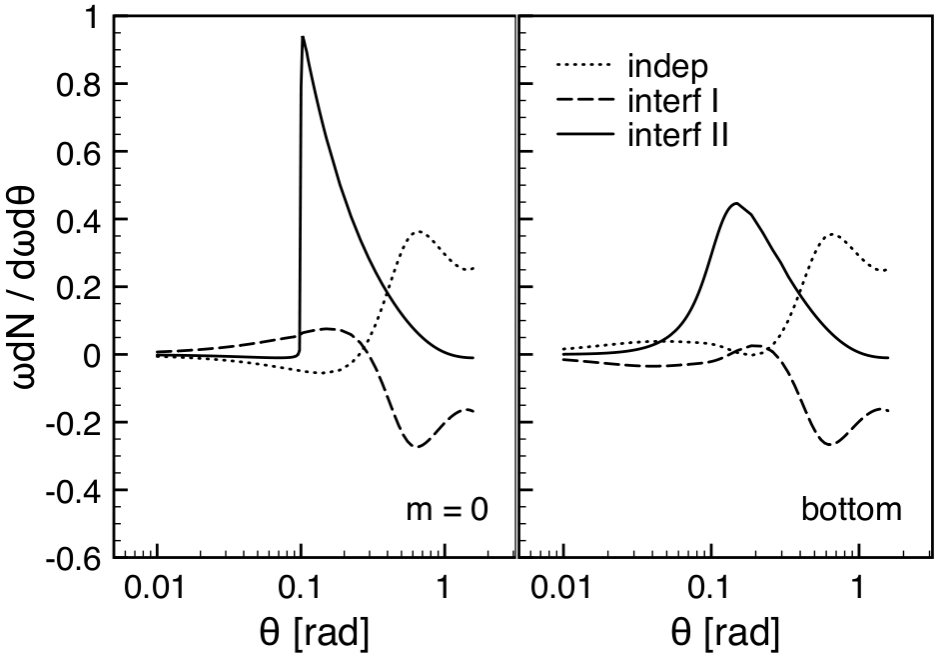

Figure 4.5: Cancellation between the sum of the independent spectra for a quark-antiquark antenna and the interference spectrum I, for massless (plot on the left) and bottom ($m = 5$ GeV, plot on the right) quarks in the soft limit [2] (Quark and antiquark energies are $E = \bar{E} = 100$ GeV, gluon energy $\omega = 2$ GeV, Debye mass $m_D = 0.5$ GeV, medium length $L = 4$ fm and antenna opening angle $\theta_{q\bar{q}} = 0.1$. The dotted curve corresponds to the independent spectra for the antenna, the dashed curve corresponds to the interference spectrum I and the solid curve corresponds to the interference spectrum II.)

The main difference between $\mathcal{I}^{\rm indep}_{q\bar{q}}$ in Eq.(4.55) and the complete antenna spectrum is the existence of the extra novel contributions stemming from the gluon exchange between the emitters of the antenna, i.e. the quark and the antiquark. These contributions can be further separated according to their infrared behaviors, what will be called in the following type I and type

II. The former is infrared safe while the latter is infrared divergent. It has a simple diagrammatic interpretation, visualized in figure 4.4. This diagrammatic interpretation is in the spirit of classical currents, which is valid for soft emissions, and strictly speaking not in terms of Feynman diagrams due to the existence of the contact terms. Namely, all interferences of the type I include at least one gluon exchange with the medium, while the type II includes only the case that gluon does not interact with the medium. The interaction of the off-shell gluon with the medium screens both the soft and the collinear divergences in $\mathcal{I}_{q\bar{q}}^{\text{interf I}}$ as is the case for the independent spectrum. It is therefore the interference spectrum II that gives the dominant contribution in the soft limit.
The interference spectrum I reads

$$\begin{aligned}\mathcal{I}_{q\bar{q}}^{\text{interf I}} = & -2\,(4\,\pi)^2\,\alpha_s^2\,C_A\,C_F\,n_0\int_0^{L^+}\mathrm{d}x^+\int\frac{\mathrm{d}^2\mathbf{q}}{(2\,\pi)^2}\,\frac{m_D^2}{\left(\mathbf{q}^2+m_D^2\right)^2}\\ & \times\frac{1}{x\,\bar{x}}\Bigg\{\frac{\boldsymbol{\kappa}\cdot\bar{\boldsymbol{\kappa}}}{(p\cdot k)\,(\bar{p}\cdot k)}\left[\cos\left(\Omega_{q\bar{q}}^0\,x^+\right)-1\right]\\ & +\frac{\boldsymbol{\nu}\cdot\bar{\boldsymbol{\nu}}}{(p\cdot v)\,(\bar{p}\cdot v)}\left[1+\cos\left(\Omega_{q\bar{q}}\,x^+\right)-\cos\left(\Omega_q\,x^+\right)-\cos\left(\Omega_{\bar{q}}\,x^+\right)\right]\\ & +\frac{\boldsymbol{\nu}\cdot\bar{\boldsymbol{\kappa}}}{(p\cdot v)\,(\bar{p}\cdot k)}\left[\cos\left(\Omega_{\bar{q}}\,x^+\right)-\cos\left(\Omega_{q\bar{q}}\,x^+\right)\right]\\ & +\frac{\bar{\boldsymbol{\nu}}\cdot\boldsymbol{\kappa}}{(\bar{p}\cdot v)\,(p\cdot k)}\left[\cos\left(\Omega_q\,x^+\right)-\cos\left(\Omega_{q\bar{q}}\,x^+\right)\right]\Bigg\},\end{aligned} \tag{4.57}$$

with $\Omega_{q\bar{q}}=p\cdot v/p^+-\bar{p}\cdot v/\bar{p}^+$ and $\Omega_{q\bar{q}}^0=p\cdot k/p^+-\bar{p}\cdot k/\bar{p}^+$. The interference spectrum II reads

$$\begin{aligned}\mathcal{I}_{q\bar{q}}^{\text{interf II}} = & -2\,(4\,\pi)^2\,\alpha_s^2\,C_A\,C_F\,n_0\int_0^{L^+}\mathrm{d}x^+\int\frac{\mathrm{d}^2\mathbf{q}}{(2\,\pi)^2}\,\frac{m_D^2}{\left(\mathbf{q}^2+m_D^2\right)^2}\\ & \times\frac{\boldsymbol{\kappa}\cdot\bar{\boldsymbol{\kappa}}}{x\,\bar{x}\;(p\cdot k)\,(\bar{p}\cdot k)}\left[\cos\left(\Omega_{q\bar{q}}\,x^+\right)-\cos\left(\Omega_{q\bar{q}}^0\,x^+\right)\right].\end{aligned} \tag{4.58}$$

The divergent structure of Eq.(4.58) is apparent from the fraction in the second line. Furthermore, arranged in this way the novel contributions exhibit a cancellation between $\mathcal{I}_{q\bar{q}}^{\text{indep}}$ and $\mathcal{I}_{q\bar{q}}^{\text{interf I}}$ in the soft limit. This cancellation as first observed in [26] still holds numerically in the massive case (see figure 4.5).
In the following, we will be concerned with comparing the coherent spectrum off one of the constituents, say the quark, defined as

$$\mathcal{I}_q^{\rm coh} = \mathcal{I}_q^{\rm indep} + \left(\mathcal{I}_{q\bar{q}}^{\rm interf\,I} + \mathcal{I}_{q\bar{q}}^{\rm interf\,II}\right)/2, \tag{4.59}$$

with the purely independent component $\mathcal{I}_q^{\rm indep}$. In vacuum, it is well knowm [18] that the coherent spectrum off the quark (antiquark) differs from the independent spectrum only by the angular ordering condition.
For the medium-induced spectrum, on the other hand, since only the $\mathcal{I}_{q\bar{q}}^{\rm interf\,II}$ component contains an infrared divergence, the main contribution to Eq.(4.54) is readily found for soft gluon emissions. In the ultrarelativistic limit, after averaging over the azimuthal angle with respect to the quark direction, one obtains

$$\omega\,\frac{{\rm d}N_q}{{\rm d}\omega\,{\rm d}\theta} = \frac{\alpha_s\,C_F}{\pi}\,\frac{\sin\theta}{1-\eta\,\cos\theta}\,\frac{1+\eta^2}{1+\cos\theta}\,H\left(\theta_{q\bar{q}},\theta;\theta_0\right)\,\Delta_{\rm med}\left(\theta_{q\bar{q}},\theta_0,L^+\right), \tag{4.60}$$

where $\eta = \sqrt{1-\theta_0^2}$. Note that the collinear divergence in the second fraction on the right-hand-side of Eq.(4.60) is explicitly regulated by the quark mass due to the dead-cone effect. In Eq.(4.60), the expression for $H\left(\theta_{q\bar{q}},\theta;\theta_0\right)$ reads

$$H\left(\theta_{q\bar{q}},\theta;\theta_0\right) = \frac{1}{2}\left[1 + \frac{\eta\,\cos\theta_{q\bar{q}} - \cos\theta}{\sqrt{\left(1-\eta\,\cos\theta_{q\bar{q}}\,\cos\theta\right)^2 - \eta^2\,\sin^2\theta_{q\bar{q}}\,\sin^2\theta}}\right], \tag{4.61}$$

which reduces to the Heaviside step function in the case of massless antenna, i.e. $H\left(\theta_{q\bar{q}},\theta;\theta_0=0\right) = \Theta\left(\cos\theta_{q\bar{q}} - \cos\theta\right)$. This generalized Heaviside step function comes with the reverse ordering condition compared to the vacuum radiation, thus mainly allowing radiation to be induced at angles larger than the opening angle of the pair. This spectrum is therefore a generalization of the property of the anti-angular ordering, found for the first time in [26], for a massive quark-antiquark antenna here.
The medium decoherence parameter appearing in Eq.(4.60) reads

$$\begin{aligned}\Delta_{\rm med}\left(\theta_{q\bar{q}},L^+\right) &= \frac{\hat{q}}{m_D^2}\int_0^{L^+}{\rm d}x^+\left[1 - \frac{|\mathbf{r}|\,m_D\,x^+}{L^+}\,K_1\left(\frac{|\mathbf{r}|\,m_D\,x^+}{L^+}\right)\right] \\ &\approx \frac{1}{6}\,\hat{q}\,L^+\,|\mathbf{r}|^2\left(\log\frac{1}{|\mathbf{r}|\,m_D} + \text{const.}\right),\end{aligned} \tag{4.62}$$

where K_1 is the modified Bessel function of the second kind and $|\mathbf{r}| = |\delta\mathbf{n}|\, L^+$ is the transverse separation between the emitters of the antenna when they leave the medium. The transverse angular separation of the quark-antiquark pair is given by

$$\delta\mathbf{n} = \frac{\mathbf{p}}{p^+} - \frac{\bar{\mathbf{p}}}{\bar{p}^+} = -\frac{\sqrt{2}\,\sin\theta_{q\bar{q}}}{1+\sqrt{1-\theta_0^2}\,\cos\theta_{q\bar{q}}}\,\hat{\mathbf{n}}, \tag{4.63}$$

where $\hat{\mathbf{n}}$ denotes the direction of $\delta\mathbf{n}$. $\delta\mathbf{n}$ contains only a weak dependence on the quark mass. The medium transport parameter is defined in Eq.(4.46). Note that the approximation performed in the second line of Eq.(4.62) is strictly valid as long as $|\mathbf{r}|\, m_D \ll 1$. Under the same condition, one can further simplify Eq.(4.62) by observing that the medium decoherence parameter exhibits only a mild logarithmic dependence on $|\mathbf{r}|\, m_D$. Then one simply has

$$\Delta_{\rm med}\left(\theta_{q\bar{q}}, L^+\right) \propto \hat{q}\, L^+\, |\mathbf{r}|^2 \propto \hat{q}\, L^3\, \theta_{q\bar{q}}^2. \tag{4.64}$$

Keeping in mind the angular ordered vacuum contribution, it becomes evident that the medium decoherence parameter controls the onset of decoherence or, in other words, the breakdown of the angular ordering for soft gluons. For a dense medium, one has to go beyond the single scattering approach and resum multiple interactions [29, 35, 36]. It is easy to check that the medium decoherence parameter in Eq.(4.62) is in fact the leading order contribution to the full result. In the opaque medium limit, i.e. $\Delta_{\rm med} \to 1$, all sensitivity on the medium characteristics are thus lost.

Above, we have relied on the fact that $\Omega^0_{q\bar{q}} \to 0$ in the soft limit. This approximation breaks down for the emitted gluon energy $\omega \gg 0$, when one also has to keep the factor $\cos\left(\Omega_{q\bar{q}}\, x^+\right)$ in Eq.(4.58). Moreover, for hard gluons one has to take into account all the components of the spectrum on equal footing. This gives rise to a characteristic cut-off scale that governs the transition between the independent and interference-dominated parts of the spectrum. This cut-off scale is independent of the quark mass.

In order to analyze the new interference contributions, to compare them with the already known independent ones and to explore phenomenological consequences, we turn to the numerical evaluation of the results.

Due to symmetry reason, one only needs to consider the emissions off one of the antenna constituents, e.g. the quark. Its propagation establishes a preferred direction such that all azimuthal averages are performed with respect to it, and additionally the vector of the momentum exchange with

the medium is perpendicular to it. These approximations are valid in the high-energy limit, where all angles are assumed to be small enough. Furthermore, the medium density is normalized by $n_0\, L^+ = 1$ and $\alpha_s = 1/3$. If not specified explicitly, all calculations are made for the quark and the antiquark energies of $E = \bar{E} = 100$ GeV. The heavy quark masses are chosen to be $m = 1.5$ GeV for the charm quark and $m = 5$ GeV for the bottom one.

The choice of the remaining medium parameters reflects two extreme scenarios: the moderate medium interaction with $m_D = 0.5$ GeV and $L = 4$ fm and the dense medium interaction with $m_D = 2$ GeV and $L = 10$ fm. In a realistic situation both of these quantities depend strongly on local medium properties and its global evolution.

We first study the antenna angular spectrum and decoherence features, then we analyze the transition between the antenna spectrum and independent spectrum, to finally examine the average radiative energy loss and the transverse momentum broadening. In all cases, both the difference between the antenna and the independent radiation and the mass effect on them are discussed.

The angular distribution of the medium-induced gluon radiation spectrum off a quark-antiquark antenna at first order in the opacity expansion is shown in figures 4.5 and 4.6, where the massless antenna (solid curve) exhibits the anti-angular ordering for the emitted gluon energy $\omega = 2$ GeV. As already mentioned, this emerging feature is the result of cancellations between various components of the spectrum, which also holds for the massive spectrum (see figure 4.5 and the discussion above).

For the charm and the bottom antennas, on the other hand, such strict anti-angular ordering is modified by the non-zero quark (antiquark) mass for small opening angles of the pair (see the right panel of figure 4.5 and the left one of figure 4.6). This is due to the screening of the collinear singularity and the appearance of the generalized Heaviside step function in Eq.(4.61). The heavier the quark is, the stronger the suppression of the radiation spectrum is. Since the dead-cone suppression mostly affects small angle emissions, this effect becomes weaker and weaker with an increasing opening angle of the pair (see the right panel of figure 4.6). In this situation, medium-induced large angle emission does not display a strong mass ordering as expected from the dead-cone suppression.

Both the massless antenna [29] and the massive one exhibit complete decoherence in the opaque medium limit [29, 35, 36], i.e. $\Delta_{\rm med} \to 1$ in Eq.(4.60) (see figure 4.7, where we have also included the corresponding coherent vacuum spectra for the charm and the bottom quarks, respectively). This illustrates that the quark-antiquark system decoheres and behaves like two independent emitters which radiate as if propagating in vacuum. The mass effect

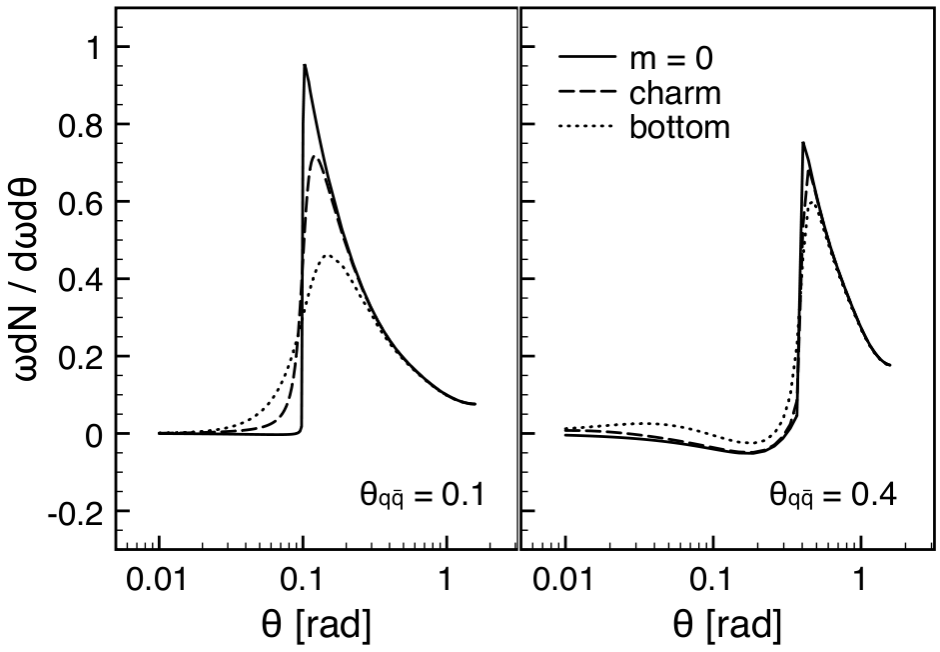

Figure 4.6: The angular distribution of the medium-induced gluon radiation spectrum off a quark-antiquark antenna at first order in the opacity expansion in the soft limit [2] (The parameters are chosen to be the same as in figure 4.5. The solid curve corresponds to the massless antenna, the dashed curve corresponds to the charm antenna and the dotted curve corresponds to the bottom antenna.)

smears out the angular separation between vacuum and medium-induced radiation, which holds strictly in the massless case. Due to the small angle nature of the dead-cone suppression, the intensity of the vacuum radiation is suppressed almost by a factor of 3 between the charm and the bottom quark spectra while the medium-induced spectrum is almost unaffected (see also figure 4.6).
Let us now consider the medium-induced gluon energy spectrum calculated via

$$\omega \frac{\mathrm{d}N}{\mathrm{d}\omega} = \int_0^{\pi/2} \mathrm{d}\theta\, \omega \frac{\mathrm{d}N}{\mathrm{d}\omega\, \mathrm{d}\theta}, \tag{4.65}$$

where the upper limit for the integration over the gluon emission angle is chosen so that $|\mathbf{k}|_{\max} = \omega$. In figure 4.8 we plot the antenna and the

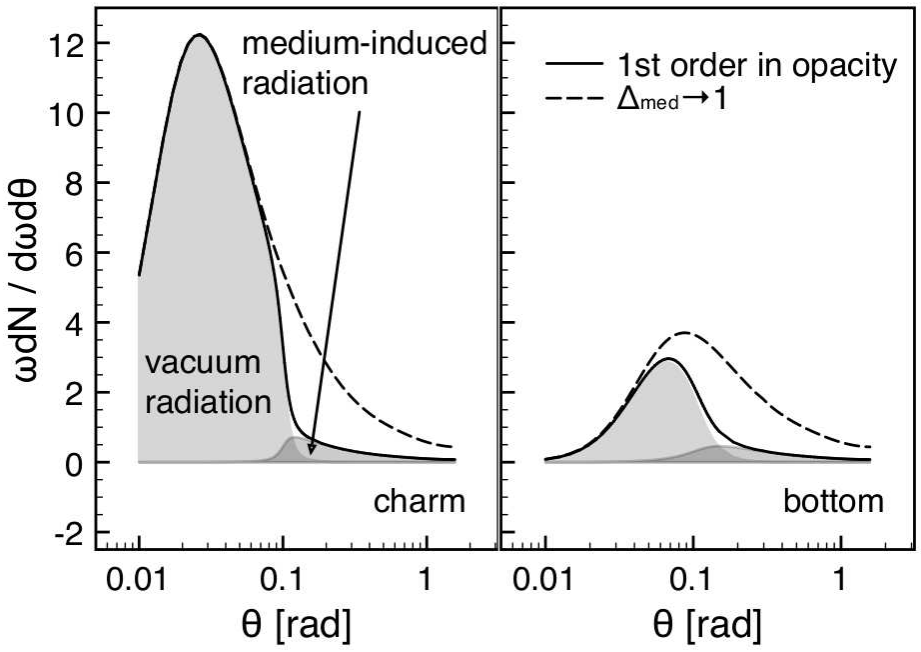

Figure 4.7: The decoherence limit of the angular distribution of the gluon radiation spectrum off charm (plot on the left) and bottom (plot on the right) antennas in the presence of a medium [2] (The parameters are chosen to be the same as in figure 4.5. The solid curve corresponds to the spectrum computed up to first order in the opacity expansion, and the dashed curve corresponds to the antenna spectrum in the presence of a completely opaque medium, i.e. $\Delta_{\mathrm{med}} \to 1$.)

independent spectra off a massless quark and a quark with mass $m = 10$ GeV (for the purpose of illustration), respectively. In the left column of figure 4.8 we show calculations for a moderate medium, while the right column contains the same curves in the case of a dense medium. First: We notice the different behaviors in the soft sector of the two types of spectra reflecting the infrared properties of the independent spectrum and the coherent spectrum off the quark. Second: We notice that the coherent spectrum matches the independent one for the emitted gluon energy $\omega > \omega_{\mathrm{coh}}$ as expected. In between these extremes, the cancellations that dominate for the moderate medium, cf. upper left panel of figure 4.8, turn to be an enhancement of the coherent spectrum, cf. lower left panel of figure 4.8. These general features of the medium-induced coherent spectrum hold for both the massless and the massive cases.

The effects of the quark mass are found both in the soft and the hard sectors and are highlighted by the shaded area in figure 4.8. Starting with the former, for the antenna spectrum this is a manifestation of the dead-cone effect which is sizeable at small opening angles (see the upper row of figure 4.8), and vanishes with an increasing opening angle (see the lower row of figure 4.8). Clearly the dead-cone effect is more pronounced in the soft gluon regime for the antenna spectrum. The independent spectrum, on the other hand, is not noticeably modified due to the compensation between the dead-cone suppression and the formation time effect. The typical medium-induced soft gluon radiation takes place at large angles. In the hard sector, one is only left with the independent components as mentioned before, and the medium-induced hard gluon radiation happens at small angles. We therefore observe that the spectra off the massive quarks are more steeply falling than the ones off the massless quarks. This is a well-known effect from the constraint on the phase space of the perpendicular momentum, which ultimately gives a manifestation of the dead-cone effect. As seen in the right column of figure 4.8, this effect is independent of the opening angle of the pair. Finally we notice that the independent spectrum off a massive quark is in fact enhanced for the small medium parameters, i.e. in the moderate medium scenario in the left column of figure 4.8, as compared with the massless one. This reflects the situation when the formation time effect prevails over the dead-cone suppression, leading to a net enhancement of medium-induced radiation as already noticed in [28].
The amount of energy taken away by the radiated gluon can be interpreted as an energy loss of the emitter. Thus one defines the radiative energy loss for the emission of gluons with energies in a certain energy interval, i.e. $\omega_{\min} < \omega < \omega_{\max}$, as

$$\Delta E = \int_{\omega_{\min}}^{\omega_{\max}} \mathrm{d}\omega \int_0^{\pi/2} \mathrm{d}\theta\, \omega\, \frac{\mathrm{d}N}{\mathrm{d}\omega\, \mathrm{d}\theta}. \tag{4.66}$$

The ratio $\Delta E/E$ as a function of the antenna opening angle is shown in figure 4.9 for three distinct gluon energy ranges. In the soft and semi-soft gluon energy regions, i.e. $0 \leq \omega \leq 2$ GeV and 2 GeV $\leq \omega \leq 6$ GeV, both the massless and the massive antenna fractional energy losses grow monotonously with an increasing opening angle and the former energy loss is larger than the latter. In the hard gluon radiation sector, i.e. 6 GeV $\leq \omega \leq E = 100$ GeV, the situation is similar for the large medium parameters, i.e. for the dense medium scenario, while for the small medium parameters, i.e. for the moderate medium scenario, there is a reversal of the behaviors between the massless and the bottom antennas due to the formation time

effect, which results in a larger energy loss for larger masses as discussed above. For the large medium parameters the dead-cone suppression is the main mass effect in all gluon energy sectors.
Both the results of the massless and the massive antennas approach the ones of independent emitters when the antenna opening angle is large enough, displaying that the interference between the quark and the antiquark reduces with an increasing opening angle as expected. Besides, in the soft gluon emission region and for the large medium parameters there is apparently more energy loss for the antenna than for the independent emitters in both the massless and the massive cases. This reflects the fact that the antenna spectrum exhibits a soft divergence while the independent spectrum is infrared finite (see figure 4.8 and the discussion below). In the semi-soft and the hard gluon emission sectors, the antenna average radiative energy loss increases and gradually approaches the independent average radiative energy loss with an increasing antenna opening angle, which indicates that in general more collimated projectiles lose less energy. Naturally there is no medium-induced antenna radiation for a vanishing opening angle due to the conservation of the color charge. Overall, the phase space restriction for gluon radiation implied by the dead-cone effect is similar for both the antenna of large opening angles and the independent emitters.
In order to further investigate the relation between the radiative energy loss and its angular structure, we compute the medium-induced radiative energy loss outside of a specific gluon emission angle:

$$\Delta E\left(\theta\right)=\int_{\omega_{\min}}^{\omega_{\max}}\mathrm{d}\omega\int_{\theta}^{\pi/2}\mathrm{d}\theta'\,\omega\,\frac{\mathrm{d}N}{\mathrm{d}\omega\,\mathrm{d}\theta'}. \tag{4.67}$$

The ratio $\Delta E\left(\theta\right)/E$ as a function of the gluon emission angle is shown in figures 4.10 and 4.11 for the moderate and the dense medium scenarios, respectively. Note that the behavior of $\Delta E\left(\theta\right)$ with the gluon emission angle traces the angular behavior of the differential energy spectrum. A decrease slower than linear of $\Delta E\left(\theta\right)$ comes from an increasing energy spectrum. A decreasing linear behavior of $\Delta E\left(\theta\right)$ results from a flat energy spectrum. A decrease stronger than linear of $\Delta E\left(\theta\right)$ traces a falling energy spectrum. A flat behavior of $\Delta E\left(\theta\right)$ indicates the null contribution, which is due to the anti-angular ordering for the antenna. An increasing behavior of $\Delta E\left(\theta\right)$ indicates the existence of negative contributions at small angles due to the destructive interferences, which is a well-known phenomenon in the BDMPS-Z/ASW/GLV framework [22, 28] for the small medium parameters. The first behavior points to $\mathbf{k}$-broadening of the radiation which reaches the upper bound at a finite gluon emission angle. Recall that the

medium-induced gluon radiation spectrum off a single emitter is known to exhibit **k**-broadening, and a proportionality relation between $\langle \mathbf{k}^2 \rangle$ and ΔE holds there (see Eq.(4.6)).

Examining figures 4.10 and 4.11, one can see that the independent emitter exhibits **k**-broadening in the regions of soft and semi-soft gluon emission, i.e. $0 \leq \omega \leq 2$ GeV and 2 GeV $\leq \omega \leq 6$ GeV. **k**-broadening emerges due to the rescattering of the emitted off-shell gluon with the medium. Since the interference spectrum II dominates in the soft limit $\omega \to 0$, and it only contains the on-shell gluon bremsstrahlung and the rescatterings of the quark and the antiquark with the medium, there is no **k**-broadening for the antenna. For the antenna opening angle $\theta_{q\bar{q}} = 0.1$ in the regions of soft and semi-soft gluon emission, $\Delta E\,(\theta)$ of the massless antenna is almost a constant for the gluon emission angle $\theta \leq \theta_{q\bar{q}}$ due to the anti-angular ordering. For the gluon emission angle $\theta > \theta_{q\bar{q}}$, the curve of the massless antenna drops monotonously and faster than linear with an increasing gluon emission angle. The suppression of the gluon radiation off the bottom antenna (dotted curve) as compared with the one off the massless antenna (solid curve) can be clearly seen at the gluon emission angle $\theta \leq \theta_{q\bar{q}}$, because most of the gluons are emitted around the antenna opening angle. For the antenna opening angle $\theta_{q\bar{q}} = 0.4$, the antenna still keeps the interference feature, i.e. the flat behavior for the gluon emission angle $\theta < \theta_{q\bar{q}}$ in the soft gluon emission sector, but it shows some **k**-broadening in the semi-soft gluon emission sector (more evident for the large medium parameters).

Note that in figure 4.10 the interference between the emitters included in the antenna generates more gluon radiation at the antenna opening angle $\theta_{q\bar{q}} = 0.4$ than at $\theta_{q\bar{q}} = 0.1$ for the specific choice of the parameters, i.e. $m_D = 0.5$ GeV, $L = 4$ fm and $0 \leq \omega \leq 2$ GeV. It agrees with the medium-induced gluon energy spectrum (see the left column in figure 4.8). In the region of large gluon emission energy, i.e. 6 GeV $\leq \omega \leq E = 100$ GeV, for both the antenna opening angles $\theta_{q\bar{q}} = 0.1$ and 0.4, the antenna and the independent spectra exhibit similar features with respect to the transverse momentum broadening in both the massless and the massive cases. One can see that the interference spectrum dominates gluon radiation when the antenna opening angle is small and the emitted gluon is soft. In this case, the antenna exhibits a new type of broadening, i.e. anti-angular ordering; while the antenna behaves like a superposition of independent emitters when the opening angle is large and the radiated gluon is hard, and then the antenna shows the typical **k**-broadening.

As a short summary, we notice that more collimated antennas lose less energy and the size of the mass effect on the energy loss for a quark-antiquark antenna with increasing opening angles becomes more and more similar to

the one resulting from independent emitters (see figure 4.12). Therefore only a superposition of two independent radiation exists in a back-to-back quark-antiquark system.

USC UNIVERSIDADE DE SANTIAGO DE COMPOSTELA

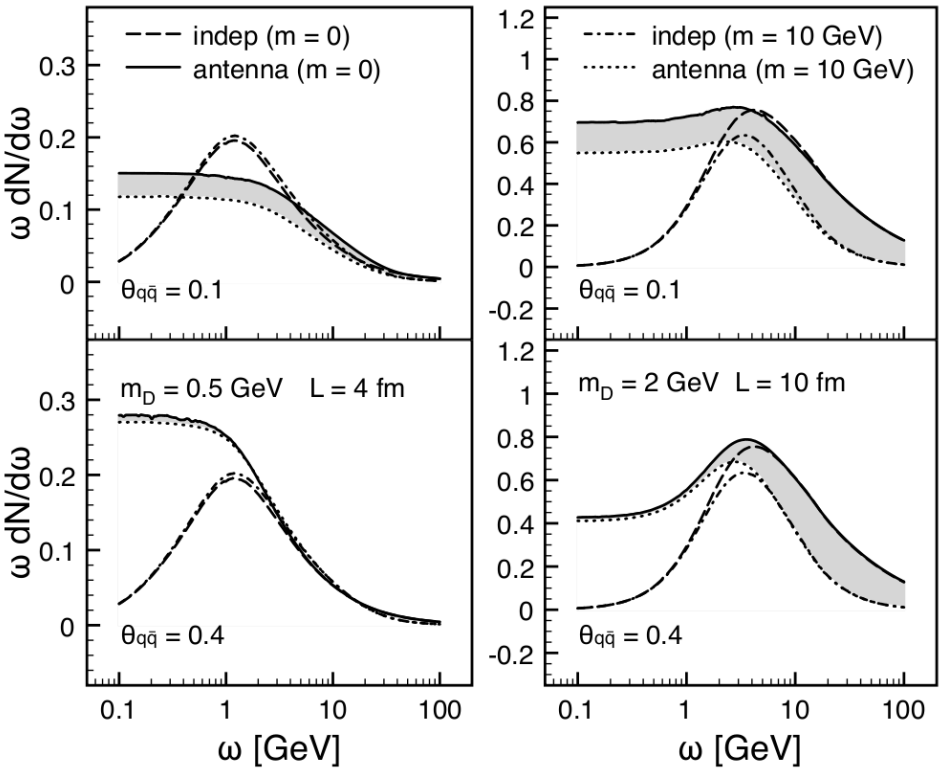

Figure 4.8: The medium-induced gluon energy spectrum [2] (We present calculations for the moderate medium scenario in the left column and the dense medium scenario in the right, where the opening angle is $\theta_{q\bar{q}} = 0.1$ in the upper row and $\theta_{q\bar{q}} = 0.4$ in the lower row. The solid curve corresponds to the massless antenna, the dotted curve corresponds to the massive antenna, the dashed curve corresponds to the massless independent spectrum and the dash-dotted curve corresponds to the massive independent one. The use of rest mass $m = 10$ GeV is for the purpose of illustration.)

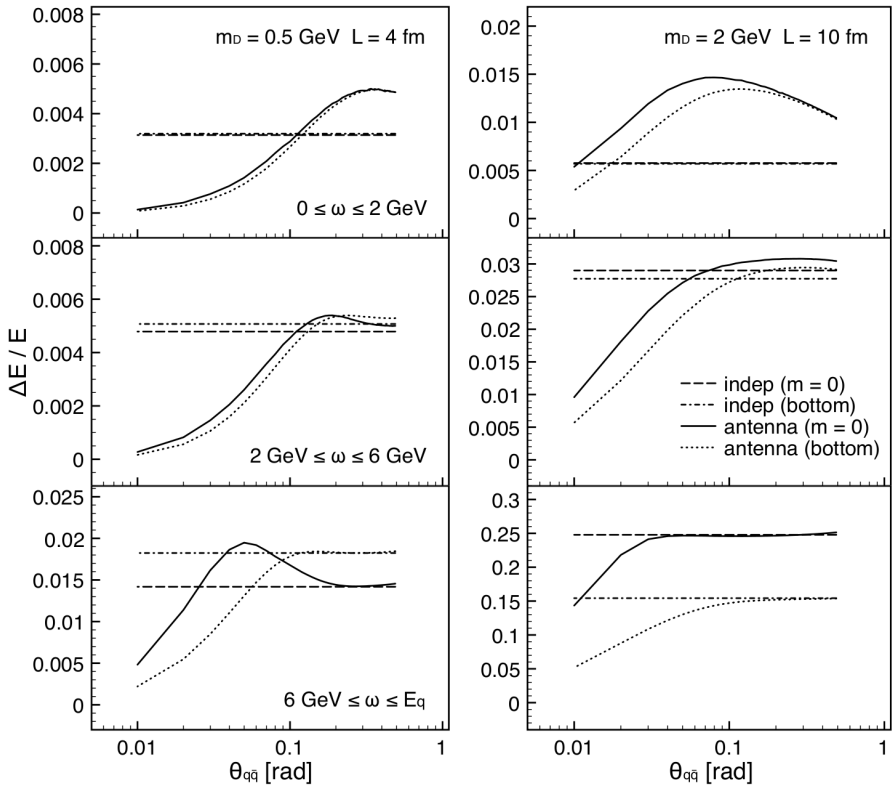

Figure 4.9: Dependence of the relative medium-induced radiative energy loss on the antenna opening angle [2] (The parameters are: Debye mass $m_D = 0.5\ (2)$ GeV and medium length $L = 4\ (10)$ fm for the plots on the left (right). The solid curves correspond to the massless antenna, the dotted curves to the bottom antenna, the dashed curves to the massless independent spectra and the dash-dotted curves to the bottom independent spectra. From top to bottom, the values used for $\omega_{\min}$ are 0, 2 GeV and 6 GeV, while those for $\omega_{\max}$ are 2 GeV, 6 GeV and $E_q = E = 100$ GeV.)

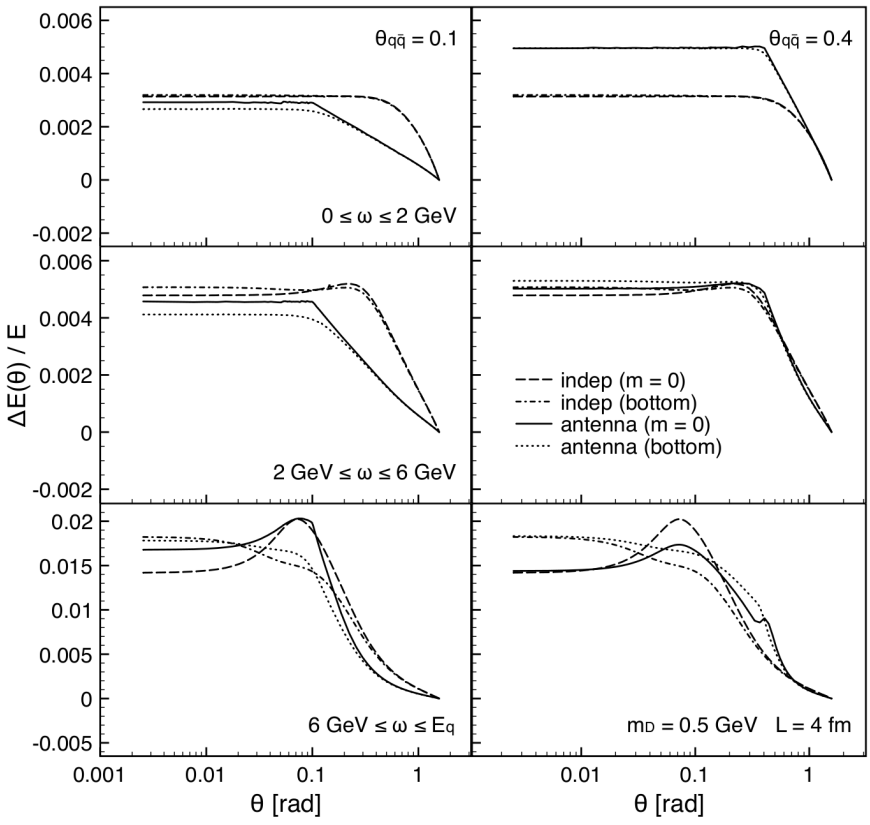

Figure 4.10: Dependence of the relative medium-induced radiative energy loss outside of a cone on the angle defining the cone [2] (The parameters are: Debye mass $m_D = 0.5$ GeV, medium length $L = 4$ fm, and antenna opening angle $\theta_{q\bar{q}} = 0.1\ (0.4)$ for the plots on the left (right). The solid curves correspond to the massless antenna, the dotted curves to the bottom antenna, the dashed curves to the massless independent spectra and the dash-dotted curves to the bottom independent spectra. From top to bottom, the values used for $\omega_{\min}$ are 0, 2 GeV and 6 GeV, while those for $\omega_{\max}$ are 2 GeV, 6 GeV and $E_q = E = 100$ GeV.)

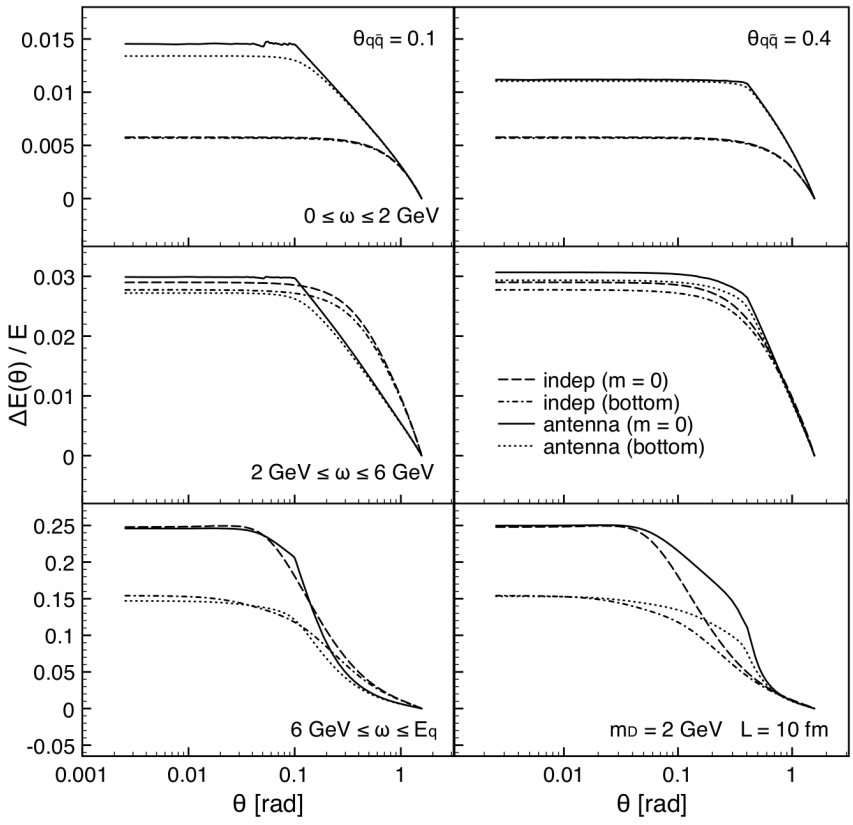

Figure 4.11: Dependence of the relative medium-induced radiative energy loss outside of a cone on the angle defining the cone [2] (The parameters are: Debye mass $m_D = 2$ GeV, medium length $L = 10$ fm, and antenna opening angle $\theta_{q\bar{q}} = 0.1$ (0.4) for the plots on the left (right). The solid curves correspond to the massless antenna, the dotted curves to the bottom antenna, the dashed curves to the massless independent spectra and the dash-dotted curves to the bottom independent spectra. From top to bottom, the values used for $\omega_{\min}$ are 0, 2 GeV and 6 GeV, while those for $\omega_{\max}$ are 2 GeV, 6 GeV and $E_q = E = 100$ GeV.)

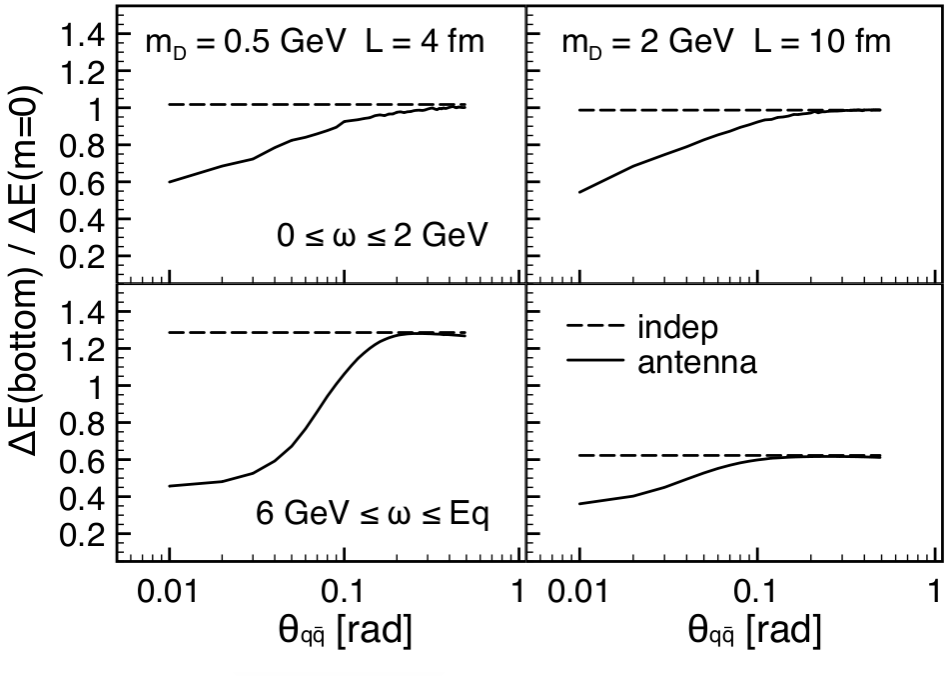

Figure 4.12: Summary plot on mass effects for medium-induced radiation [2] (The solid line refers to the antenna spectrum, while the dashed line to the independent one.)

Chapter 5

Antenna in t-channel

5.1 t-channel antenna radiation in vacuum

Studies of medium-induced QCD radiation usually rely on the calculation of single-gluon radiation spectrum off an energetic parton traversing an extended colored medium. In 4.2.5, the importance of interference effects between two emitters in the medium has been explored. As an extension to the study of the s-channel antenna radiation, the t-channel antenna radiation is studied in [3], i.e. the color coherence pattern between initial and final state radiation.

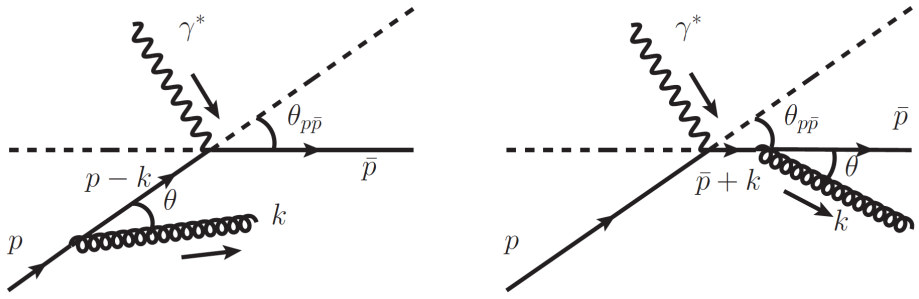

Figure 5.1: Soft gluon radiation in the quark scattering process without color transfer in t-channel in vacuum [30] (Note that $\theta_{p\bar{p}} = \theta_{qq}$ as introduced in the text.)

A Deep Inelastic Scattering process with an exchange of a virtual space-like photon is considered (see figure 5.1). The virtual photon exchange is denoted as hard scattering in the following. The calculation is again performed in the light cone gauge $A^+ = 0$ with $n = (0, 1, \mathbf{0})$. The classical current that describes the incoming and the outgoing quarks with the hard scattering

taking place at a certain time $t = t_0$ reads

$$J_{(0)} = J_{in,(0)} + J_{out,(0)}, \tag{5.1}$$

where the subscript (0) denotes vacuum quantities, and the currents for the incoming and the outgoing quarks are given by

$$\begin{aligned} J^{\mu,a}_{in,(0)} &= g\,\frac{p^\mu}{E}\,\delta^{(3)}\left(\vec{x} - \frac{\vec{p}}{E}\,t\right)\,\Theta\left(t_0 - t\right)\,Q^a_{in}, \\ J^{\mu,a}_{out,(0)} &= g\,\frac{\bar{p}^\mu}{\bar{E}}\,\delta^{(3)}\left(\vec{x} - \frac{\vec{\bar{p}}}{\bar{E}}\,t\right)\,\Theta\left(t - t_0\right)\,Q^a_{out}. \end{aligned} \tag{5.2}$$

In Eq.(5.2), Q^a_{in} and Q^a_{out} are the color charges of the incoming and the outgoing quarks, respectively, and the overline is used here to denote the momentum and other related quantities of the outgoing quark. By current conservation, one has $Q^a_{in} = Q^a_{out}$ and $Q^{a\,2}_{in} = Q^{a\,2}_{out} = C_F$. Here we will follow the approach of the last chapter and we start again by the vacuum. By linearizing the classical Yang-Mills equations, cf. Eq.(4.10), the solution of the classical gauge field at leading order of the strong coupling constant in momentum space reads

$$-k^2\,A^{i,a}_{(0)} = 2\,i\,g\left(\frac{\kappa^i}{\boldsymbol{\kappa}^2}\,Q^a_{in} - \frac{\bar{\kappa}^i}{\bar{\boldsymbol{\kappa}}^2}\,Q^a_{out}\right), \tag{5.3}$$

where the forms of the transverse vectors κ^i and $\bar{\kappa}^i$ are the same as in Eq.(4.19), but here the transverse vectors describe the transverse momenta of the gluon relative to the ones of the incoming and the outgoing quarks, respectively. Taking the solution of the classical gauge field, i.e. Eq.(5.3), into the reduction formula and summing over the physical polarizations, the vacuum spectrum of a soft gluon radiation in the quark scattering process without color transfer in t-channel reads

$$\omega\,\frac{\mathrm{d}N^{\mathrm{vac}}}{\mathrm{d}^3\vec{k}} = \frac{\alpha_s\,C_F}{\left(2\,\pi\right)^2\,\omega^2}\left(\mathcal{R}_{in} + \mathcal{R}_{out} - 2\,\mathcal{J}\right), \tag{5.4}$$

where

$$\mathcal{R}_{in} \equiv \frac{4\,\omega^2}{\boldsymbol{\kappa}^2}, \qquad \mathcal{R}_{out} \equiv \frac{4\,\omega^2}{\bar{\boldsymbol{\kappa}}^2} \tag{5.5}$$

are the independent radiation spectra off the incoming and the outgoing quarks, respectively, and

$$\mathcal{J} \equiv 4\,\omega^2\,\frac{\boldsymbol{\kappa}\cdot\bar{\boldsymbol{\kappa}}}{\boldsymbol{\kappa}^2\,\bar{\boldsymbol{\kappa}}^2} \tag{5.6}$$

denotes the interference between the incoming and the outgoing quarks. The same as the case of the s-channel antenna radiation in vacuum, one can separate the collinear divergences belonging to either the incoming quark or the outgoing one by defining the coherent spectra $\mathcal{P}_{in}^{\rm vac} = \mathcal{R}_{in} - \mathcal{J}$ and $\mathcal{P}_{out}^{\rm vac} = \mathcal{R}_{out} - \mathcal{J}$, respectively. The vacuum spectrum in Eq.(5.4) presents both the soft and the collinear divergences. In addition, the inclusive spectrum is suppressed at large gluon emission angles due to the destructive interference between the emitters, i.e. taking the azimuthal angle average along the longitudinal axis of, e.g. the incoming quark:

$$\langle dN_{in}^{\rm vac}\rangle_{\varphi} = \frac{\alpha_s\,C_F}{\pi}\,\frac{\mathrm{d}\omega}{\omega}\,\frac{\sin\theta\,\mathrm{d}\theta}{1-\cos\theta}\,\Theta\left(\cos\theta-\cos\theta_{qq}\right), \tag{5.7}$$

where the gluon emission angle is defined as before, and θ_{qq} is the scattering angle between the incoming and the outgoing quarks which is related to the virtuality of the off-shell particle in the hard scattering, e.g. the virtual photon in Deep Inelastic Scattering. Eq.(5.7) indicates that the gluon emissions are confined in the cone set by the scattering angle along either the incoming or the outgoing quark. The procedure described here can be extended to higher orders and constitutes the basic building block for the construction of a coherent parton branching formalism [31].

5.2 t-channel antenna radiation in a medium

5.2.1 Dilute medium set-up

One way to include medium modifications to the t-channel antenna radiation spectrum is to consider an asymptotic highly energetic quark produced in the remote past that suffers a hard scattering at $x^+ = x_0^+$ and afterwards

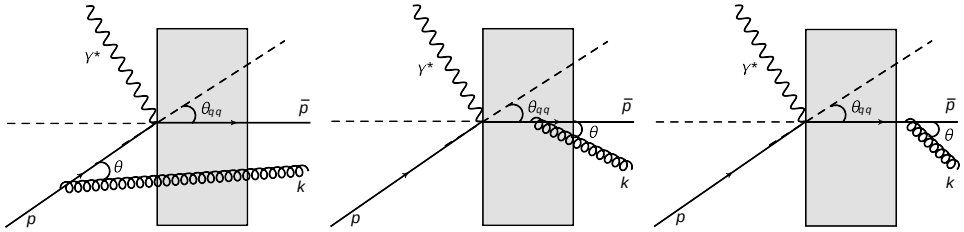

Figure 5.2: Medium-induced soft gluon radiation in the quark scattering process without color transfer in t-channel [3]

traverses a static color deconfined medium of finite size $L^+ = \sqrt{2}\,L$. Here the color deconfined medium is assumed to appear at exactly the same moment as the hard scattering, i.e. at $x^+ = x_0^+$. Gluon is radiated either before or after the hard scattering (see figure 5.2 for an illustration of the physical configuration under consideration). In the classical gauge field approximation, the quark fields act as a perturbation around the strong medium field (the shaded rectangle in figure 5.2). The total field is written as

$$A \equiv A_{\rm med} + A_{(0)} + A_{(1)}, \tag{5.8}$$

where $A_{(0)}$ is the gauge field of the quarks in vacuum, and $A_{(1)}$ is the induced gauge field, i.e. the response of the medium field at first order. The medium field in Eq.(5.8) is the solution of the 2-dimensional Poisson equation, cf. Eq.(4.30). In Fourier transform the medium field reads

$$A^-_{\rm med}\left(x^+,\mathbf{x}\right) = \int \frac{{\rm d}^4 q}{\left(2\,\pi\right)^4}\, 2\,\pi\,\delta\left(q^+\right)\, A^-_{\rm med}\left(q^-,\mathbf{q}\right)\, e^{-i\,q\cdot x}, \tag{5.9}$$

At first order in the medium field, the continuity equation for the induced eikonalized current is the same as in Eq.(4.34). Its solution can be written as the sum of the currents of the incoming and the outgoing quarks:

$$J^\mu_{(1)} = i\,g\,\frac{p^\mu}{p\cdot\partial}\left[A^-_{\rm med}, J^+_{in,(0)}\right] + i\,g\,\frac{\bar{p}^\mu}{\bar{p}\cdot\partial}\left[A^-_{\rm med}, J^+_{out,(0)}\right], \tag{5.10}$$

where $J^+_{in,(0)}$ and $J^+_{out,(0)}$ are given by the expressions in Eq.(5.2). The current of the incoming quark at first order in the medium field is

$$J^{\mu,a}_{in,(1)}\left(k\right) = \left(i\,g\right)^2 \frac{p^\mu}{-i\,p\cdot k}\int\frac{\mathrm{d}^4q}{\left(2\,\pi\right)^4}\,\frac{p^+}{p\cdot\left(k-q\right)-i\,\epsilon}\,i \\ \times\left[T\cdot A^-_{\mathrm{med}}\left(q\right)\right]^{ab}Q^b_{in}, \tag{5.11}$$

where $\left[T\cdot A^-_{\mathrm{med}}\left(q\right)\right]^{ab}Q^b_{in} \equiv -i\,f^{abc}\,A^c_{\mathrm{med}}\left(q\right)\,Q^b_{in}$. An analogous expression is readily obtained for the current of the outgoing quark. After linearizing the classical Yang-Mills equations in α_s, the equation of motion for the transverse components of the induced gauge field reads

$$\partial^2 A^i_{(1)} - 2\,i\,g\left[A^-_{\mathrm{med}},\partial^+\,A^i_{(0)}\right] = -\frac{\partial^i}{\partial^+}\,J^+_{(1)} + J^i_{(1)}. \tag{5.12}$$

While the calculation of the amplitude associated to the outgoing quark is identical to the one associated to the quark in the case of the s-channel antenna, the treatment to the incoming quark is slightly different due to the difference of the Heaviside step functions in Eq.(5.2). The solution of Eq.(5.12) in momentum space for the induced gauge field of the incoming quark can be written as

$$-k^2\,A^-_{in,(1)} = 2\,g\int\frac{\mathrm{d}^4q}{\left(2\,\pi\right)^4}\,\left(k-q\right)^+\left[A^-_{\mathrm{med}}\left(q\right),A^i_{in,(0)}\left(k-q\right)\right] \\ -\frac{k^i}{k^+}\,J^+_{in,(1)} + J^i_{in,(1)}, \tag{5.13}$$

where $A^i_{in,(0)}\left(k-q\right)$ can be identified with the vacuum field induced by the incoming quark, cf. Eq.(5.3). Integrating out q^- in Eq.(5.13) and assuming that the medium starts to appear at $x^+ = x^+_0$, one obtains

$$-k^2\,A^{i,a}_{in,(1)} = -2\,i\,g^2\int\frac{\mathrm{d}^2\mathbf{q}}{\left(2\,\pi\right)^2}\int_{x^+_0}^{+\infty}\mathrm{d}x^+\left[T\cdot A^-_{\mathrm{med}}\left(x^+,\mathbf{q}\right)\right]^{ab} \\ \times Q^b_{in}\,e^{\,i\left[k^- - \frac{(\mathbf{k}-\mathbf{q})^2}{2\,k^+}\right]x^+}\,\frac{\left(\kappa-q\right)^i}{\left(\boldsymbol{\kappa}-\mathbf{q}\right)^2}. \tag{5.14}$$

On the other hand, the solution of the induced gauge field due to the outgoing quark reads [17, 26]

$$
\begin{aligned}
-k^2\, A^{i,a}_{out,(1)} = & \, 2\, i\, g^2 \int \frac{\mathrm{d}^2\mathbf{q}}{(2\,\pi)^2} \int_{x_0^+}^{+\infty} \mathrm{d}x^+ \left[T \cdot A^-_{\mathrm{med}}\left(x^+, \mathbf{q}\right)\right]^{ab} \\
& \times Q^b_{out}\, e^{\, i\left[k^- - \frac{(\mathbf{k}-\mathbf{q})^2}{2\,k^+}\right] x^+} \\
& \times \left\{ \frac{(\bar{\kappa} - q)^i}{(\bar{\boldsymbol{\kappa}} - \mathbf{q})^2} \left[1 - \exp\left(i\, \frac{(\bar{\boldsymbol{\kappa}} - \mathbf{q})^2}{2\,k^+}\, x^+\right)\right] \right. \\
& \left. + \frac{\bar{\kappa}^i}{\bar{\boldsymbol{\kappa}}^2} \exp\left(i\, \frac{(\bar{\boldsymbol{\kappa}} - \mathbf{q})^2}{2\,k^+}\, x^+\right) \right\},
\end{aligned}
\tag{5.15}
$$

which is identical to Eq.(4.40) as expected. By using the reduction formula together with the induced gauge fields for both the incoming and the outgoing quarks, one gets the total scattering amplitude for soft gluon radiation off the incoming and the outgoing quarks:

$$
\begin{aligned}
\mathcal{M}^a_\lambda = & \, \mathcal{M}^a_{\lambda,in} + \mathcal{M}^a_{\lambda,out} \\
= & \, -2\, i\, g^2 \int \frac{\mathrm{d}^2\mathbf{q}}{(2\,\pi)^2} \int_{x_0^+}^{L^+} \mathrm{d}x^+ \left[T \cdot A^-_{\mathrm{med}}\left(x^+, \mathbf{q}\right)\right]^{ab} \left\{ Q^b_{in}\, \frac{\boldsymbol{\kappa} - \mathbf{q}}{(\boldsymbol{\kappa} - \mathbf{q})^2} \right. \\
& \left. - Q^b_{out} \left[\frac{\bar{\boldsymbol{\kappa}} - \mathbf{q}}{(\bar{\boldsymbol{\kappa}} - \mathbf{q})^2} - \bar{\mathbf{L}} \exp\left(i\, \frac{(\bar{\boldsymbol{\kappa}} - \mathbf{q})^2}{2\,k^+}\, x^+\right) \right] \right\}.
\end{aligned}
\tag{5.16}
$$

Here we use the definition of the transverse components of the Lipatov vertex in the light cone gauge:

$$
\bar{\mathbf{L}} = \frac{\bar{\boldsymbol{\kappa}} - \mathbf{q}}{(\bar{\boldsymbol{\kappa}} - \mathbf{q})^2} - \frac{\bar{\boldsymbol{\kappa}}}{\bar{\boldsymbol{\kappa}}^2}. \tag{5.17}
$$

From Eq.(5.16), one observes that the contribution to the total scattering amplitude from the incoming and the outgoing quarks is not symmetric. Such difference arises due not only to kinematic constraints but also because gluons off the outgoing quark may be radiated and rescatter with the color deconfined medium, while gluons off the incoming quark are created prior to their passage through the medium, and their momenta are going to be simply reshuffled once they interact with the medium during the interval $x_0^+ \leq x^+ \leq L^+$. To evaluate the cross section one must average the medium field and include the virtual corrections. The medium average is performed in the same fashion as in Eq.(4.44). The contact terms required by unitarity

are the interferences between the gluon emission amplitude in vacuum and the one accompanied by two scatterings with the medium with no net momentum transfer. These can be added to the radiative cross section through a redefinition of the potential, cf. Eq.(4.49).

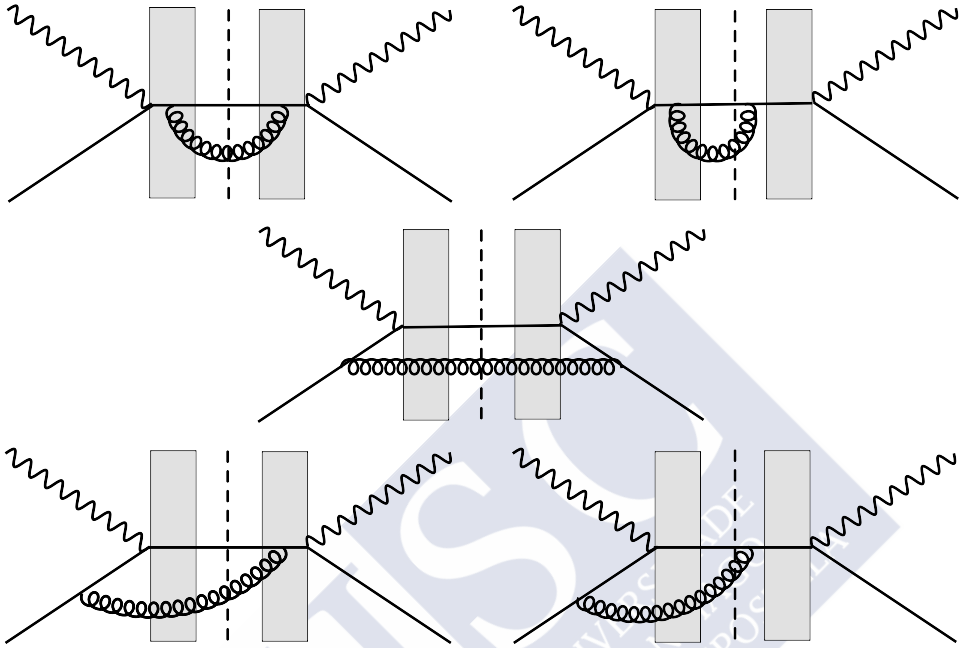

Figure 5.3: All types of Feynman diagrams contributing to the radiative cross section in the light-cone gauge [3]

When calculating the radiative cross section in the light-cone gauge, the contributions to the gluon spectrum can be separated according to the position of the emission vertex in the amplitude and its complex conjugate. In our setup, we have three possible cases. First: Gluons radiated independently off the incoming quark, which corresponds to the square of the amplitude where the emission vertex is before the hard scattering, so that the gluon entering the medium is fully formed. Second: Gluons radiated independently off the outgoing quark, which corresponds to the square of the amplitudes with both emission vertices after the hard scattering. Third: Gluons radiated in a fashion of inference between the cases where one gluon emission vertex is before the hard scattering in amplitude and another is after the hard scattering in the complex conjugate of the amplitude. Figure 5.3 illustrates this classification in terms of Feynman diagrams. Note that the same result as presented here can be obtained by using the Feynman diagram language instead of the classical gauge field approximation.

In this case, there are 2 vacuum amplitudes, 5 amplitudes with one scattering and 7 amplitudes with two scatterings that contribute to the contact terms. The medium-induced gluon radiation spectrum is proportional to the sum of the medium averages, which consists of 39 diagrams in total. After squaring the amplitude, averaging the colors, summing over the physical polarizations and considering the interferences, the spectrum of the medium-induced gluon radiation reads

$$\begin{aligned}
\omega \frac{\mathrm{d}N^{\mathrm{med}}}{\mathrm{d}^3\vec{k}} = \frac{4\,\alpha_s\,C_F\,\hat{q}}{\pi} \int \frac{\mathrm{d}^2\mathbf{q}}{(2\,\pi)^2}\,\mathcal{V}^2\left(\mathbf{q}\right) \int_0^{L^+} \mathrm{d}x^+ \left\{ \frac{1}{\left(\boldsymbol{\kappa}-\mathbf{q}\right)^2} - \frac{1}{\boldsymbol{\kappa}^2} \right. \\
+ 2\,\frac{\bar{\boldsymbol{\kappa}}\cdot\mathbf{q}}{\bar{\boldsymbol{\kappa}}^2\left(\bar{\boldsymbol{\kappa}}-\mathbf{q}\right)^2}\left[1-\cos\left(\frac{\left(\bar{\boldsymbol{\kappa}}-\mathbf{q}\right)^2}{2\,k^+}\,x^+\right)\right] \\
+ 2\left[\frac{\bar{\boldsymbol{\kappa}}\cdot\boldsymbol{\kappa}}{\bar{\boldsymbol{\kappa}}^2\,\boldsymbol{\kappa}^2} - \frac{\bar{\boldsymbol{\kappa}}\cdot\left(\boldsymbol{\kappa}-\mathbf{q}\right)}{\bar{\boldsymbol{\kappa}}^2\left(\boldsymbol{\kappa}-\mathbf{q}\right)^2}\right] \\
\left. + 2\left[\frac{\bar{\boldsymbol{\kappa}}\cdot\left(\boldsymbol{\kappa}-\mathbf{q}\right)}{\bar{\boldsymbol{\kappa}}^2\left(\boldsymbol{\kappa}-\mathbf{q}\right)^2} - \frac{\left(\bar{\boldsymbol{\kappa}}-\mathbf{q}\right)\cdot\left(\boldsymbol{\kappa}-\mathbf{q}\right)}{\left(\bar{\boldsymbol{\kappa}}-\mathbf{q}\right)^2\left(\boldsymbol{\kappa}-\mathbf{q}\right)^2}\right]\left[1-\cos\left(\frac{\left(\bar{\boldsymbol{\kappa}}-\mathbf{q}\right)^2}{2\,k^+}\,x^+\right)\right] \right\},
\end{aligned} \tag{5.18}$$

where the medium transport parameter is defined in Eq.(4.46) and one sets $x_0^+ = 0$. The first line in Eq.(5.18) is the contribution to the gluon radiation spectrum off the incoming quark. It corresponds to the bremsstrahlung of the accelerated color charge, which subsequently undergoes rescattering. The second line in Eq.(5.18) corresponds to emissions off the outgoing quark. It is identified with the so-called GLV spectrum [25] or equivalently the first order in the opacity expansion of the BDMPS-Z-W spectrum [24]. The novel contributions associated to the interferences between both emitters are contained in the rest. Note that the interference contributions show both the soft and the collinear divergencies. We observe that in the limit when the scattering angle between both emitters vanishes, i.e. $\theta_{qq} \to 0$, the medium-induced gluon radiation spectrum (see Eq.(5.18)) reduces to the well known Gunion-Bertsch spectrum [37] (see Eq.(4.2)). This is expected since the Gunion-Bertsch spectrum is the genuine induced emission due to a scattering of an asymptotic charge with the medium.

In our notation, the hard emission is the one in which the emitted gluon undergoes no scattering with the color deconfined medium. The pattern of interferences between the hard and the medium-induced emissions is involved. In order to better elucidate its physics, we consider here three interesting asymptotic regimes, namely the incoherent, the coherent and the soft limits. The GLV spectrum shows an interplay between the hard and

the medium-induced gluon emissions. The phase achieved by color rotation relates the effective formation time of the emitted gluon $\tau_f \sim \omega/\left(\bar{\boldsymbol{\kappa}}-\mathbf{q}\right)^2$ to the position of the interaction with the medium which is the main cause of the interference between both mechanisms of emission. The spectrum reaches its maximum in the incoherent limit $\tau_f \ll L^+$, where these mechanisms can be clearly separated since the phases cancel. In addition, this limit permits a clear probabilistic interpretation [24]. When one takes the incoherent limit, the contribution with the cosines in Eq.(5.18) can be neglected and the spectrum can be written as

$$\omega \left.\frac{\mathrm{d}N^{\mathrm{med}}}{\mathrm{d}^3\vec{k}}\right|_{\tau_f \ll L^+} = \frac{4\,\alpha_s\,C_F\,\hat{q}}{\pi}\int \frac{\mathrm{d}^2\mathbf{q}}{\left(2\,\pi\right)^2}\,\mathcal{V}^2\left(\mathbf{q}\right)\int_0^{L^+}\mathrm{d}x^+ \times\left[\bar{\mathbf{L}}^2+\mathbf{C}^2\left(\mathbf{k}-\mathbf{q}\right)-\mathbf{C}^2\left(\mathbf{k}\right)\right], \tag{5.19}$$

where we use the definition of the transverse emission current (an identical definition follows for $\mathbf{C}\left(\mathbf{k}-\mathbf{q}\right)$ by changing $\mathbf{k}\to\mathbf{k}-\mathbf{q}$, cf. Eq.(4.50))

$$\mathbf{C}\left(\mathbf{k}\right)=\frac{\boldsymbol{\kappa}}{\boldsymbol{\kappa}^2}-\frac{\bar{\boldsymbol{\kappa}}}{\bar{\boldsymbol{\kappa}}^2}. \tag{5.20}$$

Note that the gluon spectrum in vacuum, i.e. Eq.(5.4), can be rewritten in terms of $\mathbf{C}^2\left(\mathbf{k}\right)$, so this term takes into account the independent hard gluon emissions as well as their interferences. A similar interpretation applies for $\mathbf{C}^2\left(\mathbf{k}-\mathbf{q}\right)$ but by the transverse momentum broadening of the emitted on-shell gluon due to its rescattering with the medium. The incoherent limit of the gluon spectrum given by Eq.(5.19) allows a similar probabilistic interpretation as in the case of the GLV spectrum but further including the interferences. In the incoherent limit, one observes two mechanisms of gluon radiation. The first term of Eq.(5.19) corresponds to the genuine medium-induced gluon radiation off an asymptotic quark that suffers a scattering with the medium, i.e. the Gunion-Bertsch spectrum. The last two terms in Eq.(5.19) correspond to the radiation pattern in Eq.(5.4), i.e. the bremsstrahlung associated to the hard scattering, followed by the radiated on-shell gluon suffering a classical sequential process of rescattering with the medium. In addition, these last two terms include the interferences between the incoming and the outgoing quarks.

For the large formation time $\tau_f \gg L^+$, the medium-induced gluon radiation spectrum off a quark created at finite time is completely suppressed due to the LPM effect. When the coherent limit is taken for the gluon spectrum (see Eq.(5.18)), the cosine does not oscillate, i.e. $\cos\left(L^+/\tau_f\right)\to 1$, and therefore the gluon spectrum is further simplified to be

$$\omega \frac{\mathrm{d}N^{\mathrm{med}}}{\mathrm{d}^3\vec{k}}\bigg|_{\tau_f \gg L^+} = \frac{4\,\alpha_s\,C_F\,\hat{q}}{\pi}\int \frac{\mathrm{d}^2\mathbf{q}}{(2\,\pi)^2}\,\mathcal{V}^2\,(\mathbf{q})\int_0^{L^+}\mathrm{d}x^+ \times\left[\frac{1}{(\boldsymbol{\kappa}-\mathbf{q})^2}-\frac{1}{\boldsymbol{\kappa}^2}+2\,\frac{\bar{\boldsymbol{\kappa}}\cdot\boldsymbol{\kappa}}{\bar{\boldsymbol{\kappa}}^2\,\boldsymbol{\kappa}^2}-2\,\frac{\bar{\boldsymbol{\kappa}}\cdot(\boldsymbol{\kappa}-\mathbf{q})}{\bar{\boldsymbol{\kappa}}^2\,(\boldsymbol{\kappa}-\mathbf{q})^2}\right]. \tag{5.21}$$

The first two terms in Eq.(5.21) correspond simply to the transverse momentum broadening of the on-shell gluon emission off the incoming quark and the conservation of the gluon radiation probability. The last two terms are the interferences between the initial and the final states. The fact that there is no contribution exclusively associated to the outgoing quark, i.e. the GLV spectrum, is caused mainly by the destructive interferences between the hard and the medium-induced emissions taking place completely inside the medium. So, in this case the LPM effect becomes subleading and some of the interferences between the initial and the final quarks remain. Note that if one integrates out $\mathbf{k}$ in Eq.(5.21) and neglects the finite kinematics of the gluon, one can recover the result shown in Eq.(3.4) of [38], where a similar setup as the one presented here has been advocated to be of relevance for the energy loss of quarkonia in nuclear matter. In the coherent limit the position of the scattering center becomes close to the hard scattering point where the medium starts, and thus it looks as if the hard gluon radiated off the outgoing quark does not rescatter and is produced completely outside the medium. This hard gluon produced outside the medium is precisely the one that interferes with any of the hard and the medium-induced gluon emissions associated to the incoming quark.

The medium-induced gluon spectrum (5.18) can be further simplified in the soft limit $\omega \to 0$. In this limit, the dominating contribution to the cross section is

$$\lim_{\omega\to 0}|\mathcal{M}|^2 = \frac{4\,\alpha_s\,C_F\,\hat{q}}{\pi}\left(2\,\frac{\boldsymbol{\kappa}\cdot\bar{\boldsymbol{\kappa}}}{\boldsymbol{\kappa}^2\,\bar{\boldsymbol{\kappa}}^2}-\frac{1}{\boldsymbol{\kappa}^2}\right). \tag{5.22}$$

From this result, one can conclude that in the soft limit the medium-induced gluon emissions contain the same structures as the vacuum ones (see Eq.(5.4)). Thus, in the soft limit the medium-induced gluon radiation spectrum can be written as

$$\omega \frac{\mathrm{d}N^{\mathrm{med}}}{\mathrm{d}^3\vec{k}}\bigg|_{\omega\to 0} = \frac{\alpha_s\,C_F}{(2\,\pi)^2}\,\Delta\,(2\,\mathcal{J}-\mathcal{R}_{in})\,, \tag{5.23}$$

where $\Delta = \hat{q}\, L^+/m_D^2 \approx L/\lambda$ is the opacity expansion parameter, i.e. the effective number of scattering centers. In the soft limit, the full gluon spectrum in the presence of a medium is

$$\mathrm{d}N^{\mathrm{tot}}\big|_{\omega\to 0} = \left(\mathrm{d}N^{\mathrm{vac}} + \mathrm{d}N^{\mathrm{med}}\right)\big|_{\omega\to 0}. \tag{5.24}$$

Following the similar procedure as the vacuum case, one separates the independent and interference contributions to the incoming and the outgoing quarks in such a way that the total spectrum reads

$$\omega\,\frac{\mathrm{d}N^{\mathrm{tot}}}{\mathrm{d}^3\vec{k}}\bigg|_{\omega\to 0} = \frac{\alpha_s\, C_F}{(2\,\pi)^2}\left(\mathcal{P}_{in}^{\mathrm{tot}} + \mathcal{P}_{out}^{\mathrm{tot}}\right)\bigg|_{\omega\to 0}, \tag{5.25}$$

where

$$\begin{aligned} \mathcal{P}_{in}^{\mathrm{tot}} &= (1-\Delta)\,(\mathcal{R}_{in} - \mathcal{J})\,, \\ \mathcal{P}_{out}^{\mathrm{tot}} &= \mathcal{R}_{out} - (1-\Delta)\,\mathcal{J}. \end{aligned} \tag{5.26}$$

In the absence of a medium, i.e. $\Delta \to 0$, one naturally recovers the radiation pattern observed in vacuum, i.e. Eq.(5.4). In the opposite case of an opaque medium, i.e. $\Delta \to 1$, there is a significant reduction of soft gluon coherent radiation from the incoming quark, which is in qualitative agreement with the expectations from the saturation of parton densities [39]. Note that the boundary condition $\Delta \leq 1$, although not evident in the first order in the opacity expansion, is given by unitarity. When multiple soft scatterings, i.e. dense medium, are considered, we expect that the soft gluon emission from the incoming quark to be exponentially suppressed. In the soft limit, the total spectrum (5.25) presents both the soft and the collinear divergences. The separation of the gluon radiation, i.e. Eq.(5.26), allows not only a separation of the collinear divergences but also a simple and intuitive probabilistic interpretation. $\mathcal{P}_{in}^{\mathrm{tot}}$ is the gluon emission off the incoming quark reduced by the probability Δ that an interaction of the emitted on-shell gluon occurs inside the medium. After performing an azimuthal angle average, $\mathcal{P}_{in}^{\mathrm{tot}}$ has the same angular ordering constraint as the vacuum case, i.e. the emitted gluons will be confined inside a cone set by the scattering angle around the incoming quark, but the soft gluon radiation decreases by a quantity proportional to Δ. $\mathcal{P}_{out}^{\mathrm{tot}}$ accounts for the partial decoherence of the emitted gluon due to the scatterings with the color deconfined medium.

Such decoherence is measured by the probability of an interaction with the medium Δ. $\mathcal{P}_{out}^{\rm tot}$ shows resemblance to the radiation pattern already observed for the s-channel antenna radiation in a dilute color deconfined medium [17, 26], which tells us that the interaction with the medium opens more phase space for large angle emissions and there is a strict geometrical separation between the vacuum and the medium-induced radiation, a property called anti-angular ordering. The soft limit remains valid for a range of finite gluon energies as far as $\omega\,\theta_{qq} \ll m_D$ and $|\mathbf{k}| \ll m_D$. Hence, the analysis for finite values of gluon energy involves two regimes related to the relevant scales of the problem, the scattering angle θ_{qq} between the incoming and the outgoing quarks and the typical transverse momentum transfer $|\mathbf{q}| \sim m_D$ from the medium. So one has either $\theta_{qq} \lesssim m_D/\omega$ or $\theta_{qq} \gtrsim m_D/\omega$.

5.2.2 Dense medium set-up

In this section we outline the calculation of the emission amplitude by using the semiclassical methods of perturbative QCD. We introduce the notations followed through this work. This theoretical framework has shown to be a powerful tool in calculating observables involving soft gluon emissions at high energies [39, 41, 42]. Within this approach, soft gluon emissions can be seen as solutions of the linearized classical Yang Mills (CYM) equations in the presence of a background field (the target) and a color source which is a parton with large momentum fraction (the projectile). Through this work we limit ourselves to the eikonal approximation, which is valid as far as the gluon is soft relative to the parent partons. In addition we will also consider the region of small angles defined by $p^+,\, \bar{p}^+ \gg |\boldsymbol{p}|$, $|\bar{\boldsymbol{p}}| \gg k^+ \gg |\boldsymbol{k}|$, which is the interesting region in intrajet physics.
We first recall the standard reduction formula which relates the amplitude of gluon emission with 4-momentum $k = (w, \vec{k})$ with the classical gauge field A_μ^a (see for instance [14], pp. 217-224)

$$\mathcal{M}_\lambda^a(\vec{k}) = \lim_{k^2\to 0} \int d^4x\, e^{ik\cdot x}\, \Box_x\, A_\mu^a(x) \epsilon_\lambda^\mu(\vec{k}), \tag{5.27}$$

where $\epsilon_\lambda^\mu(\vec{k})$ is the gluon polarization vector. The classical gauge field A_μ^a is the solution of the classical Yang Mills (CYM) equations

$$[D_\mu, F^{\mu\nu}] = \mathcal{J}^\nu, \tag{5.28}$$

with $D_\mu \equiv \partial_\mu - igA_\mu$ and $F_{\mu\nu} \equiv \partial_\mu A_\nu - \partial_\nu A_\mu - ig[A_\mu, A_\nu]$. In addition to Eq.(5.28), one must consider the continuity equation for the classical color current $[D_\mu, \mathcal{J}^\mu] = 0$, which describes the space-time evolution of the projectiles. We concentrate on asymptotic states far from the region where

the physical process happens, i.e. at $x^+ \to \infty$. Therefore, Eq.(5.27) can be rewritten as [35, 42]

$$\mathcal{M}^a_\lambda(\vec{k}) = \lim_{x^+\to\infty} \int dx^- d^2\boldsymbol{x}\, e^{ik\cdot x}\, 2\partial^+_x \boldsymbol{A}^a(x)\cdot\boldsymbol{\epsilon}_\lambda(\vec{k})\,. \tag{5.29}$$

We perform our calculations in the light-cone gauge (LCG) $A^+ = 0$. Only the transverse polarization contributes to the radiative cross-section since $\sum_\lambda \epsilon^i_\lambda(\epsilon^j_\lambda)^* = \delta^{ij}$, where $i(j) = 1, 2$. Finally, the gluon spectrum reads as

$$(2\pi)^3 2k^+ \frac{dN}{d^3k} = \sum_{\lambda=1,2} |\mathcal{M}^a_\lambda(\vec{k})|^2, \tag{5.30}$$

where the phase space volume in momentum space is $d^3k \equiv d^2\boldsymbol{k}\, dk^+$. We first review within this approach the coherence pattern in DIS for the singlet case. Then we describe the set-up implemented in this work to study the medium modifications to the interference pattern between the initial and the final state radiation.

Let us first discuss a DIS process when there is no color transfer in the t-channel exchange (e.g. an electroweak quark scattering) at finite angle θ_{qq}. We denote the t-channel scattering in what follows as the *hard scattering*. In the absence of a QCD medium, the classical eikonalized current that describes the quark current that scatters before (bef) or after (aft) the hard scattering at $x_0^+ = 0$ reads as $\mathcal{J}^\mu_{(0)} = \mathcal{J}^\mu_{bef,(0)} + \mathcal{J}^\mu_{aft,(0)}$, where $\mathcal{J}^\mu_{bef,(0)}$ and $\mathcal{J}^\mu_{aft,(0)}$ are

$$\mathcal{J}^{\mu,a}_{bef,(0)}(x) = g u^\mu \Theta(x_0^+ - x^+)\delta(x^- - u^- x^+)\delta^{(2)}(\boldsymbol{x} - \boldsymbol{u}x^+) Q^a_{bef}, \tag{5.31a}$$

$$\mathcal{J}^{\mu,a}_{aft,(0)}(x) = g \bar{u}^\mu \Theta(x^+ - x_0^+)\delta(x^- - \bar{u}^- x^+)\delta^{(2)}(\boldsymbol{x} - \bar{\boldsymbol{u}}x^+) Q^a_{aft} \tag{5.31b}$$

In the last expression we have used the definition of the 4-velocity for each parton in the light-cone (LC) coordinates $u^\mu = p^\mu/p^+ \equiv (1, u^-, \boldsymbol{u})$ and $Q^a_{bef(aft)}$ denotes the color charge of the incoming (outgoing) parton. Color current conservation implies that $Q^a_{bef} = Q^a_{aft}$. An overline $^-$ is used hereafter to denote the related quantities of the outgoing parton. In momentum space, the total current $\mathcal{J}^\mu_{(0)}$ can be written as

$$J^\mu_{(0),a} = ig\left(-\frac{p^\mu}{p\cdot k + i\epsilon} Q^a_{bef} \;+\; \frac{\bar{p}^\mu}{\bar{p}\cdot k + i\epsilon} Q^a_{aft}\right). \tag{5.32}$$

By taking the square of the total color current, one gets the gluon spectrum [18]

$$k^+\frac{dN}{d^3k} = \frac{\alpha_s C_F}{\pi^2}\left(\frac{1}{\boldsymbol{\kappa}^2} + \frac{1}{\bar{\boldsymbol{\kappa}}^2} - 2\frac{\boldsymbol{\kappa}\cdot\bar{\boldsymbol{\kappa}}}{\boldsymbol{\kappa}^2\bar{\boldsymbol{\kappa}}^2}\right), \tag{5.33}$$

where $\boldsymbol{\kappa} = \boldsymbol{k} - x\boldsymbol{p}$ is the transverse momenta of the gluon with respect to the incoming quark (similar definition follows for the outgoing quark denoted by $\bar{\boldsymbol{\kappa}} = \boldsymbol{k} - x\bar{\boldsymbol{p}}$). In order to obtain the expression (5.33) we simply consider that the scalar product of two color charges is given by $Q_i Q_j = C_F$ for the color singlet configuration. A generalization for any color configuration is straightforward [18, 43].

In addition to the soft and collinear divergences, the gluon spectrum (5.33) is suppressed at large angles. This is due to the destructive interferences between both emitters and it is the physical origin of the angular ordering in parton cascades [18]. For a more complete discussion about the coherence phenomena in jet physics in vacuum see Refs. [18, 31, 43].

We are interested in calculating the gluon emission off a parton created in the remote past, which suffers a hard scattering at $x_0^+ = 0$ and subsequently passes through a dense QCD medium of finite size. For simplicity we consider that the medium is formed immediately after the hard scattering. The QCD medium is described by a background gauge field $\mathcal{A}^{a,-}_{med}$ which is a solution of the two dimensional Poisson equation $-\partial_{\boldsymbol{x}} A^{a,-}_{med} = \rho^a(x^+\boldsymbol{x})$, where $\rho^a(x^+, \boldsymbol{x})$ is the static distribution of medium color charges.

From the continuity equation $[D_\mu, \mathcal{J}^\mu] = 0$, one finds that the classical quark currents (5.31) behave different when a QCD medium is present. The eikonalized current (5.31b) of the outgoing parton gets color rotated due to the multiple soft scatterings with the background field $\mathcal{A}^-_{med}$ and its solution is given by [15, 41, 42]

$$\mathcal{J}^{\mu,a}_{aft}(x) = \mathcal{U}^{ab}(x^+, 0)\mathcal{J}^{b,\mu}_{aft,(0)}(x)\,, \tag{5.34}$$

where $\mathcal{U}^{ab}(x^+, 0)$ is a Wilson line in the adjoint representation and its general definition is

$$\mathcal{U}^{ab}(x^+, y^+, [\boldsymbol{r}]) = \mathcal{P}_\xi \exp\left[ig\int_{y^+}^{x^+} dz^+\, T\cdot\mathcal{A}^-_{med}\left(z^+, \boldsymbol{r}(z^+)\right)\right]\,, \tag{5.35}$$

where $\mathcal{P}_\xi$ denotes path ordering along ξ and the trajectory of the probe along the transverse path is denoted by $\boldsymbol{r} = \boldsymbol{u}z^+$.

In the case of the classical current of the incoming parton (5.31a), this one does not get color rotated even when a QCD medium is present since the latter is formed after the hard scattering. As we shall see below, the gluon radiation off the incoming parton will be simply a classical broadening process. In addition, we notice that the conservation of color charge is still satisfied $Q^{bef} = Q^{aft}$, i.e. the presence of the medium does not change the values of the color charges of the projectile as one expects.

We require to solve Eq.(5.28) for the total gauge field $A^\mu = \delta^{\mu-}\mathcal{A}^-_{med} + a^\mu$, where a^μ is a small perturbation around the background field $\mathcal{A}^-_{med}$. In the

light-cone gauge the linearized version of Eq.(5.28) are [41, 15]

$$\partial_- a^- + \partial_i a^i = -\tfrac{\mathcal{J}^+}{\partial_-}, \tag{5.36a}$$

$$\begin{aligned}\Box a^- - 2ig\big[\mathcal{A}^-_{med}, \partial_- a^-\big] - 2ig\big[a^i, \partial_i \mathcal{A}^-_{med}\big] \\ + i\,g[\mathcal{A}^-_{med}, \partial_- a^- + \partial_i a^i] = \mathcal{J}^-,\end{aligned} \tag{5.36b}$$

$$\big(\Box - 2ig(T\cdot\mathcal{A}^-_{med})\partial_-\big)a^i = \mathcal{J}^i_a - \partial^i\Big(\tfrac{\mathcal{J}^+}{\partial_-}\Big). \tag{5.36c}$$

In the last equations, the total current $\mathcal{J}^\mu = \mathcal{J}^\mu_{bef,(0)} + \mathcal{J}^\mu_{aft}$, where $\mathcal{J}^\mu_{bef,(0)}$ and $\mathcal{J}^\mu_{aft}$ are given by Eqs.(5.31a) and (5.34), respectively. Due to the gauge choice only the transverse components a^i contribute to the gluon emission amplitude, so we will concentrate only on its equation of motion. In principal one can also find the component a^- either by solving directly Eq.(5.36b) or use the constraint Eq.(5.36a) provided a known solution for a^i. See Refs.[41, 42], where this procedure was done in the CGC context. The solution of Eq.(5.36c) is given by [15, 42]

$$a^i_a(x^+, \boldsymbol{x}, k^+) = \int d^4y\, G_{ab}(x,y)\tilde{\mathcal{J}}^i_b(y), \tag{5.37}$$

where the modified current reads

$$\tilde{\mathcal{J}}^i = \mathcal{J}^i_a - \partial^i\Big(\frac{\mathcal{J}^+}{\partial_-}\Big). \tag{5.38}$$

and G_{ab} is the retarded Green function of the differential equation

$$\big(\Box - 2\,ig\,T\cdot A^-_{\text{med}}\partial^+\big)\; G(x,y) = \delta^{(4)}(x-y). \tag{5.39}$$

The background field does not depend on x^- which implies that the Green function $G(x,y)$ is invariant under translations along this direction. It is convenient to introduce here a Fourier transform of the Green function G_{ab}

$$\mathcal{G}(x^+, \boldsymbol{x}\,;\, y^+, \boldsymbol{y}|k^+) = \int_{-\infty}^{+\infty} dx^- e^{i(x-y)^- k^+} 2\partial^+_x G(x,y)\,, \tag{5.40}$$

which obeys the Schrödinger-like equation

$$\left(i\partial^- + \frac{\boldsymbol{\partial}^2}{2k^+} + gT\cdot A^-_{\text{med}}\right)\mathcal{G}(x^+, \boldsymbol{x}; y^+, \boldsymbol{y}|k^+) = i\delta(x^+ - y^+)\delta(\boldsymbol{x}-\boldsymbol{y}) \tag{5.41}$$

and its solution is written as a path integral along the transverse plane[15]

$$\mathcal{G}\left(x^+, \boldsymbol{x}; y^+, \boldsymbol{y}|k^+\right) = \int \mathcal{D}[\boldsymbol{r}]\,\exp\left[i\frac{k^+}{2}\int_{y^+}^{x^+} d\xi\,\dot{\boldsymbol{r}}^2(\xi)\right]\mathcal{U}(x^+, y^+; [\boldsymbol{r}])\,. \tag{5.42}$$

This propagator takes into account the non eikonal corrections to the emitted gluon due to the momentum broadening acquired due to the multiple soft scatterings with the medium. Finally, by taking the solution of the radiation field a^i (5.37) and replacing it into Eq.(5.29), we get the total gluon emission amplitude

$$\begin{aligned}\mathcal{M}^a_{tot,\lambda}(\vec{k}) &= \lim_{x^+\to\infty}\int d^2\boldsymbol{x}\, d^4y\, e^{i(k^-x^+-\boldsymbol{k}\cdot\boldsymbol{x})}\, e^{ik^+y^-} \\ &\times \mathcal{G}_{ab}\left(x^+,\boldsymbol{x};y^+,\boldsymbol{y}|k^+\right)\tilde{\mathcal{J}}^b(y)\cdot\boldsymbol{\epsilon}_\lambda\,. \end{aligned} \tag{5.43}$$

We can separate and interpret at the level of the amplitude what contribution comes from the parton before or after the hard scattering since the total current has two components (see figure 5.2). In the following we describe both contributions.
Depending on the longitudinal position y^+ where the gluon is emitted, the scattering amplitude of the outgoing parton can be split in two pieces: when $y^+\in[0,L^+]$ the emission occurs inside the medium (in), and when $y^+\geq L^+$ the emission takes place outside the medium (out) (see figure 5.2). This is easily achieved by separating the integral over y^+ as

$$\int_0^\infty dy^+ = \left(\int_0^{L^+} + \int_{L^+}^\infty\right) dy^+.$$

Then one replaces the color current (5.34) into Eq.(5.43) and after a bit of algebra, the scattering amplitude associated to the outgoing quark current reads as $\mathcal{M}^a_{\lambda,aft}(\vec{k}) = \mathcal{M}^a_{\lambda,in}(\vec{k}) + \mathcal{M}^a_{\lambda,out}(\vec{k})$, where [15, 35, 36]

$$\begin{aligned}\mathcal{M}^a_{\lambda,in}(\vec{k}) &= \frac{g}{k^+}\int d^2\boldsymbol{x} e^{i(k^-L^+-\boldsymbol{k}\cdot\boldsymbol{x})}\int_0^{L^+} dy^+ e^{ik^+\bar{u}^-y^+}\boldsymbol{\epsilon}_\lambda\cdot\left(i\boldsymbol{\partial}_y + k^+\bar{\boldsymbol{u}}\right) \\ &\times \mathcal{G}_{ab}\big(L^+,\boldsymbol{x},y^+,\boldsymbol{y}=\bar{\boldsymbol{u}}y^+|k^+\big)\,\mathcal{U}_{bc}(y^+,0)Q^{out}_c, \end{aligned} \tag{5.44a}$$

$$\mathcal{M}^a_{\lambda,out}(\vec{k}) = -2i\frac{\boldsymbol{\epsilon}_\lambda\cdot\bar{\boldsymbol{\kappa}}}{\bar{\boldsymbol{\kappa}}^2}\, e^{i(k\cdot\bar{\boldsymbol{u}})L^+}\,\mathcal{U}_{ab}(L^+,0)Q^{out}_b. \tag{5.44b}$$

It must be understood in Eq.(5.44a) that after performing the transverse derivatives $\partial_{\boldsymbol{y}}$ one sets $\boldsymbol{y}=\bar{\boldsymbol{u}}y^+$. The emission amplitude inside the medium $\mathcal{M}_{in}$ can be understood as a two-step process. Initially the highly energetic parton gets color precessed from 0 until y^+, which is taken into account by the product $\mathcal{U}_{bc}(y^+,0)Q^{out}_c$. Afterwards, the gluon is emitted at y^+ and it gets broadened until the edge of the medium at L^+. The physical information regarding the broadening of the gluon is encoded in the retarded propagator $\mathcal{G}$. In the case of $\mathcal{M}_{out}$ the projectile suffers completely the color rotation along the total length of the medium and the gluon is emitted by bremsstrahlung outside of the medium.

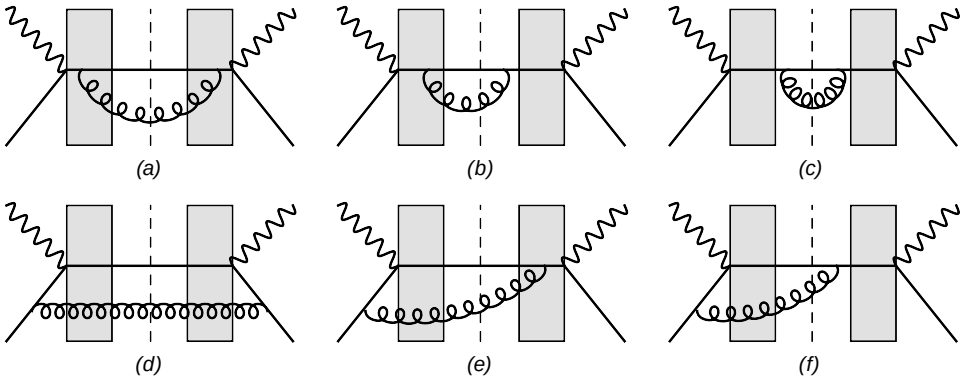

Figure 5.4: Different components of the gluon spectrum when a QCD medium is present: (a) the "in-in" component, (b) the "in-out" component, (c) the "out-out" component, (d) the "bef-bef" component, (e) the "bef-in" component and (f) the "bef-out" component. The dashed line represents the cut which divides the amplitude on the right and its complex conjugate on the left. See the text for further details.

As we shall see in the following, the square of amplitude associated to the outgoing parton given by the last expression will give us the BDMPS-Z spectrum [19, 23, 24, 32, 44, 45, 46].
The gluon radiation off the incoming parton happens completely before of the hard scattering, i.e. the longitudinal position $y^+ \in [-\infty, 0]$. The emission amplitude in this case is found after replacing Eq.(5.31a) into Eq.(5.43), so finally the contribution from the incoming parton reads

$$\begin{aligned} \mathcal{M}^a_{\lambda,bef}(\vec{k}) &= \frac{g}{k^+}\int_{x^+=\infty} d^2\boldsymbol{x}\, e^{i(k^- x^+ - \boldsymbol{k}\cdot\boldsymbol{x})}\int_{-\infty}^{0} dy^+ e^{ik^+u^-y^+} \\ &\times \boldsymbol{\epsilon}_\lambda\cdot\big(i\boldsymbol{\partial}_y + k^+\boldsymbol{u}\big)\mathcal{G}_{ab}\big(x^+,\boldsymbol{x},y^+,\boldsymbol{y}=\boldsymbol{u}y^+|k^+\big)Q_b^{in}. \end{aligned} \quad (5.45)$$

As we pointed out previously, there is no color precession in the classical current describing the incoming parton due to the absence of a QCD medium before the hard scattering. So $\mathcal{M}_{bef}$ takes into account the emission by bremsstrahlung of the gluon and its subsequent classical broadening considered in the propagator $\mathcal{G}$.
We conclude here by recalling that the total scattering amplitude is the sum of the contributions $\mathcal{M}_{tot} = \mathcal{M}_{aft} + \mathcal{M}_{bef}$, where $\mathcal{M}_{aft}$ and $\mathcal{M}_{bef}$ are given by Eqs. (5.44) and (5.45), respectively.
The contributions to the gluon spectrum can be separated in different components according to the longitudinal position where the gluon is emitted in the amplitude and the complex conjugate with respect to the hard scat-

tering, i.e. if the gluon emission happens before (bef) or after the hard scattering. When the emission takes place after the hard scattering, the gluon can be produced either inside (in) or outside (out) the QCD medium. Therefore, we have six different possibilities (see figure 5.2.2 for a sketch in terms of Feynman diagrams): the direct emissions of the incoming parton ("bef-bef") and the outgoing one ("in-in","in-out" and "out-out") and the interferences between both emitters ("bef-in" and "bef-out"). So the gluon spectrum is written as follows

USC UNIVERSIDADE DE SANTIAGO DE COMPOSTELA

$$k^+\frac{dN_{tot}}{d^3k} = \sum_{i=1}^{6} k^+\frac{dN_i}{d^3k}, \tag{5.46}$$

where the different contributions $k^+ dN_i/d^3k$ are given by

$$k^+\frac{dN_{bef-bef}}{d^3k} = \frac{\alpha_s\, C_F}{\pi^2}\,\mathrm{Re}\Bigg\{\int d^2\boldsymbol{r}d^2\boldsymbol{r}'d^2\boldsymbol{l}d^2\boldsymbol{l}'\frac{d^2\boldsymbol{p}}{(2\pi)^2}\frac{d^2\boldsymbol{p}'}{(2\pi)^2}e^{ik^+\boldsymbol{u}\cdot(\boldsymbol{l}-\boldsymbol{l}')}e^{-i\boldsymbol{k}\cdot(\boldsymbol{r}-\boldsymbol{r}')}e^{i(\boldsymbol{p}\cdot\boldsymbol{l}-\boldsymbol{p}'\cdot\boldsymbol{l}')}$$
$$\times\ \frac{\boldsymbol{p}\cdot\boldsymbol{p}'}{\boldsymbol{p}^2\,\boldsymbol{p}'^2}\frac{\big\langle\mathcal{G}\big(L^+,\boldsymbol{r},0,\boldsymbol{l}|k^+\big)\mathcal{G}^\dagger\big(L^+,\boldsymbol{r}',0,\boldsymbol{l}'|k^+\big)\big\rangle}{N_c^2-1}\Bigg\}, \tag{5.47a}$$

$$k^+\frac{dN_{in-in}}{d^3k} = \frac{\alpha_s\, C_F}{2\pi^2}\frac{1}{(k^+)^2}\,Re\Bigg\{\int_0^{L^+}dy^+\int_0^{y^+}dy'^+\int d^2\boldsymbol{z}d^2\boldsymbol{z}'e^{-i\boldsymbol{k}\cdot(\boldsymbol{z}-\boldsymbol{z}')}e^{ik^+\bar{u}^-(y^+-y'^+)}$$
$$\times\ \big(i\partial_{\boldsymbol{y}}+k^+\bar{\boldsymbol{u}}\big)\cdot\big(-i\partial_{\boldsymbol{y}'}+k^+\bar{\boldsymbol{u}}\big)$$
$$\times\ \frac{\big\langle\mathcal{G}\big(L^+,\boldsymbol{z},y^+,\boldsymbol{y}=\bar{\boldsymbol{u}}y^+|k^+\big)\mathcal{U}(y^+,y'^+)\mathcal{G}^\dagger\big(L^+,\boldsymbol{z}',y'^+,\boldsymbol{y}'=\bar{\boldsymbol{u}}y'^+|k^+\big)\big\rangle}{N_c^2-1}\Bigg\}, \tag{5.47b}$$

$$k^+\frac{dN_{in-out}}{d^3k} = \frac{\alpha_s\, C_F}{\pi^2}\frac{1}{k^+}\,\mathrm{Re}\Bigg\{ie^{i(k^--k\cdot\bar{\boldsymbol{u}})L^+}\int_0^{L^+}dy^+\int d^2\boldsymbol{z}e^{i(k^+\bar{u}^-y^+-\boldsymbol{k}\cdot\boldsymbol{z})}$$
$$\times\ \frac{\bar{\boldsymbol{\kappa}}\cdot(i\partial_{\boldsymbol{y}}+k^+\boldsymbol{u})}{\bar{\boldsymbol{\kappa}}^2}\frac{\big\langle\mathcal{G}\big(L^+,\boldsymbol{z},y^+,\boldsymbol{y}=\bar{\boldsymbol{u}}y^+|k^+\big)\mathcal{U}^\dagger\big(L^+,y^+\big)\big\rangle}{N_c^2-1}\Bigg\}, \tag{5.47c}$$

$$k^+\frac{dN_{out-out}}{d^3k} = \frac{\alpha_s\, C_F}{\pi^2}\,\frac{1}{\bar{\boldsymbol{\kappa}}^2}, \tag{5.47d}$$

$$k^+\frac{dN_{bef-in}}{d^3k} = \frac{\alpha_s\, C_F}{\pi^2}\frac{1}{k^+}\mathrm{Re}\Bigg\{i\int_0^{L^+}dy^+\int\frac{d^2\boldsymbol{k}'}{(2\pi)^2}\,d^2\boldsymbol{r}\,d^2\boldsymbol{z}\,d^2\boldsymbol{l}\,e^{-ik^+\bar{u}^-y^+}e^{i\boldsymbol{l}\cdot(\boldsymbol{k}'+k^+\bar{\boldsymbol{u}})}e^{-i\boldsymbol{k}\cdot(\boldsymbol{r}-\boldsymbol{z})}$$
$$\times\ \frac{\boldsymbol{k}'\cdot(-i\partial_{\boldsymbol{y}}+k^+\bar{\boldsymbol{u}})}{\boldsymbol{k}'^2}$$
$$\times\ \frac{\big\langle\mathcal{G}\big(L^+,\boldsymbol{r},0,\boldsymbol{l}|k^+\big)\mathcal{U}^\dagger\big(y^+,0\big)\mathcal{G}^\dagger\big(L^+,\boldsymbol{z},y^+,\boldsymbol{y}=\bar{\boldsymbol{u}}y^+|k^+\big)\big\rangle}{N_c^2-1}\Bigg\}, \tag{5.47e}$$

$$k^+\frac{dN_{bef-out}}{d^3k} = -2\frac{\alpha_s\, C_F}{\pi^2}\,Re\Bigg\{e^{iL^+(k^--k\cdot\bar{u})}\int\frac{d^2\boldsymbol{k}'}{(2\pi)^2}\,d^2\boldsymbol{r}\,d^2\boldsymbol{l}\,e^{-i\boldsymbol{k}\cdot\boldsymbol{r}}e^{i\boldsymbol{l}\cdot(\boldsymbol{k}'+k^+\boldsymbol{u})}$$
$$\times\ \frac{\boldsymbol{k}'\cdot\bar{\boldsymbol{\kappa}}}{\bar{\boldsymbol{\kappa}}^2\boldsymbol{k}'^2}\frac{\big\langle\mathcal{G}\big(L^+,\boldsymbol{r},0,\boldsymbol{l}|k^+\big)\mathcal{U}^\dagger\big(L^+,0\big)\big\rangle}{N_c^2-1}\Bigg\}. \tag{5.47f}$$

Eqs.(5.47) are valid for a given configuration of the classical gauge fields and therefore, it is necessary to average over the proper ensemble of the medium field configurations. Different techniques have been developed to carry out such averages. In this work we consider that the medium averages are given by a Gaussian white noise in the harmonic oscillator approximation which we describe in the following.

A necessary ingredient to calculate observables in high-energy AA collisions is related to the distribution of the color charges in the target. Since this information is not known from first principles, it is usually assumed that

the background field $\mathcal{A}^{-}_{med}$ is distributed along the medium as a Gaussian white noise, i.e.

$$\langle \mathcal{A}^{a}_{med}(x^+,\boldsymbol{q})\mathcal{A}^{*b}_{med}(x'^+,\boldsymbol{q}')\rangle = \delta^{ab} n(x^+)\delta(x^+-x'^+)\delta^{(2)}(\boldsymbol{q}-\boldsymbol{q}')\mathcal{V}^2(\boldsymbol{q}), \quad (5.48)$$

where $\mathcal{V}(\boldsymbol{q})$ is the medium interaction potential and $n(x^+)$ is the volume density of scattering centers. In this work we consider that for a static medium $\mathcal{V}(\boldsymbol{q})$ is a color screened Coloumb potential [19, 23, 24, 25, 32, 44, 47].
In the gaussian white noise approximation Eq.(5.48) and for the present calculation, we require to evaluate the correlators $\langle \mathcal{G}\mathcal{U}^\dagger\rangle$ and $\langle \mathcal{G}\mathcal{G}^\dagger\rangle$. The two point function $\langle \mathcal{G}\mathcal{U}^\dagger\rangle$ is related with the quark-gluon dipole in the medium and it is given by

$$\frac{1}{N_c^2-1}\langle \mathrm{Tr}\,\mathcal{G}(x^+,\boldsymbol{x};y^+,\boldsymbol{y}|k^+)\mathcal{U}^\dagger(x^+,y^+)\rangle = e^{ik^+\boldsymbol{u}\cdot\left[\bar{\boldsymbol{x}}(x^+)-\bar{\boldsymbol{y}}(y^+)\right]}$$
$$\times e^{ik^+u^-(x^+-y^+)}\mathcal{K}\left(x^+,\bar{\boldsymbol{x}}(x^+)\,;\,y^+,\bar{\boldsymbol{y}}(y^+)|k^+\right)\,, \quad (5.49)$$

where $\bar{\boldsymbol{x}}(x^+)=\boldsymbol{x}-\boldsymbol{u}x^+$ and $\bar{\boldsymbol{y}}(y^+)=\boldsymbol{y}-\boldsymbol{u}y^+$. The multiple soft scattering of the gluon with the medium is taken into account by evaluating the path integral $\mathcal{K}$ [16, 24, 32],

$$\mathcal{K}(x^+,\boldsymbol{x};y^+,\boldsymbol{y}|k^+) = \int \mathcal{D}[\boldsymbol{r}]\exp\left[\int_{y^+}^{x^+} d\xi\left(i\frac{k^+}{2}\dot{\boldsymbol{r}}^2(\xi)-\frac{1}{2}n(\xi)\sigma(\boldsymbol{r})\right)\right], \quad (5.50)$$

which describes the Brownian motion of the gluon in the transverse plane from $\boldsymbol{r}(y^+)=\boldsymbol{y}$ to $\boldsymbol{r}(x^+)=\boldsymbol{x}$. The correlator $\langle \mathcal{G}\mathcal{G}^\dagger\rangle$ is related to the medium average involving the gluon from y^+ to x^+ reads

$$\int d^2\boldsymbol{x}\int d^2\boldsymbol{x}'\frac{e^{-i\boldsymbol{k}\cdot(\boldsymbol{z}-\boldsymbol{z}')}}{N_c^2-1}\langle \mathrm{Tr}\,\mathcal{G}(x^+,\boldsymbol{z};y^+,\boldsymbol{x}|k^+)\mathcal{G}^\dagger(x^+,\boldsymbol{z}';y^+,\boldsymbol{y}|k^+)\,\rangle =$$
$$e^{-i\boldsymbol{k}\cdot(\boldsymbol{x}-\boldsymbol{y})}\mathcal{S}(x^+,y^+,\boldsymbol{x}-\boldsymbol{y})\,. \quad (5.51)$$

where the $\mathcal{S}(x^+,y^+,\boldsymbol{x}-\boldsymbol{y})$ is formally the scattering S-matrix for a dipole which is defined as

$$\mathcal{S}(x^+,y^+,\boldsymbol{x}-\boldsymbol{y}) = \exp\left[-\frac{1}{2}\int_{y^+}^{x^+} d\xi\, n(\xi)\,\sigma(\boldsymbol{x}-\boldsymbol{y})\right]\,. \quad (5.52)$$

Both the medium averages (5.50) and (5.51) depend on the dipole cross section $\sigma(\boldsymbol{r})$, whose general expression reads

$$\sigma(\boldsymbol{r}) = \int \frac{d^2\boldsymbol{q}}{(2\pi)^2}\mathcal{V}(\boldsymbol{q})\left[1-\cos(\boldsymbol{r}\cdot\boldsymbol{q})\right]. \quad (5.53)$$

Following the procedure usually found in the literature, we make use of the "harmonic oscillator approximation", where the product $n(\xi)\sigma(\boldsymbol{r}) \approx \frac{1}{2}\hat{q}\boldsymbol{r}^2$ [22]. This approximation is valid in the limit of multiple soft scatterings. Here $\hat{q}$ is the medium transport coefficient, which probes the accumulated transverse momentum squared per unit length. The harmonic oscillator approximation allows to calculate exactly the path integral (5.50) in a static and homogeneous medium which is given by

$$\mathcal{K}_{osc}(x^+, \boldsymbol{x}; y^+, \boldsymbol{y}|k^+) = \frac{A}{\pi i}\, \exp\left[i\, AB(\boldsymbol{x}^2 + \boldsymbol{y}^2) - 2iA\, \boldsymbol{x}\cdot\boldsymbol{y}\right]. \qquad (5.54)$$

where

$$A = \frac{k^+\Omega}{2\sin(\Omega(x^+ - y^+))}, \qquad B = \cos(\Omega(x^+ - y^+))\,. \qquad (5.55)$$

In these expressions the parameter $\Omega = \frac{(1-i)}{2}\sqrt{\frac{\hat{q}}{k^+}}$. In addition, the S-matrix for a dipole (5.52) in the harmonic oscillator approximation takes a simple form

$$\mathcal{S}_{osc}(y^+, x^+, \boldsymbol{r}) = \exp\left[-\frac{1}{4}\hat{q}\boldsymbol{r}^2(y^+ - x^+)\right]. \qquad (5.56)$$

Now we calculate the different components of the gluon spectrum (5.47) by evaluating the medium averages within the harmonic oscillator approximation as it was described above. After a lengthy calculation, the contributions

of the gluon spectrum can be finally written as

$$k^+\frac{dN_{bef-bef}}{d^3k} = \frac{\alpha_s\,C_F}{\pi^2}\,\mathrm{Re}\left\{\int d^2\boldsymbol{b}\frac{d^2\boldsymbol{k}'}{(2\pi^2)}\frac{e^{i(\boldsymbol{k}'-\boldsymbol{\kappa})\cdot\boldsymbol{b}}}{\boldsymbol{k}'^2}\mathcal{S}_{osc}(L^+,0,\boldsymbol{b})\right\}, \quad (5.57a)$$

$$k^+\frac{dN_{in-in}}{d^3k} = \frac{\alpha_s\,C_F}{2\pi^2}\frac{1}{(k^+)^2}\,Re\left\{\int_0^{L^+}dy'^+\int_0^{y'^+}dy^+\int d^2\boldsymbol{b}\,e^{i\bar{\boldsymbol{\kappa}}\cdot\boldsymbol{b}}\right.$$
$$\left.\times\ \mathcal{S}_{osc}(L^+,y'^+,\boldsymbol{b})\partial_{\boldsymbol{b}}\cdot\partial_{\boldsymbol{y}}\,\mathcal{K}_{osc}(y'^+,\boldsymbol{b},y^+,\boldsymbol{y}|k^+)\big|_{\boldsymbol{y}=0}\right\}, \quad (5.57b)$$

$$k^+\frac{dN_{in-out}}{d^3k} = -\frac{\alpha_s\,C_F}{\pi^2}\frac{1}{k^+}\mathrm{Re}\left\{\int_0^{L^+}dy^+\int d^2\boldsymbol{b}\,\frac{e^{-i\bar{\boldsymbol{\kappa}}\cdot\boldsymbol{b}}}{\bar{\boldsymbol{\kappa}}^2}\right.$$
$$\left.\times\ \bar{\boldsymbol{\kappa}}\cdot\partial_{\boldsymbol{y}}\,\mathcal{K}_{osc}(L^+,\boldsymbol{b},y^+,\boldsymbol{y}|k^+)\big|_{\boldsymbol{y}=0}\right\}, \quad (5.57c)$$

$$k^+\frac{dN_{out-out}}{d^3k} = \frac{\alpha_s\,C_F}{\pi^2}\,\frac{1}{\bar{\boldsymbol{\kappa}}^2}, \quad (5.57d)$$

$$k^+\frac{dN_{bef-in}}{d^3k} = \frac{\alpha_s\,C_F}{\pi^2}\frac{1}{k^+}\mathrm{Re}\left\{\int_0^{L^+}dy^+\int\frac{d^2\boldsymbol{k}'}{(2\pi)^2}\,d^2\boldsymbol{b}\,d^2\boldsymbol{l}\,e^{-i\bar{\boldsymbol{\kappa}}\cdot\boldsymbol{b}}e^{i\boldsymbol{k}'\cdot\boldsymbol{l}}e^{ik^+\delta\boldsymbol{n}\cdot\boldsymbol{l}}\right.$$
$$\left.\times\ \mathcal{S}_{osc}(L^+,y^+,\boldsymbol{b})\frac{\boldsymbol{k}'\cdot\partial_{\boldsymbol{b}}\mathcal{K}_{osc}(y^+,\boldsymbol{b},0,\boldsymbol{l}|k^+)}{\boldsymbol{k}'^2}\right\}, \quad (5.57e)$$

$$k^+\frac{dN_{bef-out}}{d^3k} = -2\,\frac{\alpha_s\,C_F}{\pi^2}Re\left\{\int\frac{d^2\boldsymbol{k}'}{(2\pi)^2}\,d^2\boldsymbol{b}\,d^2\boldsymbol{l}\frac{\boldsymbol{k}'\cdot\bar{\boldsymbol{\kappa}}}{\boldsymbol{k}'^2\,\bar{\boldsymbol{\kappa}}^2}e^{i\boldsymbol{k}'\cdot\boldsymbol{l}}e^{-i\bar{\boldsymbol{\kappa}}\cdot\boldsymbol{b}}e^{ik^+\delta\boldsymbol{n}\cdot\boldsymbol{l}}\right.$$
$$\left.\times\ \mathcal{K}_{osc}(L^+,\boldsymbol{b},0,\boldsymbol{l}|k^+)\right\}. \quad (5.57f)$$

Before the analysis regarding the formation time, we consider the limit when there is no QCD medium. In this limit $\hat{q}\to 0$ the different components of

the medium-induced gluon spectrum (5.57) reduce to

$$k^+\frac{dN_{bef-bef}}{d^3k} = \frac{\alpha_s C_F}{\pi^2}\frac{1}{\boldsymbol{\kappa}^2}, \tag{5.58a}$$

$$k^+\frac{dN_{in-in}}{d^3k} = 2\frac{\alpha_s C_F}{\pi^2}\frac{1}{\bar{\boldsymbol{\kappa}}^2}\left[1-\cos\left(\frac{\bar{\boldsymbol{\kappa}}^2}{2k^+}L^+\right)\right], \tag{5.58b}$$

$$k^+\frac{dN_{in-out}}{d^3k} = -2\frac{\alpha_s C_F}{\pi^2}\frac{1}{\bar{\boldsymbol{\kappa}}^2}\left[1-\cos\left(\frac{\bar{\boldsymbol{\kappa}}^2}{2k^+}L^+\right)\right], \tag{5.58c}$$

$$k^+\frac{dN_{out-out}}{d^3k} = \frac{\alpha_s\, C_F}{\pi^2}\frac{1}{\bar{\boldsymbol{\kappa}}^2}, \tag{5.58d}$$

$$k^+\frac{dN_{bef-in}}{d^3k} = 2\frac{\alpha_s\, C_F}{\pi^2}\frac{\boldsymbol{\kappa}\cdot\bar{\boldsymbol{\kappa}}}{\boldsymbol{\kappa}^2\,\bar{\boldsymbol{\kappa}}^2}\left[\cos\left(\frac{\bar{\boldsymbol{\kappa}}^2}{2k^+}L^+\right)-1\right], \tag{5.58e}$$

$$k^+\frac{dN_{bef-out}}{d^3k} = -2\frac{\alpha_s\, C_F}{\pi^2}\frac{\boldsymbol{\kappa}\cdot\bar{\boldsymbol{\kappa}}}{\boldsymbol{\kappa}^2\,\bar{\boldsymbol{\kappa}}^2}\cos\left(\frac{\bar{\boldsymbol{\kappa}}^2}{2k^+}L^+\right). \tag{5.58f}$$

After summing together the those expressions one finds

$$\begin{aligned} k^+\frac{dN_{tot}}{d^3k}\bigg|_{\hat{q}\to 0} &= \sum_{i=1}^{6} k^+\frac{dN_i}{d^3k}\bigg|_{\hat{q}\to 0} \\ &= \frac{\alpha_s C_F}{\pi^2}\left(\frac{1}{\boldsymbol{\kappa}^2}+\frac{1}{\bar{\boldsymbol{\kappa}}^2}-2\frac{\boldsymbol{\kappa}\cdot\bar{\boldsymbol{\kappa}}}{\boldsymbol{\kappa}^2\,\bar{\boldsymbol{\kappa}}^2}\right), \end{aligned} \tag{5.59}$$

which reduces as expected to the vacuum gluon spectrum, i.e. Eq. (5.33). The physical meaning of the gluon spectrum (5.57) can be better understood by considering formation time arguments. The coherent limit corresponds to the case when the emitted gluon remains coherent while crossing the QCD medium, i.e. $\tau_d \gg L^+$. Hence, the emitted gluon is not able to acquire Brownian motion while passing through the QCD medium. In this case, one enters to the fully complete LPM regime where the medium acts as a unique scattering center and therefore the effective momentum transfer is $\sim Q_s = \hat{q}L^+$, which is constant. As a consequence, in this limit dN_{in-in} and dN_{in-out} are suppressed. Therefore, the total spectrum is given by the sum of three components

$$k^+\frac{dN_{tot}}{d^3k}\bigg|_{\tau_d\gg L^+} = k^+\frac{dN_{bef-bef}}{d^3k}+k^+\frac{dN_{bef-out}}{d^3k}+k^+\frac{dN_{out-out}}{d^3k}. \tag{5.60}$$

In this limit, the dipole $\mathcal{S}$ and the path integral $\mathcal{K}$ become [32]

$$\lim_{L^+\to 0}\mathcal{S}(L^+,0,\boldsymbol{r})\big|_{Q_s=const.} = e^{-\frac{Q_s^2\boldsymbol{r}^2}{4}}, \tag{5.61a}$$

$$\lim_{L^+\to 0}\mathcal{K}_{osc}(L^+,\boldsymbol{x};0,\boldsymbol{y}|k^+)\big|_{Q_s=const.} = \delta^{(2)}(\boldsymbol{x}-\boldsymbol{y})e^{-\frac{Q_s^2\boldsymbol{y}^2}{4}}. \tag{5.61b}$$

Next we make explicit use of the above expressions to simplify the non-vanishing components of the gluon spectrum in this limit. The final result can be written as

$$k^+\frac{dN_{bef-bef}}{d^3k} = \frac{\alpha_s C_F}{\pi^2}\,\frac{e^{-\boldsymbol{\kappa}^2/Q_s^2}}{Q_s^2}\left[\log\left(\frac{Q_s^2}{\Lambda^2}\right) - \Gamma\left(0,-\frac{\boldsymbol{\kappa}^2}{Q_s^2}\right) - \gamma_E - \log\left(-\frac{\boldsymbol{\kappa}^2}{Q_s^2}\right)\right], \tag{5.62a}$$

$$k^+\frac{dN_{out-out}}{d^3k} = \frac{\alpha_s\, C_F}{\pi^2}\,\frac{1}{\bar{\boldsymbol{\kappa}}^2}, \tag{5.62b}$$

$$k^+\frac{dN_{bef-in}}{d^3k} = -2\frac{\alpha_s\, C_F}{\pi^2}\,\frac{\boldsymbol{\kappa}\cdot\bar{\boldsymbol{\kappa}}}{\boldsymbol{\kappa}^2\bar{\boldsymbol{\kappa}}^2}\left(1-e^{-\boldsymbol{\kappa}^2/Q_s^2}\right). \tag{5.62c}$$

If we consider the case when the hard scattering does not affect the trajectory of the projectile, i.e. in the high-energy limit where $\delta\boldsymbol{\kappa}\sim 0$, then $\boldsymbol{\kappa}\sim\bar{\boldsymbol{\kappa}}=\boldsymbol{k}$, so Eqs.(5.62) coincide with the well known result obtained by Kovchegov and Mueller, see Eqs. 59-61 of Ref. [48]. The high-energy limit of the gluon production in the dilute-dense regime has also been studied in the past by different authors [42, 48, 49, 50, 51, 52].

Chapter 6

Conclusions

In the end, let us refresh our knowledge and see what we have just understood in this thesis.

- The study of the spectrum of two-photon radiation off a quark in a medium is presented in this thesis. In the Moliére limit, we find similar features as in the case of one-photon radiation off a quark in a medium, namely the appearance of Gaussian distribution of the total momentum transfer from the medium. In the two-photon case, this is quite surprising since the corresponding vacuum spectrum is just a superposition of two independent emissions.

- The above conclusions hold, strictly speaking, only for the ladder emission diagram, depicted in figure 3.4. For the two-photon case, there appears Feynman diagrams with much more complicated emission sequences, in addition to the diagrams including interference with vacuum emissions.

- The medium-induced gluon radiation spectrum off a $q\bar{q}$ antenna at first order in opacity expansion is generalized to the massive case. In this calculation, performed in the high-energy limit, both the formation time effect and the dead-cone effect for massive quarks and the interference between emissions off the quark and the antiquark are included. The results and techniques presented here can also be applied to tagged heavy-quark jets.

- We find that the anti-angular ordering obtained in the massless case is modified by the dead-cone effect. The decoherence phenomenon extends to the massive case. The interference between two emitters included in the antenna opens more phase space for soft gluon radiation at relatively large opening angles for some specific choices of the

parameters. More collimated antenna loses less energy and the size of the mass effect on the energy loss for the antenna of large opening angles is similar to the one resulting from independent emitters. The average energy loss outside of a given emission angle is studied, and we find that there is no typical **k**-broadening in the antenna in either the massless or the massive cases for small antenna opening angles and small energies of the emitted gluon, which is just the anti-angular ordering regime. The antenna spectrum is found to be dominated by the contribution from independent emitters for large antenna opening angles and large energies of the emitted gluon.

- The breakdown of the traditional relation between radiative energy loss and **k**-broadening that we obtain in our formalism is very suggestive of an interpretation of the recent experimental findings on reconstructed jets in nuclear collisions at the LHC. Indeed, the data indicate that the main observed effect is the emission of soft particles at large angles, while there is no strong modification of the fragmentation function or the dijet azimuthal asymmetry. At the same time, a large energy loss is observed in the energy imbalance between two back-to-back jets. These two features are difficult to reconcile in a traditional formalism as the relation between energy loss and broadening is a rather general one. However, they qualitatively admit a natural interpretation in terms of the partial decoherence, which is found when more than one emitter is considered, as done here, and where the vacuum-like soft radiation is found. Although several issues need to be clarified before interpreting these data in terms of an underlying physical mechanism, e.g. the sample of jets studied retains some bias as demonstrated by the suppression in R_{CP} measured by ATLAS, the findings presented in this thesis are very encouraging for a full description of the data in terms of a medium-modified parton shower.

- The interference pattern between initial and final radiation in a color deconfined medium is presented in this thesis. We derive an analytic expression for the medium-induced gluon spectrum off an asymptotic parton created in the remote past which suffers a hard collision and subsequently crosses a color deconfined medium. The medium-induced gluon spectrum has three contributions: the independent gluon emissions associated to the incoming and the outgoing partons, and the interference terms between both emitters. The angular distribution of gluon emission is affected by the presence of these interferences between the emitters when one compares with the radiation

pattern in vacuum.

- The setup studied here shows in a transparent manner how the interferences affect the angular distribution of the gluon radiation under the presence of a color deconfined medium. Note that, the same as the previous studies in vacuum and in the medium, the results presented here for the t-channel exchange of a color singlet object hold in the soft limit for arbitrary color representations. In this way, they are applicable to medium-induced soft gluon production for any t-channel hard scattering. The possible phenomenological consequences of our findings can be considered at the level of the inclusive spectra of produced gluons, and the opening of more phase space for large angle soft emissions, which is evident in the soft limit, should lead to an increase of soft hadron multiplicities.

My doctorate studies are the first steps towards jet calculus in a color deconfined medium, and they may give an improved guidance to the construction of the building blocks for the Monte Carlo simulators.

USC UNIVERSIDADE DE SANTIAGO DE COMPOSTELA

USC
UNIVERSIDADE
DE SANTIAGO
DE COMPOSTELA

Bibliography

[1] H. Ma, C. A. Salgado and K. Tywoniuk, "Medium-induced multi-photon radiation," J. Phys. Conf. Ser. **270** (2011) 012034 [arXiv:1105.5801 [hep-ph]].

[2] N. Armesto, H. Ma, Y. Mehtar-Tani, C. A. Salgado and K. Tywoniuk, "Coherence effects and broadening in medium-induced QCD radiation off a massive $q\bar{q}$ antenna," JHEP **1201** (2012) 109 [arXiv:1110.4343 [hep-ph]].

[3] N. Armesto, H. Ma, M. Martinez, Y. Mehtar-Tani and C. A. Salgado, "Interference between initial and final state radiation in a QCD medium," Phys. Lett. B **717** (2012) 280 [arXiv:1207.0984 [hep-ph]].

[4] N. Armesto, H. Ma, M. Martinez, Y. Mehtar-Tani and C. A. Salgado, "Coherence effects on gluon production in a dense medium," work in progress.

[5] J. Beringer *et al.* [Particle Data Group Collaboration], "Review of Particle Physics (RPP)," Phys. Rev. D **86** (2012) 010001.

[6] D. J. Gross and F. Wilczek, "ULTRAVIOLET BEHAVIOR OF NON-ABELIAN GAUGE THEORIES," Phys. Rev. Lett. **30** (1973) 1343.

[7] H. D. Politzer, "RELIABLE PERTURBATIVE RESULTS FOR STRONG INTERACTIONS?," Phys. Rev. Lett. **30** (1973) 1346.

[8] G. S. Bali, "QCD forces and heavy quark bound states," Phys. Rept. **343** (2001) 1 [arXiv:hep-ph/0001312].

[9] F. Karsch, "Lattice results on QCD thermodynamics," Nucl. Phys. A **698** (2002) 199 [arXiv:hep-ph/0103314].

[10] O. Kaczmarek, F. Karsch, E. Laermann and M. Lutgemeier, "Heavy quark potentials in quenched QCD at high temperature," Phys. Rev. D **62** (2000) 034021 [hep-lat/9908010].

[11] K. Aamodt and C. A. Loizides [ALICE Collaboration], "Suppression of Charged Particle Production at Large Transverse Momentum in Central Pb–Pb Collisions at $\sqrt{s_{NN}} = 2.76$ TeV," Phys. Lett. B **696** (2011) 30 [arXiv:1012.1004 [nucl-ex]].

[12] S. S. Adler *et al.* [PHENIX Collaboration], "Identified charged particle spectra and yields in Au + Au collisions at s(NN)**(1/2) = 200-GeV," Phys. Rev. C **69** (2004) 034909 [arXiv:nucl-ex/0307022].

[13] M. Gyulassy and X. n. Wang, "Multiple collisions and induced gluon Bremsstrahlung in QCD," Nucl. Phys. B **420** (1994) 583 [arXiv:nucl-th/9306003].

[14] C. Itzykson and J. B. Zuber, "Quantum Field Theory," New York, Usa: Mcgraw-hill (1980) 705 P.(International Series In Pure and Applied Physics)

[15] Y. Mehtar-Tani, "Relating the description of gluon production in pA collisions and parton energy loss in AA collisions," Phys. Rev. C **75** (2007) 034908 [hep-ph/0606236].

[16] U. A. Wiedemann and M. Gyulassy, "Transverse momentum dependence of the Landau-Pomeranchuk-Migdal effect," Nucl. Phys. B **560** (1999) 345 [hep-ph/9906257].

[17] Y. Mehtar-Tani, C. A. Salgado and K. Tywoniuk, "The radiation pattern of a QCD antenna in a dilute medium," JHEP **1204** (2012) 064 [arXiv:1112.5031 [hep-ph]].

[18] Y. L. Dokshitzer, V. A. Khoze, A. H. Mueller and S. I. Troian, "Basics of perturbative QCD," Gif-sur-Yvette, France: Ed. Frontieres (1991) 274 p. (Basics of)

[19] R. Baier, Y. L. Dokshitzer, A. H. Mueller, S. Peigne and D. Schiff, "Radiative energy loss of high-energy quarks and gluons in a finite volume quark - gluon plasma," Nucl. Phys. B **483** (1997) 291 [hep-ph/9607355].

[20] E. A. Kuraev, L. N. Lipatov and V. S. Fadin, "The Pomeranchuk Singularity in Nonabelian Gauge Theories," Sov. Phys. JETP **45** (1977) 199 [Zh. Eksp. Teor. Fiz. **72** (1977) 377].

[21] I. I. Balitsky and L. N. Lipatov, "The Pomeranchuk Singularity in Quantum Chromodynamics," Sov. J. Nucl. Phys. **28** (1978) 822 [Yad. Fiz. **28** (1978) 1597].

[22] C. A. Salgado and U. A. Wiedemann, "Calculating quenching weights," Phys. Rev. D **68** (2003) 014008 [hep-ph/0302184].

[23] R. Baier, Y. L. Dokshitzer, A. H. Mueller, S. Peigne and D. Schiff, "Radiative energy loss and p(T) broadening of high-energy partons in nuclei," Nucl. Phys. B **484** (1997) 265 [hep-ph/9608322].

[24] U. A. Wiedemann, "Gluon radiation off hard quarks in a nuclear environment: Opacity expansion," Nucl. Phys. B **588** (2000) 303 [hep-ph/0005129].

[25] M. Gyulassy, P. Levai and I. Vitev, "Reaction operator approach to nonAbelian energy loss," Nucl. Phys. B **594** (2001) 371 [arXiv:nucl-th/0006010].

[26] Y. Mehtar-Tani, C. A. Salgado and K. Tywoniuk, "Anti-angular ordering of gluon radiation in QCD media," Phys. Rev. Lett. **106** (2011) 122002 [arXiv:1009.2965 [hep-ph]].

[27] M. Djordjevic and M. Gyulassy, "Heavy quark radiative energy loss in QCD matter," Nucl. Phys. A **733**, 265 (2004) [arXiv:nucl-th/0310076].

[28] N. Armesto, C. A. Salgado and U. A. Wiedemann, "Medium induced gluon radiation off massive quarks fills the dead-cone," Phys. Rev. D **69** (2004) 114003 [arXiv:hep-ph/0312106].

[29] Y. Mehtar-Tani, C. A. Salgado and K. Tywoniuk, "Jets in QCD Media: From Color Coherence to Decoherence," Phys. Lett. B **707** (2012) 156 [arXiv:1102.4317 [hep-ph]].

[30] N. Armesto, H. Ma, M. Martinez, Y. Mehtar-Tani and C. A. Salgado, "Medium-induced soft gluon radiation in DIS," arXiv:1207.1207 [hep-ph].

[31] R. K. Ellis, W. J. Stirling and B. R. Webber, "QCD and collider physics", Cambridge University Press, 1996.

[32] U. A. Wiedemann, "Transverse dynamics of hard partons in nuclear media and the QCD dipole," Nucl. Phys. B **582** (2000) 409 [hep-ph/0003021].

[33] N. Armesto, L. Cunqueiro, C. A. Salgado and W. -C. Xiang, "Medium-evolved fragmentation functions," JHEP **0802** (2008) 048 [arXiv:0710.3073 [hep-ph]].

[34] N. Armesto, L. Cunqueiro and C. A. Salgado, "Q-PYTHIA: A Medium-modified implementation of final state radiation," Eur. Phys. J. C **63** (2009) 679 [arXiv:0907.1014 [hep-ph]].

[35] Y. Mehtar-Tani and K. Tywoniuk, "Jet Coherence in QCD Media: The Antenna Radiation Spectrum," arXiv:1105.1346 [hep-ph].

[36] J. Casalderrey-Solana and E. Iancu, "Interference effects in medium-induced gluon radiation," JHEP **1108** (2011) 015 [arXiv:1105.1760 [hep-ph]].

[37] J. F. Gunion and G. Bertsch, "Hadronization By Color Bremsstrahlung," Phys. Rev. D **25** (1982) 746.

[38] F. Arleo, S. Peigne and T. Sami, "Revisiting scaling properties of medium-induced gluon radiation," Phys. Rev. D **83** (2011) 114036 [arXiv:1006.0818 [hep-ph]].

[39] E. Iancu and R. Venugopalan, "The Color glass condensate and high-energy scattering in QCD," In *Hwa, R.C. (ed.) et al.: Quark gluon plasma* 249-3363 [hep-ph/0303204].

[40] S. Chatrchyan *et al.* [CMS Collaboration], "Measurement of the inclusive production cross sections for forward jets and for dijet events with one forward and one central jet in pp collisions at sqrt(s) = 7 TeV," JHEP **1206** (2012) 036 [arXiv:1202.0704 [hep-ex]].

[41] F. Gelis and Y. Mehtar-Tani, "Gluon propagation inside a high-energy nucleus," Phys. Rev. D **73** (2006) 034019 [hep-ph/0512079].

[42] J. P. Blaizot, F. Gelis and R. Venugopalan, "High-energy pA collisions in the color glass condensate approach. 1. Gluon production and the Cronin effect," Nucl. Phys. A **743** (2004) 13 [hep-ph/0402256].

[43] A. Bassetto, M. Ciafaloni and G. Marchesini, "Jet Structure and Infrared Sensitive Quantities in Perturbative QCD," Phys. Rept. **100** (1983) 201.

[44] R. Baier, Y. L. Dokshitzer, A. H. Mueller and D. Schiff, "Radiative energy loss of high-energy partons traversing an expanding QCD plasma," Phys. Rev. C **58** (1998) 1706 [hep-ph/9803473].

[45] B. G. Zakharov, "Fully quantum treatment of the Landau-Pomeranchuk-Migdal effect in QED and QCD," JETP Lett. **63** (1996) 952 [hep-ph/9607440].

[46] B. G. Zakharov, "Radiative energy loss of high-energy quarks in finite size nuclear matter and quark - gluon plasma," JETP Lett. **65** (1997) 615 [hep-ph/9704255].

[47] M. Gyulassy, P. Levai and I. Vitev, "NonAbelian energy loss at finite opacity," Phys. Rev. Lett. **85** (2000) 5535 [nucl-th/0005032].

[48] Y. V. Kovchegov and A. H. Mueller, "Gluon production in current nucleus and nucleon - nucleus collisions in a quasiclassical approximation," Nucl. Phys. B **529** (1998) 451 [hep-ph/9802440].

[49] Y. V. Kovchegov and K. Tuchin, "Inclusive gluon production in DIS at high parton density," Phys. Rev. D **65** (2002) 074026 [hep-ph/0111362].

[50] A. Dumitru and L. D. McLerran, "How protons shatter colored glass," Nucl. Phys. A **700** (2002) 492 [hep-ph/0105268].

[51] B. Z. Kopeliovich, A. V. Tarasov and A. Schafer, "Bremsstrahlung of a quark propagating through a nucleus," Phys. Rev. C **59** (1999) 1609 [hep-ph/9808378].

[52] J. Jalilian-Marian and Y. V. Kovchegov, "Saturation physics and deuteron-Gold collisions at RHIC," Prog. Part. Nucl. Phys. **56** (2006) 104 [hep-ph/0505052].